From Cooper Pairs to Molecules: Effective field theories for ultra-cold atomic gases near Feshbach resonances

by

J. N. Milstein

B.A., Northern Illinois University, 1996

A thesis submitted to the

Faculty of the Graduate School of the

University of Colorado in partial fulfillment

of the requirements for the degree of

Doctor of Philosophy

Department of Physics

2004

This thesis entitled:
From Cooper Pairs to Molecules: Effective field theories for ultra-cold atomic gases near
Feshbach resonances
written by J. N. Milstein
has been approved for the Department of Physics

Murray Holland

Prof. Paul Beale

Date

The final copy of this thesis has been examined by the signatories, and we find that both the content and the form meet acceptable presentation standards of scholarly work in the above mentioned discipline.

Milstein, J. N. (Ph.D., Physics)

From Cooper Pairs to Molecules: Effective field theories for ultra-cold atomic gases near Feshbach resonances

Thesis directed by Prof. Murray Holland

Feshbach resonances in dilute atomic gases are a powerful tool used to control the strength of atom-atom interactions. In practice, the tuning is accomplished by varying a magnetic field, affording experiments on dilute atomic gases a knob with which they can arbitrarily adjust the interactions. This precision control makes atomic gases an ideal place to study many-body phenomena. The resonance works by introducing a closed channel containing a bound, molecular state within the open channel of continuum scattering states. The molecular state greatly modifies the scattering responsible for the interactions, as it is tuned near resonance, introducing pair correlations throughout the sample. The size of these correlations may range from either very small, where they appear as molecules, to very large, where they resemble Cooper pairs. This leads to a "crossover" problem of connecting the Bardeen-Cooper-Schrieffer theory of Cooper pairing, which describes conventional superconductors, to the process of Bose-Einstein condensation of molecules. To answer this question, it is necessary to develop an appropriate field theory for both Bosons and Fermions that can account for the Feshbach processes and, therefore, properly describe resonant, ultra-cold atomic gases.

Dedication

This work is dedicated to Jack Shear for getting me to think about the world and to Terry Robinson for not letting me stop.

Acknowledgements

I should express my deepest gratitude to Murray Holland for all his support during the formation of this dissertation work. The environment in which I spent my graduate career could not have been more ideal. The independence which I was granted helped to both nurture and stimulate a variety of interests within me as can be seen in the broad range of topics present within this work.

In fact, an innumerable number of people were instrumental in the development of this dissertation such as the various members of my research group, many of the experimentalists and staff of JILA, as well as all the collaborators I have had the chance to work with on the projects discussed within. I would particulary like to acknowledge the collaboration and friendship I have had with Servaas Kokkelmans and would like to thank Christophe Salomon for hosting me at ENS in Paris where I was fortunate enough to be during the final stages of this work.

If I look back at those who helped me achieve this doctorate I should thank both George Crabtree and Art Fedro for all their encouragement. If it had not been for the kind reception I received as I entered the physical sciences with a degree in the social sciences it is not certain that I would ever have written this work.

This dissertation is dedicated, in part, to my grandfather, Jack Shear, who was not able to see it completed. I'm sure he hardly suspected that all those broken appliances he used to have me fetch from the dumpsters when I was a kid were worth anything, but they were.

Contents

Figures

Figure

Chapter 1

Introduction

1.1 Degenerate atomic gases

Dilute atomic gases provide a fascinating setting in which to study an array of fundamental questions in many-body physics. The precise control with which these gases can be manipulated, combined with a detailed understanding of the atomic interactions, allows for an unprecedented level of comparison between theory and experiment. Since the first observations of Bose-Einstein condensation(BEC)[1, 2, 3], innumerable works have been published on the nature of quantum degenerate gases. With the achievement of degeneracy within a Fermi gas [4], the next big push is toward superfluidity, a contest analogous to the race toward condensation almost a decade ago.

The main ingredient to creating a degenerate atomic gas is to cool an ensemble of atoms until the de Broglie wavelength of the particles, defined as:

$$\lambda_{db} = \hbar/(2Mk_BT)^{1/2}, \tag{1.1}$$

becomes large compared to the average inter-particle spacing. For a system of bosons, cooling leads to a condensate of atoms where a macroscopic fraction occupies a single quantum state. For fermions, cooling will cause the atoms to fill each energy level, allowing for no more than one of each spin state at a given level. The result is a degenerate "Fermi sea" of atoms.

Unfortunately, the onset of quantum degeneracy will often be proceeded by a

liquid or solid phase transition. In order to reach the quantum degenerate regime, the timescale for formation of molecules by 3-body collisions must be much longer than the time needed to reach degeneracy. Since equilibrium is reached through binary elastic collisions (a process which leads to cooling of the gas) at a rate proportional to the density $\sim n$, and 3-body inelastic collisions (which result in losses) occur at a rate proportional to $\sim n^2$, a window may open at extremely low densities in which degeneracy may be achieved. However, such low densities also depress the temperature requirement for quantum degeneracy into the nanokelvin range. As an illustration, current BEC experiments reach quantum degeneracy at temperatures between 500 nK and 2 μk at densities between 10^{14} and 10^{15} cm^{-3} [5].

The first observation of Bose-Einstein condensation(BEC) was made in a dilute alkali gas of ^{87}Rb at JILA [1], followed almost immediately by similar reports in ^{23}Na at MIT [2] and ^{7}Li at Rice [3]. This achievement was made possible by the rapid advances that had occurred in the field of laser cooling and trapping over the previous few decades. Not long after, quantum degeneracy was achieved at JILA within a two-component Fermi gas of ^{40}K atoms [4].

Although similar to the methods employed in achieving BEC, the techniques used to reach the degenerate regime within fermions had to be adapted to account for Pauli statistics. A major hurdle results from the fact that identical fermions tend to avoid each other. In this case, s-wave interactions, which dominate the low energy scattering of these gases, would vanish between a single species of fermions. To overcome this difficulty, the JILA group used a mixture of atoms within the two hyperfine levels: $|F = 9/2, m_F = 9/2\rangle$ and $|F = 9/2, m_F = 7/2\rangle$, where $F = 9/2$ is the total atomic spin and m_F is the magnetic quantum number. Runaway evaporation, by which the collision rates increase as the temperature decreases, was achieved by carefully removing equal populations of both spin states as the gas cooled. Another method for increasing elastic collisions is to sympathetically cool the fermions with an auxiliary, bosonic population.

This technique was soon employed to create degenerate mixtures of ^{7}Li and ^{6}Li at ENS [6], Rice [7], and Duke [8], a mixture of ^{6}Li and ^{23}Na at MIT [9], and a ^{40}K and ^{87}Rb mixture at Firenze [10].

1.2 Tunable interactions

One of the more unique qualities of cold atomic gases is the ability to finely tune the interatomic interactions. This control is achieved by making use of low-energy Feshbach resonances which can be precisely tuned by variation of a magnetic field. The observation of a Feshbach resonance within a dilute atomic gas is a relatively recent event, first attained within a Na BEC at MIT [11]. Quite soon after, observations of Feshbach resonances where reported in ^{85}Rb at U.T. Austin[12] and JILA[13], as well as in Cs at Stanford [14]. Feshbach resonances have also been observed in degenerate Fermi systems such as ^{40}K at JILA [15], and ^{6}Li at MIT [16], ENS [17], and Innsbruck [18], to name a few.

In cold alkali collisions, the atom-atom interactions are predominantly determined by the state of the valence electrons. If two atoms involved in a collision form a triplet, where "triplet" refers to the electronic spin configuration of the two valence electrons, the electrons will tend to avoid each other in order to preserve the overall antisymmetry of the wavefunction. This behavior acts to reduce the Coulomb repulsion felt by the two atoms resulting in a somewhat shallower potential well. For a singlet state, however, the atoms may sit upon one another resulting in a much stronger potential. Because of these considerations, singlet potentials are in general much deeper than corresponding triplet potentials.

The singlet and triplet spin states may couple to one another through hyperfine interactions with the spin of the nucleus. If two atoms are scattering within a triplet potential, for instance, the hyperfine coupling may flip the electronic and nuclear spins of one of the atoms bringing the collision into the singlet potential. Another spin flip may

then bring the collision back to the triplet potential. For large internuclear separations we may define a quantity Δ which gives the energy shift between the scattering threshold of the singlet and triplet potentials. This relative separation is determined by the Zeeman shifts of the internal states of the two atoms and may, therefore, be adjusted by variation of a magnetic field.

Since the threshold of the singlet potential generally appears above the threshold of the triplet potential it becomes energetically unfavorable for atoms to scatter out of the singlet potential. The singlet is referred to then as a closed channel potential and the triplet as an open channel potential. Of course, for real alkali atoms, the atoms appear as a linear combination of a singlet and triplet states so it is best to talk in terms of open and closed channels rather than singlet and triplet channels.

If a closed channel Q supports a bound state, we may form a Feshbach resonance by tuning this bound state near the threshold of the open channel P (see Fig. 1.1). The energy between the bound state in channel Q and the threshold of channel P is referred to as the detuning ν. Two atoms scattering within the P channel may collide to form a quasi-bound molecular state within the Q channel with a different internal spin arrangement. The molecular state is only considered to be quasi-bound since it remains coupled to the continuum states resulting in a finite lifetime for the molecular state. Another spin flip breaks apart the molecule and the system is returned to the initial P channel.

The detuning of the two channels has a dramatic impact on the scattering properties of the system and results in a scattering length which depends on the external magnetic field as:

$$a = a_{bg}\left(1 - \frac{\Delta B}{B - B_0}\right). \tag{1.2}$$

Here a_{bg} would be the background scattering length of the open channel if the closed channel was not accessible, ΔB is a measure of the width of the resonance, B_0 is the

value of the magnetic field B just on resonance, and $B - B_0 \sim \nu$. We will discuss more the details of Feshbach resonance theory in the next chapter.

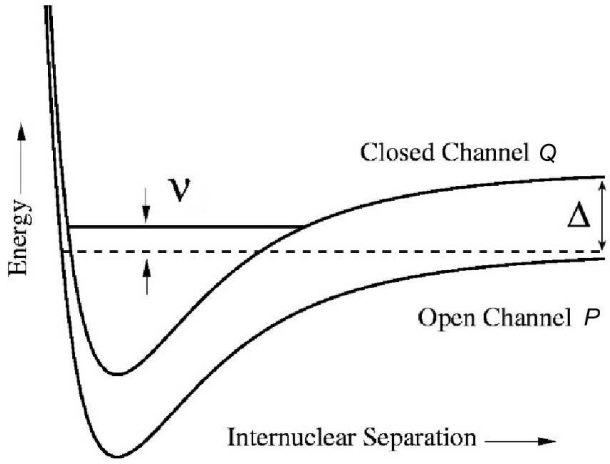

Figure 1.1: Born-Oppenheimer curves illustrating the mechanism of a Feshbach resonance. A Feshbach resonance results when a closed channel potential possesses a bound state in proximity to the scattering threshold of an open channel potential. The detuning of the bound state from the edge of the collision continuum is denoted by ν. Δ represents the energy shift between the two channels at large, relative separation.

1.3 Molecular superfluids and beyond

The introduction of a Feshbach resonance not only allows direct control over the atom-atom interactions, but inherently introduces a process of molecular formation and disassociation. The presence of molecules greatly increases the richness and utility of these systems. Molecular BECs, for instance, have remained out of reach to experiment due to the difficulty involved in cooling molecules as compared to alkali atoms. One way of overcoming this difficulty would be to create an atomic condensate through traditional laser trapping and cooling techniques and to then ramp across a Feshbach resonance converting the atomic condensate into a molecular condensate. This technique was used in the JILA ^{85}Rb experiment by Donley *et al.* [19] to create a superposition of atoms and molecules–although the question of whether a true molecular condensate was formed is

still being debated. A similar experiment was performed by Dürr *et al.* [20] where they were able to spatially separate the molecular component from the atomic population by performing a Stern-Gerlach experiment.

Surprisingly enough, degenerate Fermi gases proved more adept at forming molecules than Bose gases. Due to Pauli blocking of the available decay channels, these molecules showed extremely long lifetimes, some remaining for up to several seconds [21, 22, 23, 24]. With such long lived molecules available, reports of molecular condensates quickly appeared at JILA [25], then MIT [26] and Innsbruck [27].

The production of a molecular condensate from a Fermi gas of atoms was the first step in experimentally studying the "crossover problem" of moving between Bardeen-Cooper-Schrieffer (BCS) superfluidity and Bose-Einstein condensation (BEC). Soon after these initial observations, reports of condensate formation above the resonance, well within the crossover regime between the extremes of BCS and BEC, where made first at JILA [28] and then at MIT [29]. These reports may be the first observations of "resonance superfluidity" within Fermi gases.

1.4 Outlook and overview

The structure of this thesis will be as follows. Chapter 2 will present the formalism of Feshbach resonant scattering. In Chapter 3 we will use the ideas discussed in the previous chapter to develop a field theory for bosons and apply it to the collapse of a condensate. We will review some of the fundamental notions behind BCS theory in Chapter 4 and go on to extend these ideas to form a theory of resonance superfluidity in Chapter 5. This theory will be used to determine signatures of a superfluid phase transition in a degenerate Fermi gas. Chapter 6 will discuss the crossover problem, briefly mentioned in the previous section of this introduction, in greater detail and in Chapter 7 we will treat the crossover by extending a lowest order theory to account for the production of molecules. Chapter 8 will extend the theory of the previous chapter

to formulate a nonperturbative theory of the crossover. In Chapter 9 we introduce the fractional quantum Hall effect, properties of which are predicted to occur in a rapidly rotating Bose gas, and, in Chapter 10, discuss how a resonance may alter these properties focusing on the ground state of such a system.

Chapter 2

Feshbach resonance formalism

2.1 Feshbach resonance theory

We now briefly describe the Feshbach formalism and derive the elastic S- and T-matrices for two-body Feshbach resonant scattering. These matrices represent the transition probabilities for scattering between states within the resonant system. A more detailed and extended treatment of this formalism can be found in the literature [30, 31].

In Feshbach resonance theory, two projection operators P and Q are introduced which project onto the subspaces $\mathcal{P}$ and $\mathcal{Q}$ and satisfy the relations:

$$\begin{aligned} P = P^\dagger \quad Q = Q^\dagger \\ P^2 = P \quad Q^2 = Q \\ P + Q = 1. \end{aligned} \tag{2.1}$$

These subspaces form two orthogonal components which together span the full Hilbert space of both scattering and bound wavefunctions $|\psi\rangle = P|\psi\rangle + Q|\psi\rangle$. The open and closed channels are contained in $\mathcal{P}$ and $\mathcal{Q}$, respectively. The operators P and Q split the Schrödinger equation for the two-body problem $(E - H)|\psi\rangle = 0$ into two parts:

$$(E - H_{PP})|\psi_P\rangle = H_{PQ}|\psi_Q\rangle, \tag{2.2}$$

$$(E - H_{QQ})|\psi_Q\rangle = H_{QP}|\psi_P\rangle, \tag{2.3}$$

where $H_{PP} = PHP$, $H_{PQ} = PHQ$, etc., and ψ is the total scattering wavefunction. The projections on the two sub-spaces are indicated by $P|\psi\rangle = |\psi_P\rangle$ and $Q|\psi\rangle = |\psi_Q\rangle$.

The Hamiltonian $H = H^0 + V$ consists of the sum of single-particle interactions H^0 and the two-body interaction V. We may formally solve Eq. (2.3) to find:

$$|\psi_Q\rangle = \frac{1}{E^+ - H_{QQ}} H_{QP}|\psi_P\rangle, \tag{2.4}$$

where $E^+ = E + i\delta$, with δ approaching zero from positive values. Substituting this result into Eq. (2.2), the open channel equation can be written as

$$(E - H_{\text{eff}})|\psi_P\rangle = 0, \tag{2.5}$$

where

$$H_{\text{eff}} = H_{PP} + H_{PQ}\frac{1}{E^+ - H_{QQ}} H_{QP}. \tag{2.6}$$

If we write Eq. (2.6) in the following form:

$$H_{\text{eff}} = H^0_{PP} + V_{\text{eff}}, \tag{2.7}$$

we may identify an effective potential

$$V_{\text{eff}} = V_{PP} + H_{PQ}\frac{1}{E^+ - H_{QQ}} H_{QP}, \tag{2.8}$$

resulting from the coupling to the $\mathcal{Q}$ subspace. We have thus reduced the scattering problem to that of scattering off an effective potential composed of an additive combination of the open channel potential and a coupling to the closed channels. We will return to this result in our later discussion of the many-body physics of Feshbach resonant systems.

The trick to solving Eq. (2.5) is to expand the resolvent operator into the discrete and continuum eigenstates of H_{QQ}:

$$H_{\text{eff}} = H_{PP} + \sum_i \frac{H_{PQ}|\phi_i\rangle\langle\phi_i|H_{QP}}{E - \epsilon_i} + \int \frac{H_{PQ}|\phi(\epsilon)\rangle\langle\phi(\epsilon)|H_{QP}}{E^+ - \epsilon} d\epsilon. \tag{2.9}$$

Here the ϵ_i's and ϵ's are the uncoupled bound-state and continuum eigenvalues, respectively. In practice, only a few bound states will significantly affect the properties of

the open-channel. We will now assume that a small number of bound states dominate the problem and will neglect the continuum expansion in Eq. (2.9). Then the formal solution for $|\psi_P\rangle$ is given by

$$|\psi_P\rangle = |\psi_P^+\rangle + \frac{1}{E^+ - H_{PP}} \sum_i \frac{H_{PQ}|\phi_i\rangle\langle\phi_i|H_{QP}|\psi_P\rangle}{E - \epsilon_i}, \tag{2.10}$$

where the scattered wavefunction $|\psi_P^+\rangle$ is an eigenstate of the direct interaction H_{PP} (i.e., $(E^+ - H_{PP})|\psi_P^+\rangle = 0$) and satisfies outgoing, spherical wave boundary conditions. Likewise, we may define a scattered wavefunction $|\psi_P^+\rangle$ satisfying incoming, spherical wave boundary conditions, $(E^- - H_{PP})|\psi_P^-\rangle = 0$. The scattered wavefunctions $|\psi_P^\pm\rangle$ may be formally solved for with the result

$$|\psi_P^\pm\rangle = |\chi_P\rangle + \frac{V_{PP}}{E^\pm - H_{PP}}|\chi_P\rangle, \tag{2.11}$$

where the unscattered wavefunction $|\chi_P\rangle$ is defined as an eigenstate of H_{PP}^0.

We now quantify the scattering behavior of a Feshbach resonance system by calculating the transition matrix (T-matrix). To begin, let us define a nonresonant T-matrix for scattering within the $\mathcal{P}$ subspace as:

$$\begin{aligned} \mathcal{T}_P &= \langle\chi_P|V_{PP} + V_{PP}\frac{1}{E^+ - H_{PP}}V_{PP}|\chi_P\rangle & (2.12)\\ &= \langle\chi_P|V_{PP}|\psi_P^+\rangle. & (2.13) \end{aligned}$$

In moving from Eq. (2.12) to Eq. (2.13) we have made use of Eq. (2.11).

To calculate the full scattering T-matrix $\mathcal{T}$, which accounts for the coupling to the $\mathcal{Q}$ subspace, we must identify the effective potential as defined by Eq. (2.6). By multiplying Eq. (2.10) from the left with $\langle\chi_P|V_{\text{eff}}$, we derive the full, scattering T-matrix:

$$\begin{aligned} \mathcal{T} &= \langle\chi_P|V_{\text{eff}}|\psi_P\rangle & (2.14)\\ &= \mathcal{T}_P + \sum_i \frac{\langle\psi_P^-|H_{PQ}|\phi_i\rangle\langle\phi_i|H_{QP}|\psi_P\rangle}{E - \epsilon_i}, & (2.15) \end{aligned}$$

where we have again made use of the relation between the unscattered state $|\chi_P\rangle$ and the scattering wave-function $|\psi_P^-\rangle$ as given in Eq. (2.11).

From the T-matrix, we can easily go to the S-matrix defined as:

$$\mathcal{S} = \langle \psi_P^- | \psi_P^+ \rangle. \tag{2.16}$$

For s-wave scattering, there exists a simple relation between the S- and T-matrix [32]:

$$\mathcal{S} = 1 - 2\pi i \mathcal{T}. \tag{2.17}$$

This allows us to rewrite Eq. (2.15) as

$$\mathcal{S} = \mathcal{S}_P - \sum_i \frac{2\pi i \langle \psi_P^- | H_{PQ} | \phi_i \rangle \langle \phi_i | H_{QP} | \psi_P \rangle}{E - \epsilon_i}, \tag{2.18}$$

where the non-resonant factor $\mathcal{S}_P$ describes the direct scattering process within the subspace $\mathcal{P}$.

2.2 Single resonance

For the case of only one resonant bound state and only one open channel, Eq. (2.18) gives rise to the following elastic S-matrix element:

$$\mathcal{S} = \mathcal{S}_P \left[1 - \frac{2\pi i |\langle \psi_P^+ | H_{PQ} | \phi_1 \rangle|^2}{E - \epsilon_1 - \langle \phi_1 | H_{QP} \frac{1}{E^+ - H_{PP}} H_{PQ} | \phi_1 \rangle} \right]. \tag{2.19}$$

This relation is found by acting on both sides of Eq. (2.10)with $\langle \phi_i | H_{QP}$ and substituting the result into Eq. (2.18). The direct, non-resonant S-matrix is related to the background scattering length $a_{\rm bg}$, for $k \ll a_{\rm bg}^{-1}$, by $\mathcal{S}_P = \exp[-2ika_{\rm bg}]$. The term in the numerator gives rise to the energy-width of the resonance, $\Gamma = 2\pi |\langle \psi_P^+ | H_{PQ} | \phi_1 \rangle|^2$, which is proportional to the incoming wavenumber k and coupling constant $\bar{g}_1$ [33]. The bracket in the denominator gives rise to a shift of the bound-state energy, and to an additional width term $i\Gamma/2$. If we denote the energy-shift between the collision continuum and the bound state by $\bar{\nu}_1$, and represent the kinetic energy simply by $\hbar^2 k^2/m$, the S-matrix element can be rewritten as

$$\mathcal{S}(k) = e^{-2ika_{\rm bg}} \left[1 - \frac{2ik|\bar{g}_1|^2}{-\frac{4\pi\hbar^2}{m}(\bar{\nu}_1 - \frac{\hbar^2 k^2}{m}) + ik|\bar{g}_1|^2} \right]. \tag{2.20}$$

The resulting, total scattering length, coming from the relation

$$\lim_{k\to 0} T(k) = \frac{4\pi\hbar^2 a}{m}, \tag{2.21}$$

has a dispersive shape of the form

$$a = a_{\rm bg}\left(1 - \frac{m}{4\pi\hbar^2 a_{\rm bg}}\frac{|\bar{g}_1|^2}{\bar{\nu}_1}\right), \tag{2.22}$$

which may directly be related to Eq. (1.2). The form of Eq. (2.22) allows us to extract the parameters of the resonance model from a plot of the scattering length versus magnetic field.

2.3 Double resonance

Often more than one resonance may need to be considered. For example, the scattering properties for the $(f, m_f) = (1/2, -1/2)$ and $(1/2, 1/2)$ channel of ^{6}Li are dominated by a combination of two resonances: a triplet potential resonance and a Feshbach resonance. A mechanism of this sort may be inferred from Fig. 2.1 where the residual scattering length, which would arise in the absence of the Feshbach resonance coupling, would be very large and negative and vary with magnetic field. This should be compared with the value of the non-resonant background scattering length for the triplet potential of ^{6}Li which is only $31\,a_0$, which is an accurate measure of the characteristic range of this potential. An adequate scattering model for this system, therefore, requires inclusion of both bound-state resonances. The double-resonance S-matrix, with again only one open channel, follows then from Eq. (2.18) and includes a summation over two bound states. After solving for the ψ_P wave function, the S-matrix can be written as

$$S(k) = e^{-2ika_{\rm bg}}\left[1 - \frac{2ik(|\bar{g}_1|^2\Delta_2 + |\bar{g}_2|^2\Delta_1)}{ik(|\bar{g}_1|^2\Delta_2 + |\bar{g}_2|^2\Delta_1) - \Delta_1\Delta_2}\right], \tag{2.23}$$

with $\Delta_1 = (\bar{\nu}_1 - \hbar^2k^2/m)4\pi\hbar^2/m$, where $\bar{\nu}_1$ and $\bar{g}_1$ are the detuning and coupling strengths for state 1. Equivalent definitions are used for state 2. Later we will show that

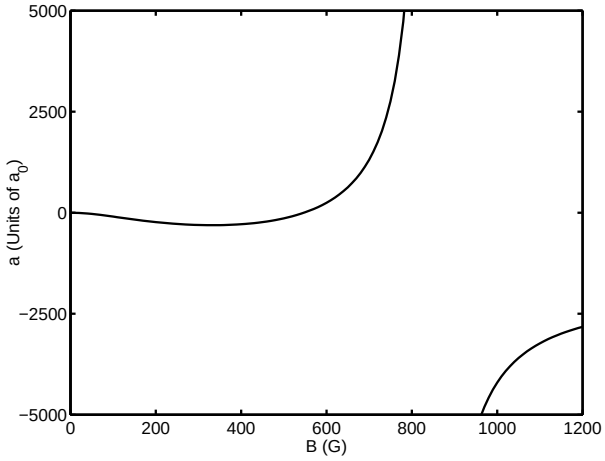

Figure 2.1: Scattering length as a function of magnetic field for the $(f, m_f) = (1/2, -1/2)$ and $(1/2, 1/2)$ mixed spin channel of ^{6}Li.

this simple analytic Feshbach scattering model mimics the coupled channels calculation of ^{6}Li.

Once again, the parameters of this model, which are related to the positions and widths of the last bound states, can be directly found from a plot of the scattering length versus magnetic field as given, for example, by Fig. 2.1. The scattering length behavior should be reproduced by the analytic expression for the scattering length following from Eq. (2.23):

$$a = a_{bg} - \frac{m}{4\pi\hbar^2}\left(\frac{|\bar{g}_1|^2}{\bar{\nu}_1} + \frac{|\bar{g}_2|^2}{\bar{\nu}_2}\right). \tag{2.24}$$

The advantage of a double-pole, over a single-pole, S-matrix parametrization is that we can account for the interplay between a potential resonance and a Feshbach resonance which, in principle, can radically change the scattering properties. This interplay is not only important for the description of ^{6}Li interactions, but also for other atomic systems which have an almost resonant triplet potential, such as bosonic ^{133}Cs [34, 35] and ^{85}Rb [36].

In the many-body theories discussed in this thesis, the scattering properties are represented by a T-matrix instead of an S-matrix. We have shown for s-wave scattering

that there exists a simple relation between the two, however, the definition for T in the many-body theory will be slightly different in order to give it the conventional dimensions of energy per unit density:

$$\mathcal{T}(k) = \frac{2\pi\hbar^2 i}{mk}\left[\mathcal{S}(k) - 1\right]. \tag{2.25}$$

2.4 Coupled square-well scattering

We now describe the coupled-channels extension of a textbook single-channel square-well scattering problem [37]. Our motivation for studying this model is that we may take the limit of the potential range as $R \to 0$, resulting in an explicit representation of a set of coupled delta-function potentials. Such a set of potentials greatly simplifies the description in the many-body problem. The applicability of delta-function potentials, or contact potentials, to the many-body system is motivated by the fact that the length-scale associated with the range of the interatomic potential is, typically, much smaller than the length scale associated with the de Broglie wavelength, or other thermodynamic correlation scales. This means that we need not concern ourselves with the actual shape of the potential so long as the chosen potential reproduces the correct asymptotic scattering properties. We may, therefore, chose the simplest potential which satisfies the constraints of our problem.

The scattering equations for a system of coupled square wells may be written as

$$E_{\rm kin}\psi^P(\mathbf{r}) = \left[H_0(\mathbf{r}) + V^P(\mathbf{r})\right]\psi^P(\mathbf{r}) + g(\mathbf{r})\psi^Q(\mathbf{r}), \tag{2.26}$$

$$E_{\rm kin}\psi^Q(\mathbf{r}) = \left[H_0(\mathbf{r}) + V^Q(\mathbf{r}) + \epsilon\right]\psi^Q(\mathbf{r}) + g^*(\mathbf{r})\psi^P(\mathbf{r}), \tag{2.27}$$

with ϵ the energy-shift of the closed channel and $E_{\rm kin} = \hbar^2k^2/m$ the two-body kinetic energy. The coupled square well model encapsulates the general properties of two-body alkali interactions. In scattering events between alkalis, we can divide the internuclear separation into two regions: the inner region where the exchange interaction (the difference between the singlet and triplet potentials) is much larger than the hyperfine

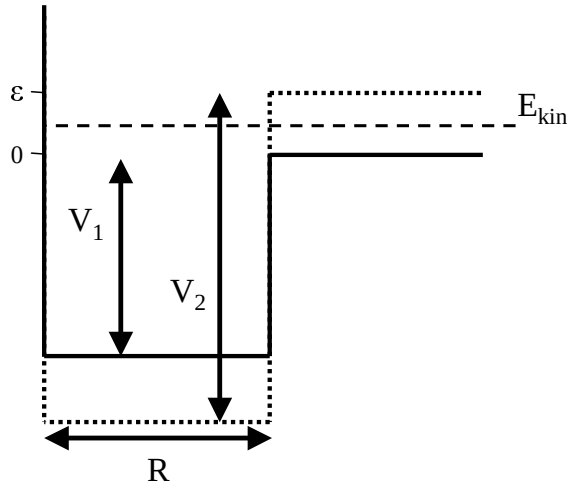

Figure 2.2: Illustration of the coupled square well system. The solid and dotted lines correspond to the molecular potentials V_1 (P) and V_2 (Q) inner $r < R$ (outer $r > R$) region, respectively. The dashed line corresponds to the kinetic energy $E_{\rm kin}$ in the open channel. The detuning ϵ can be chosen such that a bound state of the square-well potential V_2 enters the collision continuum causing a Feshbach resonance in the open channel.

splitting, and the outer region where the hyperfine interaction dominates. Here we make a similar distinction for the coupled square wells. In analogy to the real singlet and triplet potentials, we use, for the inner region, two artificial square-well potentials labelled as V_1 and V_2. We take the coupling $g(\mathbf{r})$ to be constant over the range of the potentials , $r < R$, and to be zero outside this range (see Fig. 2.2). For the outer region, $r > R$, the open and closed channel wavefunctions are given by $u_P(r) \sim \sin k_P r$ and $u_Q(r) \sim \exp(-k_Q r)$, respectively, where $u(r) = r\psi(r)$. For the inner region $r < R$ the wave functions are given by $u_1(r) \sim \sin k_1 r$ and $u_2(r) \sim \sin(k_2 r)$. The relevant wavevectors are defined as: $k_P = \sqrt{mE_{\rm kin}}/\hbar$, $k_Q = \sqrt{m(\epsilon - E_{\rm kin})}/\hbar$, $k_1 = \sqrt{m(E_{\rm kin} + V_1)}/\hbar$, and $k_2 = \sqrt{m(E_{\rm kin} + V_2 - \epsilon)}/\hbar$.

This problem may now be solved by means of a basis rotation at the boundary R which gives rise to simple analytic expressions. The efficacy of this transformation may be understood by realizing that the effect of the potentials is to cause the wavefunction to accumulate a phase $\phi_1 = k_1 R$ and $\phi_2 = k_2 R$ at the boundary R. For $r > R$, we therefore consider one open channel and one closed channel with wavenumbers $k_P(E_{\rm kin})$ and $k_Q(E_{\rm kin}, \epsilon)$. $E_{\rm kin}$ is the relative kinetic energy of the two colliding particles in the center of mass frame and ϵ is the energy-difference of the two outer-range channels. In analogy with a real physical system, we can refer to the inner range channels as a molecular basis and the channel wave functions are just linear combinations of the u_1 and u_2 wave functions. The coupling strength is effectively given by the basis-rotation angle θ for the scattering wave functions:

$$\begin{pmatrix} u_P(R) \\ u_Q(R) \end{pmatrix} = \begin{pmatrix} \cos\theta & \sin\theta \\ -\sin\theta & \cos\theta \end{pmatrix} \begin{pmatrix} u_1(R) \\ u_2(R) \end{pmatrix}, \tag{2.28}$$

allowing for an analytic solution of the scattering model. This leads to the following expression for the S-matrix:

$$\mathcal{S} = e^{-2ik_P R}[1 - (-2ik_P(k_2 \cot\phi_2 \cos^2\theta + k_Q + k_1 \cot\phi_1 \sin^2\theta)/ \tag{2.29}$$

$$(k_P k_Q + k_1 \cot\phi_1(k_P \sin^2\theta - k_Q \cos^2\theta) + ik_2 \cot\phi_2(k_1 \cot\phi_1 + k_P \cos^2\theta + k_Q \sin^2\theta)].$$

An extension to treat more than two coupled potentials, which would be required to model more than one resonance, is straightforward.

The parameters of the two wells have to be chosen such that the results of a real scattering calculation are reproduced. In fact, all the parameters are completely determined from the field dependence of the scattering length, and all other scattering properties can then be derived, such as the energy-dependence of the scattering phase shift. One way of selecting these parameters is to first chose a range R, typically of the order of an interatomic potential range (100 a_0) or less. Now we have only to determine the set of parameters V_1, V_2, and θ. The potential depth V_1 is chosen such that the scattering length is equal to the background scattering length $a_{\rm bg}$ while keeping $\theta = 0$. Also, V_1 should be large enough that the wavenumber k_1 depends only weakly on the scattering energy. Then we set θ to be non-zero and change the detuning until a bound state crosses the collision threshold giving rise to a Feshbach resonance. The value of V_2 is more or less arbitrary, but we typically chose it to be larger than V_1. Finally, we change the value of θ to give the Feshbach resonance the desired width.

In Fig. 2.3 the coupled square-well system is compared with the Feshbach scattering theory for the scattering parameters of ^{40}K. Despite the fact that there is a strong energy-dependence of the T-matrix, the two scattering representations agree very well. We will later show that the resulting scattering properties converge for $R \to 0$.

2.5 Comparison with coupled channels calculation

In the last section we argued that the double-well system is in good agreement with Feshbach scattering theory. Now we will show how well both the Feshbach theory and the $R \to 0$ coupled square-well, or contact square-well, theory agree with the full coupled channels calculation [38]. In Fig. 2.4 we show the real and imaginary parts of the

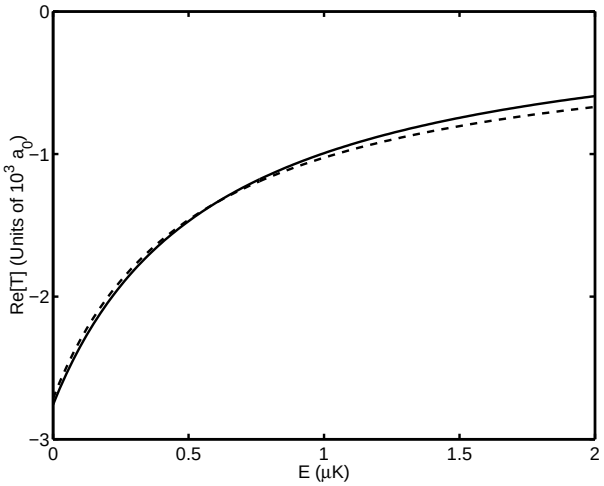

Figure 2.3: Comparison of coupled square-well scattering (solid line), with a potential range $R = 1a_0$, to Feshbach scattering (dashed line) for a detuning that yields a scattering length of about -2750 a_0. Similar agreement is found for all detunings.

T-matrix applied to the case of ^{6}Li and compare the contact square well and Feshbach scattering representations to a full coupled channels calculation. The agreement is surprisingly good and holds for all magnetic fields (i.e., similar agreement is found at all detunings).

In this section we have discovered the remarkable fact that even a complex system, including internal structure and resonances, can be described with contact potentials and a few coupling parameters. This was trivially known for off resonance scattering where only a single parameter, the scattering length, is required to encapsulate the collision physics. However, this has not be pointed out before for the resonance system where an analogous parameter set is required to describe a system with a scattering length that may pass through infinity!

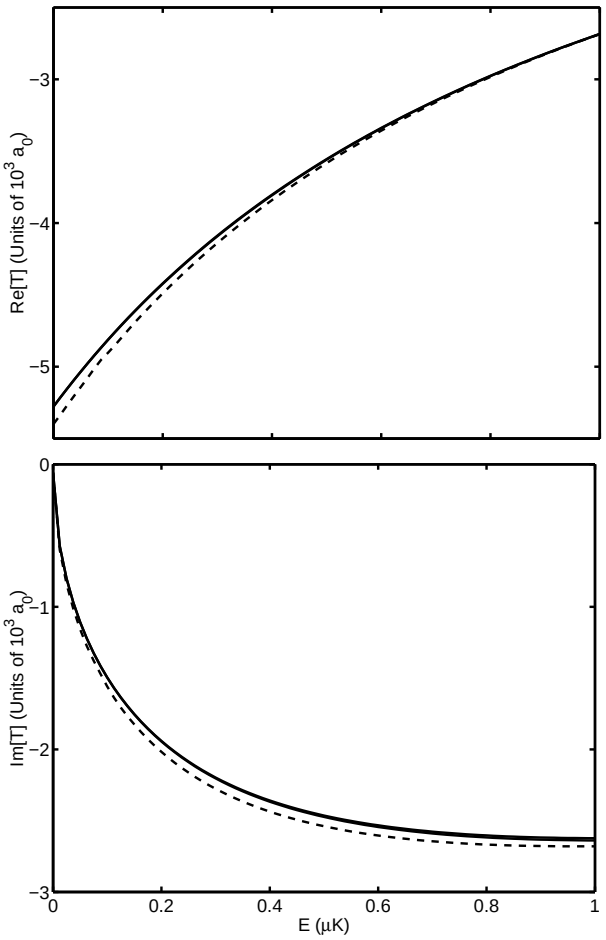

Figure 2.4: Real (top) and imaginary (bottom) part of the T-matrix , as a function of collision energy, for the Feshbach model and the contact square-well model (overlapping solid lines), and for a coupled channels calculation (dashed line). The atomic species considered is ^{6}Li, for atoms colliding in the $(f, m_f) = (1/2, -1/2)$ and $(1/2, 1/2)$ channel near 800G.

2.6 Pseudo-potential scattering and renormalization

In forming a field theory to describe Feshbach resonant interactions we would prefer not to work with the complete interatomic potentials since they contain much more information than is actually needed and severely complicate the problem. Rather, we would like to work with a suitable set of pseudo-potentials that incorporate all the relevant scattering physics. As we have shown in the previous sections, a pair of coupled square wells may be accurately used to describe a Feshbach resonance. However, we had to adjust the various parameters, such as the depth and coupling of the wells, in order to produce the desired resonance. A correct field theoretic description of a resonant system must, similarly, adjust the pseudo-potentials. This adjustment procedure is termed "renormalization" and connects the pseudo-potential parameters in the field theory to the physical parameters describing the resonance. What's more, if contact potentials are incorporated in the many-body theory, which is often done out of initial convenience, the renormalization works to remove divergences that will naturally arise due to the singularity of such a potential. To show how one properly renormalizes a Feshbach resonant field theory, we must first take a closer look at the underlying two-body physics.

We begin by solving the Lippmann-Schwinger scattering equation for a Feshbach resonance system. Our goal will be to derive explicit expressions which match the two-body scattering parameters describing the Feshbach resonance $(\bar{U}, \bar{g}_i, \bar{\nu}_i)$ to the model potential parameters (U, g, ν) entered into our field theory. The first step is to solve the scattering Eqs. (2.26) and (2.27) for these pseudo-potentials. As we have seen, we can formally solve the bound-state equations and make use of Eq. (2.9) to expand the Green's function in bound-state solutions. In this case we may write

$$\psi^Q(\mathbf{r}) = \sum_i \frac{\phi_i^Q(\mathbf{r}) \int d^3r' \phi_i^{Q*}(\mathbf{r}') g^*(\mathbf{r}') \psi^P(\mathbf{r}')}{E^+ - \epsilon_i}, \tag{2.30}$$

with $\phi_i^Q(\mathbf{r})$ a bound state wavevector and ϵ_i its eigenenergy. For the purposes of this

section we will only consider a single resonance potential so will henceforth drop the i subscript. We now define an amplitude for the system to be in the bound state $\phi = \langle \phi^Q | \psi^Q \rangle$. This definition will later prove useful in the mean-field equations. Together with the open channel equation and the definition $g(\mathbf{r}) = g(\mathbf{r})\phi^Q(\mathbf{r})$ we get a new set of scattering equations

$$\frac{\hbar^2 \mathbf{k}^2}{m}\psi(\mathbf{r}) = \left(-\frac{\hbar^2}{m}\nabla^2 + V(\mathbf{r})\right)\psi(\mathbf{r}) + g(\mathbf{r})\phi \tag{2.31}$$

$$\frac{\hbar^2 \mathbf{k}^2}{m}\phi = \nu\phi + \int d^3r' g(\mathbf{r}')\psi(\mathbf{r}'), \tag{2.32}$$

where we have dropped the P superscripts. A formal solution for $\psi(\mathbf{r})$ may be given by the following relation:

$$\psi(\mathbf{r}) = \chi(\mathbf{r}) - \frac{m}{4\pi\hbar^2}\int d^3r' \frac{e^{i|\mathbf{k}||\mathbf{r}-\mathbf{r}'|}}{|\mathbf{r}-\mathbf{r}'|}\left[V(\mathbf{r}')\psi(\mathbf{r}') + g(\mathbf{r}')\phi\right], \tag{2.33}$$

where $\chi(\mathbf{r})$ represents the unscattered component. The scattering amplitude $f(\theta)$ is defined in the limit $r \to \infty$ of the wavefunction by the relation

$$\psi(\mathbf{r}) = \chi(\mathbf{r}) + f(\theta)\frac{e^{ikr}}{r}. \tag{2.34}$$

By taking the $r \to \infty$ limit of Eq. (2.33) we have an asymptotic form for the full scattered wavefunction

$$\psi(\mathbf{r}) = \chi(\mathbf{r}) - \frac{m}{4\pi\hbar^2}\frac{e^{ikr}}{r}\int d^3r' e^{-i\mathbf{k}\cdot\mathbf{r}'}\left[V(\mathbf{r}')\psi(\mathbf{r}') + g(\mathbf{r}')\phi\right]. \tag{2.35}$$

A comparison of Eq. (2.35) to Eq. (2.34) gives the following form for the scattering amplitude:

$$f(\theta) = -\frac{m}{4\pi\hbar^2}\int d^3r' e^{-i\mathbf{k}\cdot\mathbf{r}'}\left[V(\mathbf{r}')\psi(\mathbf{r}') + g(\mathbf{r}')\phi\right]. \tag{2.36}$$

In Fourier space this becomes

$$f(\mathbf{k},\mathbf{k}') = -\frac{m}{4\pi\hbar^2}\left[\int \frac{d^3p}{(2\pi)^3}\left(V(\mathbf{k}'-\mathbf{p})\psi(\mathbf{p})\right) + g(\mathbf{k}')\phi\right]. \tag{2.37}$$

With the aid of the relationship $\mathcal{T}(\mathbf{k},\mathbf{p}) = -(4\pi\hbar^2/m)f(\mathbf{k},\mathbf{p})$, linking the T-matrix to the scattering amplitude, we may write the Fourier representation of the open channel wavefunction as

$$\psi(\mathbf{p}) = (2\pi)^3\delta(\mathbf{k}-\mathbf{p}) + \frac{\mathcal{T}(\mathbf{k},\mathbf{p})}{\frac{\hbar^2\mathbf{k}^2}{m} - \frac{\hbar^2\mathbf{p}^2}{m} + I\delta}. \tag{2.38}$$

Substituting this result into Eq. (2.37) yields

$$\mathcal{T}(\mathbf{k},\mathbf{k}') = V(\mathbf{k}'-\mathbf{k}) + \int \frac{d^3p}{(2\pi)^3}\frac{U(\mathbf{k}'-\mathbf{p})\mathcal{T}(\mathbf{k},\mathbf{p})}{\frac{\hbar^2\mathbf{k}^2}{m} - \frac{\hbar^2\mathbf{p}^2}{m} + I\delta} + g(\mathbf{k}')\phi. \tag{2.39}$$

By rewriting the original closed channel scattering equation, Eq. (2.27), as

$$\phi = \frac{1}{\frac{\hbar^2\mathbf{k}^2}{m} - \nu}\int \frac{d^3p}{(2\pi)^3}\, g(\mathbf{p})\psi(\mathbf{p}), \tag{2.40}$$

we may eliminate ϕ from Eq. (2.39). This results in the following integral equation for the off the energy-shell T-matrix

$$\mathcal{T}(\mathbf{k},\mathbf{k}') = \left[U(\mathbf{k}'-\mathbf{k}) + \frac{g(\mathbf{k}')g(\mathbf{k})}{\frac{\hbar^2\mathbf{k}^2}{m} - \nu}\right] + \int \frac{d^3p}{(2\pi)^3}\left[\frac{\left(U(\mathbf{k}'-\mathbf{p}) + \frac{g(\mathbf{k}')g(\mathbf{p})}{\frac{\hbar^2\mathbf{k}^2}{m}-\nu}\right)\mathcal{T}(\mathbf{k},\mathbf{p})}{\frac{\hbar^2\mathbf{k}^2}{m} - \frac{\hbar^2\mathbf{p}^2}{m} + I\delta}\right]. \tag{2.41}$$

We now have a general integral equation for the T-matrix. However, to make use of this relationship we will need to make some simplifying assumptions. The first being the separability of the potential $U(k-k') = \lambda(k)\lambda(k')$. The second, that the T-matrix is basically constant over the range of the integral allowing us to pull it outside of the integral. This is another way of saying that the T-matrix only contributes on the energy-shell. Third, we will assume s-wave scattering so the wavenumbers $\mathbf{k} = \mathbf{k}'$. This results in the algebraic equation for the T-matrix:

$$\mathcal{T}(\mathbf{k}) = \left[\lambda(\mathbf{k})^2 + \frac{g(\mathbf{k})^2}{\frac{\hbar^2\mathbf{k}^2}{m} - \nu}\right] + \mathcal{T}(\mathbf{k})\int \frac{d^3p}{(2\pi)^3}\left[\frac{\left(\lambda(\mathbf{k})\lambda(\mathbf{p}) + \frac{g(\mathbf{k})g(\mathbf{p})}{\frac{\hbar^2\mathbf{k}^2}{m}-\nu}\right)}{\frac{\hbar^2\mathbf{k}^2}{m} - \frac{\hbar^2\mathbf{p}^2}{m} + I\delta}\right]. \tag{2.42}$$

The renormalization is performed by matching the potentials U, g and detuning ν to the physical potentials $\bar{U}, \bar{g}$ and the physical detuning $\bar{\nu}$ as given by the form of the Feshbach theory (Eqs. (2.20) and (2.25)). Results for several types of model pseudo-potentials are given in Appendix. A.

Chapter 3

Collapsing condensates and atomic bursts

3.1 Outlook

Having thoroughly discussed the two-body physics underlying Feshbach resonant interactions, we are now in a position to apply these ideas to a many-body system. We begin, in this chapter, by discussing the formalism for Bosons and apply it to a particularly novel experiment. In the next chapter we will expand upon this formalism to account for Fermions.

3.2 The "Bosenova" problem in collapsing condensates

The ability to dynamically modify the nature of the microscopic interactions in a Bose-Einstein condensate—an ability virtually unique to the field of dilute gases—opens the way to the exploration of a range of fundamental phenomena. A striking example of this is the "Bosenova" experiment carried out in the Wieman group at JILA [39] which explored the mechanical collapse instability arising from an attractive interaction. This collapse resulted in an unanticipated burst of atoms, the nature of which is a subject of current debate.

The Bosenova experiment, conducted by the JILA group, consisted of the following elements. A conventional, stable Bose-Einstein condensate was created in equilibrium. The group then used a Feshbach resonance to abruptly switch the interactions to be attractive inducing an implosion. One might have predicted that the rapid in-

crease in density would simply lead to a rapid loss of atoms, primarily through inelastic three-body collisions. In contrast, what was observed was the formation of an energetic burst of atoms emerging from the center of the implosion. Although the energy of these atoms was much larger than that of the condensate, the energy was insignificant when compared to the molecular binding energy which characterizes the energy released in a three-body collision. In the end, what remained was a remnant condensate which appeared distorted and was believed to be in a highly excited collective state.

One theoretical method which has been extensively explored to explain this behavior has been the inclusion of a decay term into the Gross-Pitaevskii equation as a way to account for the atom loss [40, 41, 42, 43]. Aside from its physical application to the Bosenova problem, the inclusion of three-body loss as a phenomenological mechanism represents an important mathematical problem, since the nonlinear Gross-Pitaevskii equation allows for a class of self-similar solutions in the unstable regime. The local collapses predicted in this framework can generate an outflow even within this zero temperature theory. However, there are a number of aspects which one should consider when applying the extended Gross-Pitaevskii equation to account for the observations made in the JILA experiment.

The first problematic issue is the potential breakdown of the principle of attenuation of correlations. This concept is essential in any quantum or classical kinetic theory as it allows multi-particle correlations to be factorized. The assumption of attenuation of correlations is especially evident in the derivation of the Gross-Pitaevskii equation where all explicit multi-particle correlations are dropped. Furthermore, there is considerable evidence for this instability toward pair formation in the mechanically unstable quantum theory [44].

A second difficulty with motivating the Gross-Pitaevskii approach is that, by this method, one describes the energy-dependent interactions through a single parameter, the scattering length, which is determined from the s-wave scattering phase shift at

zero scattering energy. Near a Feshbach resonance, as we have seen in Chapter 1, the proximity of a bound state in a closed potential to the zero of the scattering continuum can lead to a strong energy dependence of the scattering. Exactly on resonance, the s-wave scattering length passes through infinity and, in this situation, the Gross-Pitaevskii equation is undefined.

These two fundamental difficulties with the Gross-Pitaevskii approach led us to reconsider the Bosenova problem [45]. We were motivated by the fact that the same experimental group at JILA recently performed a complementary experiment [19]– the, so called, molecular Ramsey fringe experiment. Their results provided significant insight into this problem. What was remarkable in these new experiments was that, even with a large positive scattering length, in which the interactions were repulsive, a burst of atoms and a remnant condensate were observed. Furthermore, in the large positive scattering length case, simple effective field theories, which included an explicit description of the Feshbach resonance physics, were able to provide an accurate quantitative comparison with the data [46, 47, 48]. The theory showed the burst to arise from the complex dynamics of the atom condensate which was coupled to a coherent field of exotic molecular dimers of a remarkable physical size and near the threshold binding energy.

In this Chapter, based on the work of [45], we draw connections between the two JILA experiments. We pose and resolve the question as to whether the burst of atoms in the Bosenova collapse could arise in a similar way as in the Ramsey fringe experiment—from the formation of a coherent molecular superfluid. This hypothesis is tested by applying an effective field theory for resonance superfluidity to the collapse. For fermions, the case of resonance superfluidity in an inhomogeneous system has been treated in the local density approximation using, essentially, the uniform solution at each point in space [49]. For the collapse of a Bose-Einstein condensate, as we wish to treat here, the local density approximation is not valid and the calculation must be

performed on a truly inhomogeneous system.

3.3 Development of an effective field theory for bosons

In the Feshbach resonance illustrated in Figure 1.1, the properties of the collision of two ground state atoms is controlled through their resonant coupling to a bound state in a closed channel Born-Oppenheimer potential. By adjusting an external magnetic field, the scattering length can be tuned to have any value. This field dependence of the scattering length is characterized by the detuning $\bar{\nu}$ and obeys a dispersive profile given by $a(\bar{\nu}) = a_{\rm bg}(1 - \kappa/(2\bar{\nu}))$, with κ the resonance width and $a_{\rm bg}$ the background scattering length. In fact, as described in Chapter 2.1, all the scattering properties of a Feshbach resonance system are completely characterized by just three parameters $\bar{U} = 4\pi\hbar^2 a_{\rm bg}/m$, $\bar{g} = \sqrt{\kappa \bar{U}}$, and $\bar{\nu}$. Physically, $\bar{U}$ represents the energy shift per unit density on the single particle eigenvalues due to the background scattering processes, while $\bar{g}$, which has dimensions of energy per square-root density, represents the coupling of the Feshbach resonance between the open and closed channel potentials.

We now proceed to construct a low order many-body theory which includes this resonance physics. The Hamiltonian for a dilute gas of scalar bosons with binary interactions is given in complete generality by

$$H = \int d^3x \; \psi_a^\dagger(\mathbf{x}) H_a(\mathbf{x}) \psi_a(\mathbf{x}) + \frac{1}{2} \int d^3x d^3x' \; \psi_a^\dagger(\mathbf{x}) \psi_a^\dagger(\mathbf{x}') U(\mathbf{x}, \mathbf{x}') \psi_a(\mathbf{x}') \psi_a(\mathbf{x}), \quad (3.1)$$

where $H_a(\mathbf{x})$ is the single particle Hamiltonian, $U(\mathbf{x}, \mathbf{x}')$ is the binary interaction potential, and $\psi_a(\mathbf{x})$ is a bosonic scalar field operator. In cold quantum gases, where the atoms collide at very low energy, we are only interested in the behavior of the scattering about a small energy range above zero. There exist many potentials which replicate the low energy scattering behavior of the true potential; therefore, it is convenient to carry out the calculation with the simplest one, the most convenient choice being to take the interaction potential as a delta-function pseudo-potential when possible.

For a Feshbach resonance, this choice of pseudo-potential is generally not available since the energy dependence of the scattering implies that a minimal treatment must at least contain a spread of wave-numbers which is equivalent to the requirement of a non-local potential. Since the solution of a nonlocal field theory is inconvenient, we take an alternative, but equivalent, approach. We include into the theory an auxiliary molecular field operator $\psi_m(\mathbf{x})$ which obeys Bose statistics and describes the collision between atoms in terms of two elementary components: i.) the background collisions between atoms in the absence of the resonance interactions and ii.) the conversion of atom pairs into tightly bound, molecular states. This allows us to construct a local field theory with the property that when this auxiliary field is integrated out, an effective Hamiltonian of the form given in Eq. (3.1) is recovered with a potential $V(\mathbf{x},\mathbf{x}') = V(|\mathbf{x}-\mathbf{x}'|)$ which generates the form of the two-body T-matrix predicted by Feshbach resonance theory (Eq. (2.20) with (2.25)). The local Hamiltonian which generates this scattering behavior is:

$$\begin{aligned} H &= \int d^3x\ \psi_a^\dagger(\mathbf{x}) H_a(x) \psi_a(\mathbf{x}) + \int d^3x\ \psi_m^\dagger(\mathbf{x}) H_m(x) \psi_m(\mathbf{x}) \\ &+ \frac{1}{2}\int d^3x d^3x'\ \psi_a^\dagger(\mathbf{x})\psi_a^\dagger(\mathbf{x}')U(\mathbf{x}-\mathbf{x}')\psi_a(\mathbf{x})\psi_a(\mathbf{x}) \\ &+ \frac{1}{2}\int d^3x d^3x'\ \left(\psi_m^\dagger(\frac{\mathbf{x}+\mathbf{x}'}{2})g(\mathbf{x}-\mathbf{x}')\psi_a(\mathbf{x})\psi_a(\mathbf{x}') + \text{h.c.}\right). \end{aligned} \tag{3.2}$$

Equation (3.2) has the intuitive structure of resonant atom-molecule coupling [50, 51] and was motivated by bosonic models of superfluidity [52, 53]. Here we have defined the free atomic dispersion $H_a(x) = -\frac{\hbar^2}{2m}\nabla_x^2 + V_a(\mathbf{x}) - \mu_a$ and the free molecular dispersion $H_m(x) = -\frac{\hbar^2}{4m}\nabla_x^2 + V_m(\mathbf{x}) - \mu_m$. $V_{a,m}$ are the external potentials and $\mu_{a,m}$ are the chemical potentials (the subscripts a, m represent the atomic and molecular contributions, respectively). The Feshbach resonance is controlled by the magnetic field which is incorporated into the theory by the detuning $\nu = \mu_m - 2\mu_a$ between the atomic and molecular fields.

The field operators which we have introduced $\psi_a^\dagger(\mathbf{x}), \psi_a(\mathbf{x})$ create and destroy

atoms at point $\mathbf{x}$ and $\psi_m^\dagger(\mathbf{x}), \psi_m(\mathbf{x})$ create and destroy molecules at point $\mathbf{x}$. For the bosonic gas, both sets of these operators obey Bose commutation relations:

$$\begin{aligned} \left[\psi_a(\mathbf{x}), \psi_a^\dagger(\mathbf{x}')\right] &= \delta^3(\mathbf{x}-\mathbf{x}') \\ \left[\psi_m(\mathbf{x}), \psi_m^\dagger(\mathbf{x}')\right] &= \delta^3(\mathbf{x}-\mathbf{x}'), \end{aligned} \tag{3.3}$$

and we assume that the fields ψ_a and ψ_m commute. It is important to keep in mind that the parameters introduced in the field theory are distinct from the physical parameters $\bar{U}$, $\bar{g}$, and $\bar{\nu}$ behind the resonance. In order for the local Hamiltonian given in Eq. (3.2) to be applicable, one must introduce into the field theory a renormalized set of parameters. Since we will be working with contact potentials, each will contain a momentum cutoff associated with a maximum wavenumber K_c. This need not be physical in origin but should exceed the momentum range of occupied quantum states. The relationships between the renormalized and physical parameters for the contact potentials are given in Appendix A.1 . Of course, all of our final results must be independent of this artificial cutoff; a condition which has been checked for all the results we will present.

To begin our development of a resonant field theory, we define the atomic and molecular condensates in terms of the mean-fields of their respective operators

$$\phi_a(\mathbf{x}) = \langle \psi_a(\mathbf{x}) \rangle \quad \text{and} \quad \phi_m(\mathbf{x}) = \langle \psi_m(\mathbf{x}) \rangle. \tag{3.4}$$

The remainder is associated with the fluctuations about these mean-fields and can likewise be defined:

$$\chi_a(\mathbf{x}) = \psi_a(\mathbf{x}) - \phi_a(\mathbf{x}) \quad \text{and} \quad \chi_m(\mathbf{x}) = \psi_m(\mathbf{x}) - \phi_m(\mathbf{x}). \tag{3.5}$$

Assuming the occupation of $\phi_m(\mathbf{x})$ to be small (less than 2% in the simulations we present), we drop higher-order terms arising from fluctuations about this mean-field which do not give a significant correction to our results.

Starting from Heisenberg's equation of motion

$$i\frac{\partial}{\partial t} A(\mathbf{x}, t) = [A(\mathbf{x}, t), H(\mathbf{x}', t')], \tag{3.6}$$

we may derive a hierarchy of time dependent equations for the various fields involved within our problem, each coupling to higher-order correlations. To truncate this hierarchy, we work within Hartree-Fock-Bogoliubov (HFB) theory. The simplification which this introduces into the problem is that it allows us to factorize terms to quadratic order in the field operators. Another way to say this is that we only account for correlations between pairs of fields, but neglect all higher-order correlations. For example, we use Wick's theorem to factorize a four-point interaction as:

$$\begin{aligned}\langle A(\mathbf{x}_1)A(\mathbf{x}_2)A(\mathbf{x}_3)A(\mathbf{x}_4)\rangle &= \langle A(\mathbf{x}_1)A(\mathbf{x}_2)\rangle\langle A(\mathbf{x}_3)A(\mathbf{x}_4)\rangle \\ &+ \langle A(\mathbf{x}_1)A(\mathbf{x}_3)\rangle\langle A(\mathbf{x}_2)A(\mathbf{x}_4)\rangle + \langle A(\mathbf{x}_1)A(\mathbf{x}_4)\rangle\langle A(\mathbf{x}_2)A(\mathbf{x}_3)\rangle.\end{aligned} \tag{3.7}$$

Under this set of approximations we derive four equations: two corresponding to a Schrödinger evolution of the mean fields

$$\begin{aligned}i\hbar\frac{d\phi_a(\mathbf{x})}{dt} &= \Big(-\frac{\hbar^2}{2m}\nabla^2_{\mathbf{x}} + V_a(\mathbf{x}) - \mu_a + U[|\phi_a(\mathbf{x})|^2 + 2G_N(\mathbf{x},\mathbf{x})]\Big)\phi_a(\mathbf{x}) \\ &+ [UG_A(\mathbf{x},\mathbf{x}) + g\phi_m(\mathbf{x})]\phi^*_a(\mathbf{x}),\end{aligned} \tag{3.8}$$

$$i\hbar\frac{d\phi_m(\mathbf{x})}{dt} = \Big(-\frac{\hbar^2}{4m}\nabla^2_{\mathbf{x}} + V_m(\mathbf{x}) - \mu_m\Big)\phi_m(\mathbf{x}) + \frac{g}{2}[\phi^2_a(\mathbf{x}) + G_A(\mathbf{x},\mathbf{x})], \tag{3.9}$$

and two corresponding to the Louiville space evolution of the normal density $G_N(\mathbf{x},\mathbf{x}') = \langle\chi^\dagger_a(\mathbf{x}')\chi_a(\mathbf{x})\rangle$ and of the anomalous density $G_A(\mathbf{x},\mathbf{x}') = \langle\chi_a(\mathbf{x}')\chi_a(\mathbf{x})\rangle$. The time evolution of the densities may be expressed in the compact form [54]

$$i\hbar\frac{\partial\mathcal{G}}{dt} = \Sigma\mathcal{G} - \mathcal{G}\Sigma^\dagger, \tag{3.10}$$

where the density matrix and self-energy matrix are defined respectively as

$$\mathcal{G}(\mathbf{x},\mathbf{x}') = \begin{pmatrix} \langle\chi^\dagger_a(\mathbf{x}')\chi_a(\mathbf{x})\rangle & \langle\chi_a(\mathbf{x}')\chi_a(\mathbf{x})\rangle \\ \langle\chi^\dagger_a(\mathbf{x}')\chi^\dagger_a(\mathbf{x})\rangle & \langle\chi_a(\mathbf{x}')\chi^\dagger_a(\mathbf{x})\rangle \end{pmatrix}, \tag{3.11}$$

and

$$\Sigma(\mathbf{x},\mathbf{x}') = \begin{pmatrix} H(\mathbf{x},\mathbf{x}') & \Delta(\mathbf{x},\mathbf{x}') \\ -\Delta^*(\mathbf{x},\mathbf{x}') & -H^*(\mathbf{x},\mathbf{x}') \end{pmatrix}. \tag{3.12}$$

The convenience of choosing a microscopic model in which the potential couplings are of contact form is now evident since the elements of the self-energy matrix Σ are diagonal in $\mathbf{x}$ and $\mathbf{x}'$ with non-zero elements

$$\begin{aligned} H(\mathbf{x},\mathbf{x}) &= -\frac{\hbar^2}{2m}\nabla_x^2 + V_a(\mathbf{x}) - \mu_a + 2U[|\phi_a(\mathbf{x})|^2 + G_N(\mathbf{x},\mathbf{x})], \\ \Delta(\mathbf{x},\mathbf{x}) &= U[\phi_a^2(\mathbf{x}) + G_A(\mathbf{x},\mathbf{x})] + g\phi_m(\mathbf{x}). \end{aligned} \tag{3.13}$$

3.4 Application to a spherical trap geometry

Equations (3.8), (3.9), and (3.10) form a closed set of equations for the inhomogeneous system. However, since the normal density and anomalous pairing field are both six-dimensional objects, it is very difficult to solve these equations in an arbitrary geometry. For this reason, we consider the case of greatest symmetry consisting of a spherical trap. Here we can reduce the problem to one of only three dimensions according to the following procedure. To begin, it is convenient to write the elements of the single particle density matrix in center of mass and relative coordinates:

$$\mathbf{R} = \tfrac{\mathbf{x}+\mathbf{x}'}{2} \quad \text{and} \quad \mathbf{r} = \mathbf{x} - \mathbf{x}'. \tag{3.14}$$

The normal density then takes on a familiar structure corresponding to the Wigner distribution [55]

$$\begin{aligned} G_N(\mathbf{R},\mathbf{k}) &= \int d^3r\, \langle \chi_a^\dagger(\mathbf{R}-\mathbf{r}/2)\chi_a(\mathbf{R}+\mathbf{r}/2)\rangle e^{-i\mathbf{k}\cdot\mathbf{r}} \\ &= \int d^3r\, G_N(\mathbf{R},\mathbf{r}) e^{-i\mathbf{k}\cdot\mathbf{r}}, \end{aligned} \tag{3.15}$$

which, in the high-temperature limit, will map to the particle distribution function $f(\mathbf{R},\mathbf{k})$ for a classical gas. Correspondingly, the anomalous density can be written in Fourier space as

$$\begin{aligned} G_A(\mathbf{R},\mathbf{k}) &= \int d^3r\, \langle \chi_a(\mathbf{R}-\mathbf{r}/2)\chi_a(\mathbf{R}+\mathbf{r}/2)\rangle e^{-i\mathbf{k}\cdot\mathbf{r}} \\ &= \int d^3r\, G_A(\mathbf{R},\mathbf{r}) e^{-i\mathbf{k}\cdot\mathbf{r}}. \end{aligned} \tag{3.16}$$

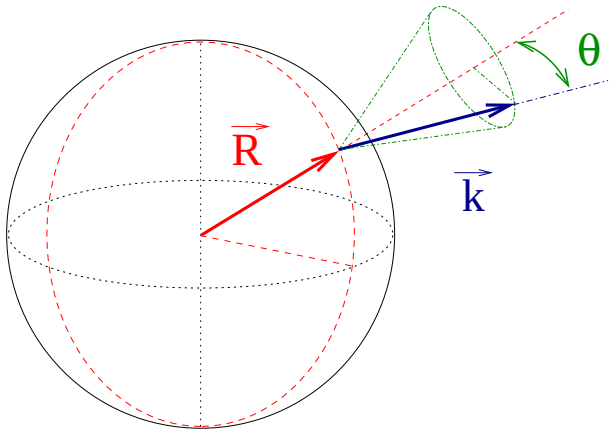

Figure 3.1: Illustration of the spherically symmetric geometry used as defined by the center of mass vector $\vec{R}$, relative momentum vector $\vec{k}$, and the angle θ between them.

In this geometry, the angular dependence of the center of mass vector $\mathbf{R}$ is irrelevant, and the cylindrical symmetry about $\mathbf{R}$ allows the wavevector $\mathbf{k}$ to be represented by its length and the one remaining angle as illustrated in Figure 3.1.

This simplification allows us to represent the density distributions in three-dimensions as

$$G(\mathbf{R}, \mathbf{k}) = G(R, k, \theta), \tag{3.17}$$

where G corresponds to either the normal (G_N) or anomalous (G_A) density. It is now straightforward to rewrite Eqs. (3.9) and (3.10) in this coordinate system. It is worth pointing out the simple structure of the kinetic energy contributions to Eq. (3.10) which, for the G_N and G_A components, take the corresponding forms, respectively:

$$\left(\nabla^2_{\mathbf{x}} - \nabla^2_{\mathbf{x}'}\right) G_N(\mathbf{x}, \mathbf{x}') = 2\left(\nabla_{\mathbf{R}} \cdot \nabla_{\mathbf{r}}\right) G_N(\mathbf{R}, \mathbf{r}) \tag{3.18}$$

$$\left(\nabla^2_{\mathbf{x}} + \nabla^2_{\mathbf{x}'}\right) G_A(\mathbf{x}, \mathbf{x}') = \left(\frac{1}{2}\nabla^2_{\mathbf{R}} + 2\nabla^2_{\mathbf{r}}\right) G_A(\mathbf{R}, \mathbf{r}). \tag{3.19}$$

One may now take the Fourier transform with respect to $\mathbf{r}$ as indicated by Eqs. (3.15) and (3.16), replacing $\nabla_{\mathbf{r}} \rightarrow i\mathbf{k}$. The gradient operator $\nabla_{\mathbf{R}}$ can be expressed in any representation, but it is most convenient to use spherical polar coordinates aligned with

the **k** direction vector

$$\nabla_{\mathbf{R}} = \hat{R}\frac{\partial}{\partial R} + \hat{\theta}\frac{1}{R}\frac{\partial}{\partial \theta} + \hat{\varphi}\frac{1}{\sin\theta}\frac{\partial}{\partial \varphi}, \tag{3.20}$$

where φ is the azimuthal angle about **k** (which will eventually drop out in our chosen symmetry), and $(\hat{R}, \hat{\theta}, \hat{\varphi})$ are the spherical unit vectors in the R, θ, and φ directions. Noting that $\hat{R} \cdot \mathbf{k} = k\cos\theta$, $\hat{\theta} \cdot \mathbf{k} = -k\sin\theta$, and $\hat{\varphi} \cdot \mathbf{k} = 0$, we arrive at the following expression for the differential operator in Eq. (3.18):

$$\nabla_{\mathbf{R}} \cdot \mathbf{k} = k\left(\cos\theta\frac{\partial}{\partial R} - \frac{\sin\theta}{R}\frac{\partial}{\partial \theta}\right). \tag{3.21}$$

Furthermore, the spherical Laplacian for a system with no azimuthal dependence, as required in Eq. (3.19), is given by

$$\nabla^2_{\mathbf{R}} = \frac{1}{R^2}\frac{\partial}{\partial R}\Big(R^2\frac{\partial}{\partial R}\Big) + \frac{1}{R^2\sin\theta}\frac{\partial}{\partial \theta}\Big(\sin\theta\frac{\partial}{\partial \theta}\Big). \tag{3.22}$$

In practice, we expand the θ dependence of G_N and G_A in terms of the orthogonal Legendre polynomials and the angular derivatives are then easily implemented via the usual recursion relations.

3.5 Numerical results and analysis

As an initial test, we expect the resonance theory to give a similar prediction to the Gross-Pitaevskii equation in the initial phase of the collapse, when the quantum depletion is small. Figure 3.2 shows a direct comparison between the Gross-Pitaevskii approach and the resonance theory. The same initial conditions were used for all our simulations: 1000 rubidium-85 atoms in the ground state of a 10 Hz harmonic trap. For all the images we present, the results of the three-dimensional calculation, in our spherical geometry, are illustrated as a two-dimensional slice through the trap center. In the Gross-Pitaevskii solution we used a scattering length of $-200\,a_0$, where a_0 is the Bohr radius. For comparison, the Feshbach resonance theory uses a positive background

scattering length of $50\,a_0$ and a resonance width and detuning , respectively, of 15 kHz and 2.8 kHz. These parameters give the same effective scattering length as the one used in the Gross-Pitaevskii evolution, but nowhere in the resonance theory does the effective scattering length appear explicitly. As is evident, there is no noticeable discrepancy between the two approaches over this short timescale. Eventually, we expect these theories to diverge significantly as the density increases and the coupling between the atomic and molecular degrees of freedom become stronger. However, at this stage, the agreement is a demonstration that our renormalized theory correctly allows us to tune the interactions in an inhomogeneous situation.

We now proceed to a more complex situation in which the timescales for the atom-molecule coupling and the collapse dynamics are more compatible. From a numerical point of view, it becomes convenient to increase the resonance width to 1.5 MHz and the detuning to 14 kHz so that the effect of the atom-molecule coupling will appear in the first stage of the collapse. This allows us to form a complete picture of the dynamics involving the atomic collapse and the simultaneous coupling to a coherent molecular field. The numerical calculation is shown in Fig. 3.3 for both the condensed and non-condensed components. We see the formation of a significant fraction of non-condensed atoms–a feature not described within the Gross-Pitaevskii framework. During a time evolution of 0.8 ms the condensate fraction falls to approximately 80% of its initial value while the non-condensate fraction reaches a peak at around 20%. The amplitude of the scalar field ϕ_m remains below the 2% level at all times.

To better illustrate the behavior of the atoms during the collapse, we present the flow of the different distributions involved. The condensate velocity field is shown in Fig. 3.4. It exhibits similar characteristics to those predicted by the Gross-Pitaevskii theory, which, without loss, predicts that the condensed atoms will always accelerate toward the trap center. In contrast, the velocity field of the atoms outside of the condensate is radially outward.

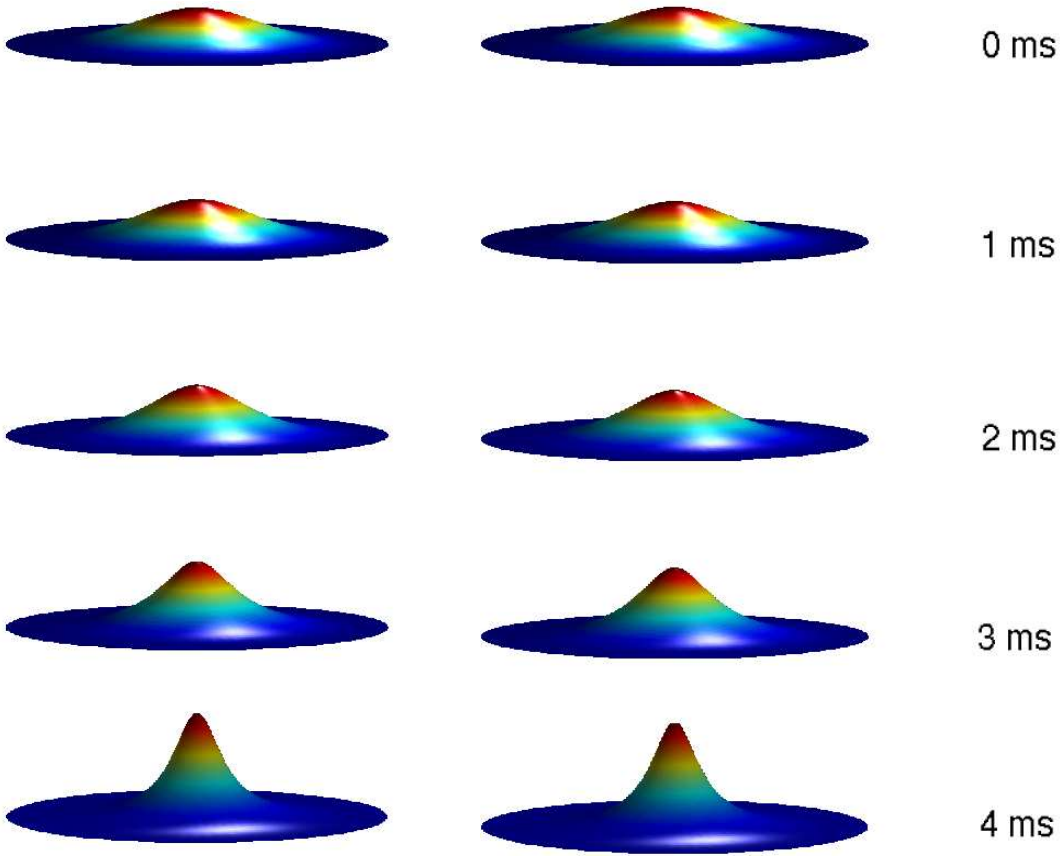

Figure 3.2: A direct comparison of the collapse between the Gross-Pitaevskii (left) and the resonance approach (right) within the regime of applicability of the Gross-Pitaevskii equation. Each horizontal pair is at the same time step with time increasing from top to bottom. As expected, we observe no appreciable difference between the two methods.

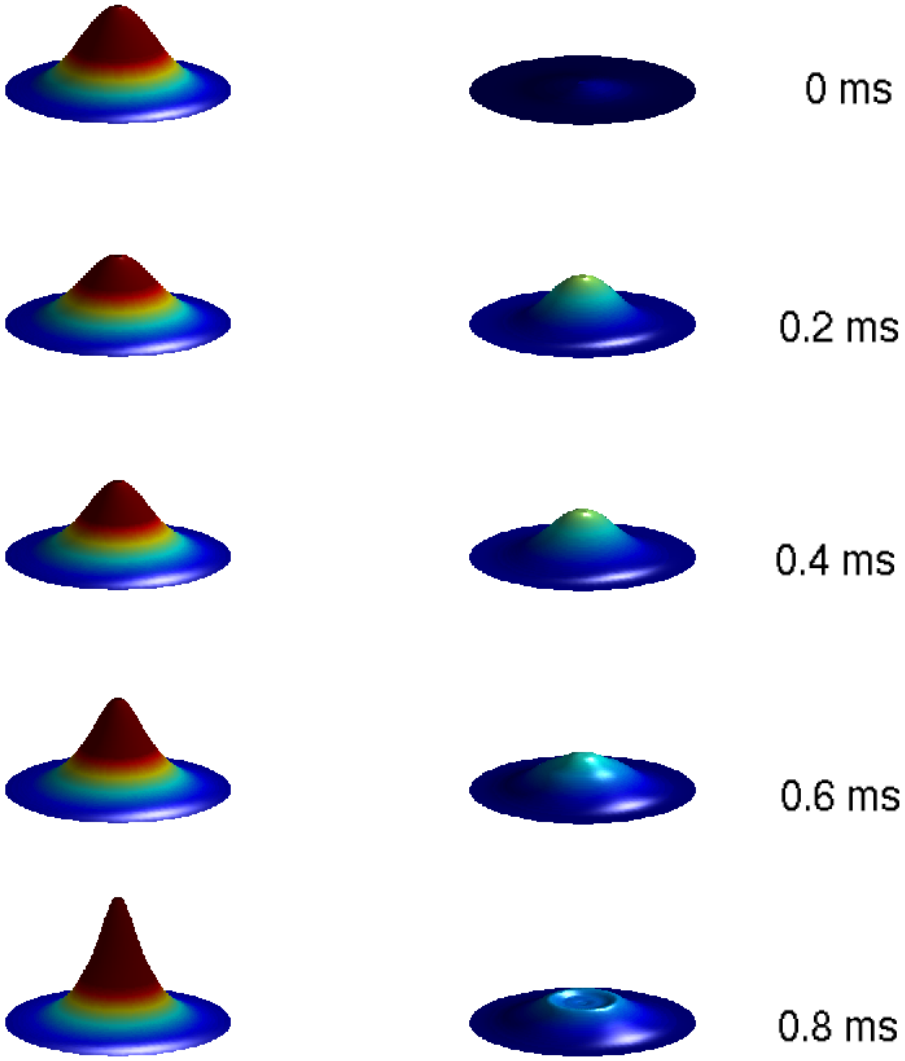

Figure 3.3: The simulation of the collapse in the resonance theory showing the time evolution of the condensed fraction $\phi_a(\mathbf{x})$ (left) and noncondensed fraction $G_N(\mathbf{x},\mathbf{x})$ (right). Each horizontal pair is taken at the same instant of time with time increasing from top to bottom. It is evident that noncondensate atoms are produced during the collapse forming rings which propagate from the center of the cloud outward.

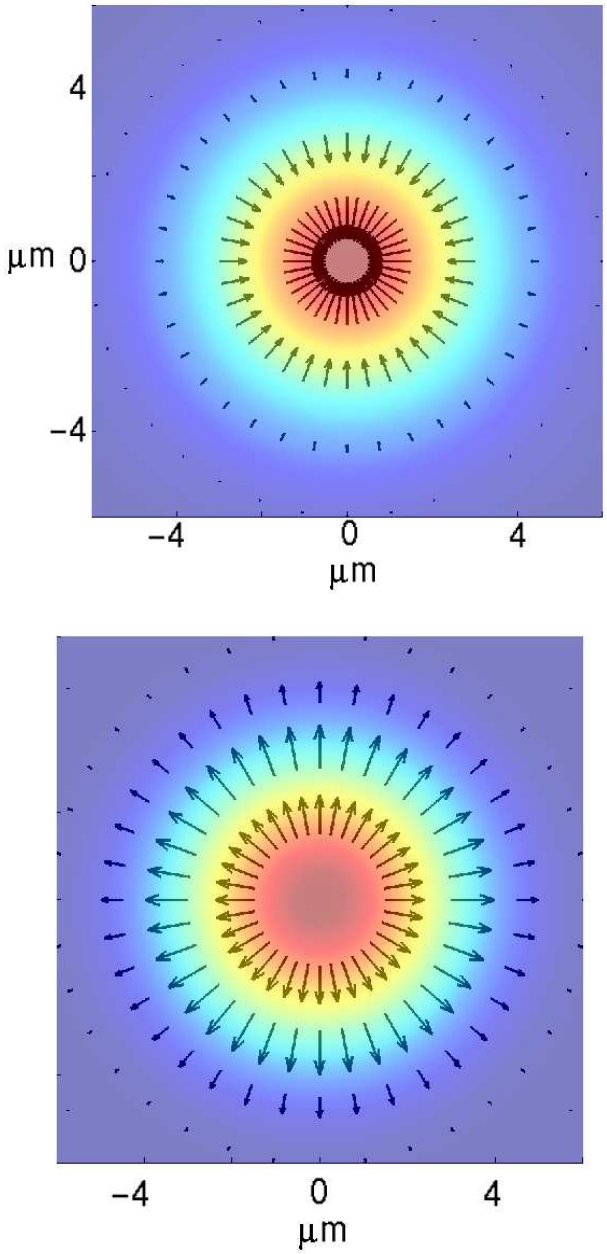

Figure 3.4: The velocity fields for the condensate component $\phi_a(\mathbf{x})$ (top) and the non-condensed component $G_N(\mathbf{x}, \mathbf{x})$ (bottom) midway through the simulation (0.4 ms). The color contours indicate the densities and the velocity fields are represented in direction and strength by the arrows. This clearly shows that in the resonance theory, as the condensate collapses inward, the non-condensate atoms that are generated flow outward.

An important quantity to calculate for these expanding non-condensed atoms is the effective temperature, or energy per particle, since this quantity is observed experimentally. This is illustrated in Fig. 3.5 where we show, superimposed on an illustration of the density, a colormap of the temperature. The hottest atoms generated in the center of the cloud are of comparable energy scale to those seen in the experiment, being on the order of 100 nK.

3.6 Conclusion

These numerical simulations illustrate the feasibility of generating atomic bursts purely through a coupling between an atomic and molecular component. However, there are a number of important distinctions with the experimental situation which would have to be accounted for before making a direct comparison. These simulations contain no inelastic three-body loss and particle number is absolutely conserved. In reality, three-body loss may be important to the experiment, but we suggest with this work that three-body loss is not the only mechanism for producing a non-condensed burst during the collapse.

It should be emphasized that, if our hypothesis for the burst generation is correct, the non-condensate atoms that are produced by this mechanism are not simply generated in a thermal component, but are instead generated in a fundamentally intriguing quantum state. The process of dissociation of molecules into atom pairs produces macroscopic correlations reminiscent of a squeezed vacuum state in quantum optics. This means that every atom in the burst with momentum $\mathbf{k}$ would have an associated partner with momentum $-\mathbf{k}$. In principle, the correlations could be directly observed in experiments through coincidence measurements providing clear evidence as to whether this is the dominant mechanism for the burst generation in the Bosenova.

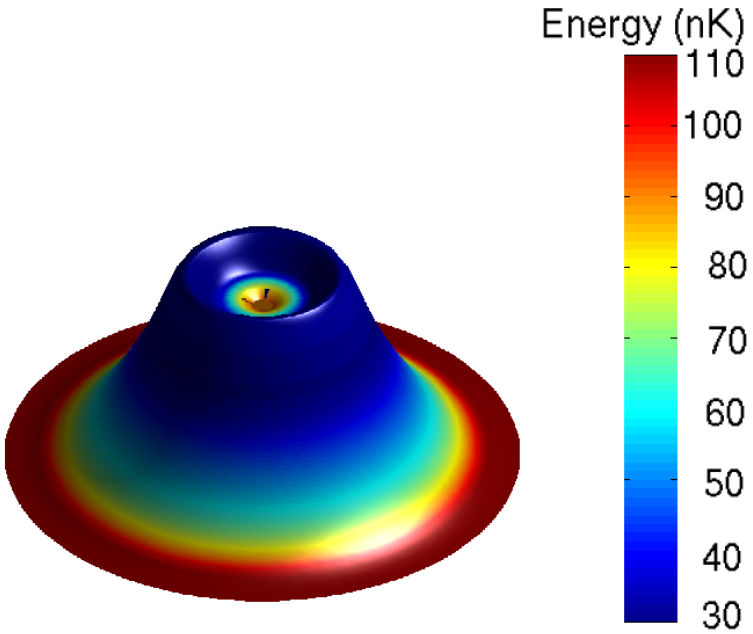

Figure 3.5: Density distribution of the non-condensate atoms near the end of the simulation (0.8 ms) on which we have superimposed the energy per particle as a colormap. The range of energies, of order 100 nK, is consistent with the characteristic scale of the burst particle energies in the Bosenova experiment. Note that hot atoms are generated in the center of the cloud during the atom-molecule oscillations since this is where the atom-molecule coupling is strongest (the coupling strength varies as the square root of the density). As the hot particles radiate outward a ring can be observed.

Chapter 4

BCS Superfluidity

4.1 Bardeen-Cooper-Schrieffer theory

The classic theory of superfluidity/superconductivity was put forth by Bardeen, Cooper, and Schrieffer in 1957 [56]. Entitled BCS theory, after its founders, the ideas presented in this seminal work were able to successfully explain almost all observed properties of conventional superconductors. We will extend BCS theory in Chapter 5 to incorporate Feshbach resonant interactions, but first it will prove instructive to review some fundamentals.

4.2 Cooper pairing

The cardinal process behind superfluidity is the formation of Cooper pairs. Cooper, who originally studied the problem [57] , showed that fermions, interacting above a closed Fermi sea, will show an instability towards forming pairs regardless of the weakness of the interaction, so long as the interaction remains attractive. Due to the sharpness of the Fermi surface, the main contribution to this population of paired states will arise between atoms on opposite ends of the Fermi surface. For instance, if we consider the s-wave pairing of a two spin state system $(\uparrow, \downarrow)$, pairs will prefer to form between atoms of $\mathbf{k}, \uparrow$ and $-\mathbf{k}, \downarrow$ (see Fig. 4.1). As long as the Fermi surface remains relatively sharp, it is unlikely that other combinations of pairs will form. This statement is more clearly illustrated in combination with Fig. 4.2.

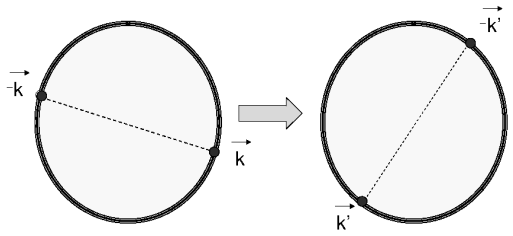

Figure 4.1: For s-wave collisions, pairs of atoms with opposite spin will form at the Fermi surface. The interior region represents the filled Fermi sea whereas the dark line around the edge shows the range of available states. In order to conserve energy the state shown on the left may scatter into any available state (right) which lies along its equipotential surface. For this example, the equipotential surface lies within the available states at the Fermi surface.

In a true many-body system, these atom pairs do not truly form bound states, but should rather be thought of as resulting from strong correlations. The energy gap, and most of the observed properties of superconductors, would be absent if it weren't for the strong correlations between these pairs. It should be noted, however, that these correlations result more from the Pauli blocking of available states within the Fermi surface than from the actual dynamical interactions. As a consequence, it is often a very good approximation to treat the system as though the interactions only occur between the Cooper pairs. This scheme may be called the BCS or pairing approximation.

4.3 BCS linearization and canonical transformation

Let us begin by discussing BCS theory as derived from the method of canonical transformation [58, 59]. We start with the following interacting Hamiltonian which accounts for the effects of pair-wise interactions:

$$H = \sum_{\mathbf{k}\sigma} \epsilon_{\mathbf{k}} a^{\dagger}_{\mathbf{k}\sigma} a_{\mathbf{k}\sigma} + \sum_{\mathbf{k}\mathbf{k}'} V_{\mathbf{k}\mathbf{k}'} a^{\dagger}_{\mathbf{k}\uparrow} a^{\dagger}_{-\mathbf{k}\downarrow} a_{-\mathbf{k}'\downarrow} a_{\mathbf{k}'\uparrow}, \tag{4.1}$$

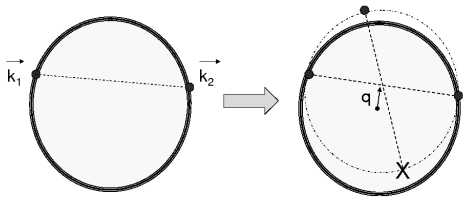

Figure 4.2: If we attempt to form a Cooper pair between $\mathbf{k},\uparrow$ and $\mathbf{k}',\downarrow$, where $\mathbf{k} \neq -\mathbf{k}'$, the number of states which the pair may scatter into is severely limited. This may be seen by transforming to a frame in which the pairs form with equal and opposite momentum, but with center of mass momentum $\mathbf{q}$. The equipotential surface is given by the dotted line and only rarely falls within the available region of states.

where $a^\dagger_{\mathbf{k}\sigma}(a_{\mathbf{k}\sigma})$ are fermion creation(annihilation) operators, $\epsilon_k = \hbar^2 k^2/2m$, and $V_{\mathbf{k}\mathbf{k}'}$ define the matrix elements of the interaction potential. A fundamental idea behind BCS theory is that the many-body wavefunction will be constructed of a phase coherent superposition of paired states

$$|\phi_N\rangle = \sum_{\mathbf{k}_1} \cdots \sum_{\mathbf{k}_{N/2}} g_{\mathbf{k}_1} \cdots g_{\mathbf{k}_{N/2}} ... a^\dagger_{\mathbf{k}_1\uparrow} a^\dagger_{-\mathbf{k}_1\downarrow} \cdots a^\dagger_{\mathbf{k}_{N/2}\uparrow} a^\dagger_{-\mathbf{k}_{N/2}\downarrow} |\varphi_0\rangle, \tag{4.2}$$

where $g_{\mathbf{k}_{N/2}}$ is the weight of each of the $N/2$ paired states and $|\varphi_0\rangle$ is the vacuum ket. Because of this phase coherence, operators such as $a_{-\mathbf{k}\downarrow} a_{\mathbf{k}\uparrow}$ may not average to zero as they would in the normal state where the phases are at random. What's more, for a large number of particles one may assume that the fluctuations about these averages should be small. With this in mind, we rewrite the paired operator as

$$a_{-\mathbf{k}\downarrow} a_{\mathbf{k}\uparrow} = \langle a_{-\mathbf{k}\downarrow} a_{\mathbf{k}\uparrow} \rangle + (a_{-\mathbf{k}\downarrow} a_{\mathbf{k}\uparrow} - \langle a_{-\mathbf{k}\downarrow} a_{\mathbf{k}\uparrow} \rangle), \tag{4.3}$$

which separates the average (first term) from the fluctuations about the average (second term). Substitution of Eq. (4.3) into Eq. (4.1) results in

$$H = \sum_{\mathbf{k}\sigma} \xi_{\mathbf{k}} a^\dagger_{\mathbf{k}\sigma} a_{\mathbf{k}\sigma} + \sum_{\mathbf{k}\mathbf{k}'} V_{\mathbf{k}\mathbf{k}'} (a^\dagger_{\mathbf{k}\uparrow} a^\dagger_{-\mathbf{k}\downarrow} \langle a_{-\mathbf{k}'\downarrow} a_{\mathbf{k}'\uparrow} \rangle + \langle a^\dagger_{\mathbf{k}\uparrow} a^\dagger_{-\mathbf{k}\downarrow} \rangle a_{-\mathbf{k}'\downarrow} a_{\mathbf{k}'\uparrow}), \tag{4.4}$$

where $\xi_{\mathbf{k}} = \epsilon_{\mathbf{k}} - \mu$. We have introduced a chemical potential since the linearized Hamiltonian no longer conserves number. The chemical potential may be adjusted to gain

the desired number of atoms. We may now define the gap

$$\Delta_{\mathbf{k}} = -\sum_{\mathbf{k}'} V_{\mathbf{k}\mathbf{k}'} \langle a_{-\mathbf{k}'\downarrow} a_{\mathbf{k}'\uparrow} \rangle. \tag{4.5}$$

For the moment, the name may seem a bit arbitrary, but this function will later be shown as equivalent to the value of the gap in the energy spectrum. The Hamiltonian may now be written as:

$$H = \sum_{\mathbf{k}\sigma} \xi_{\mathbf{k}} a^{\dagger}_{\mathbf{k}\sigma} a_{\mathbf{k}\sigma} - \sum_{\mathbf{k}} (\Delta_{\mathbf{k}} a^{\dagger}_{\mathbf{k}\uparrow} a^{\dagger}_{-\mathbf{k}\downarrow} + \Delta^{*}_{\mathbf{k}} a_{-\mathbf{k}\downarrow} a_{\mathbf{k}\uparrow}). \tag{4.6}$$

This Hamiltonian may be diagonalized by an appropriate canonical transformation (see Appendix B) of the general form

$$\begin{pmatrix} a_{\mathbf{k}\uparrow} \\ a^{\dagger}_{-\mathbf{k}\downarrow} \end{pmatrix} = \begin{pmatrix} u^{*}_{\mathbf{k}} & v_{\mathbf{k}} \\ -v^{*}_{\mathbf{k}} & u_{\mathbf{k}} \end{pmatrix} \begin{pmatrix} \gamma_{\mathbf{k}0} \\ \gamma^{\dagger}_{\mathbf{k}1} \end{pmatrix}, \tag{4.7}$$

where the γ's are a new set of Fermi operators and the weights $u_{\mathbf{k}}$ and $v_{\mathbf{k}}$ must satisfy the relationship

$$|u_{\mathbf{k}}|^2 + |v_{\mathbf{k}}|^2 = 1, \tag{4.8}$$

for the resulting transformation to remain unitary. Note that an inversion of Eq. (4.7) shows that the new operators γ have the net effect of mixing the spins. By inserting these substitutions into Eq. (4.6) we will recover a diagonal Hamiltonian, that is, one that only contains density type pairs of operators $\gamma^{\dagger}_{\mathbf{k}}\gamma_{\mathbf{k}}$, if the following condition is satisfied:

$$\Delta^{*}_{\mathbf{k}} v^{2}_{\mathbf{k}} - \Delta_{\mathbf{k}} u^{2}_{\mathbf{k}} + 2\xi u_{\mathbf{k}} v_{\mathbf{k}} = 0. \tag{4.9}$$

Multiplying through by $\Delta^{*}_{\mathbf{k}}/u^{2}_{\mathbf{k}}$ and solving the resulting quadratic equation in terms of $\Delta^{*}_{\mathbf{k}} v_{\mathbf{k}}/u_{\mathbf{k}}$ we have the following condition for the coefficients

$$\frac{v_{\mathbf{k}}}{u_{\mathbf{k}}} = \frac{E_{\mathbf{k}} - \xi_{\mathbf{k}}}{\Delta^{*}_{\mathbf{k}}}, \tag{4.10}$$

where we define $E_{\mathbf{k}} = \sqrt{\xi^{2}_{\mathbf{k}} + |\Delta_{\mathbf{k}}|^2}$. Equation (4.10), which is the positive root, is chosen since it corresponds to the stable minimum (as opposed to the unstable maximum)

energy solution. By combining Eq. (4.8) and Eq. (4.10) we have the following result for the value of the coefficients:

$$|v_{\mathbf{k}}|^2 = 1 - |u_{\mathbf{k}}|^2 = \frac{1}{2}\left(1 - \frac{\xi_{\mathbf{k}}}{E_{\mathbf{k}}}\right). \tag{4.11}$$

It should be noted that, although the phases up until know are written arbitrarily, the phase of $u_{\mathbf{k}}$, $v_{\mathbf{k}}$, and $\Delta_{\mathbf{k}}$ must occur so that $\Delta^*_{\mathbf{k}} v_{\mathbf{k}}/u_{\mathbf{k}}$ is real, as implied by Eq. (4.10).

4.4 The appearance of an energy gap

The resulting diagonal Hamiltonian (Eq. (4.6) written in terms of the basis defined in Eq. (4.7)) is

$$H = \sum_{\mathbf{k}} (\xi_k - E_{\mathbf{k}}) + \sum_{\mathbf{k}} E_{\mathbf{k}} (\gamma^\dagger_{\mathbf{k}0}\gamma_{\mathbf{k}0} + \gamma^\dagger_{\mathbf{k}1}\gamma_{\mathbf{k}1}). \tag{4.12}$$

The first term gives a constant shift to the energy spectrum while the second term describes the elementary quasi-particle excitations of the system. The energy of these excitations is given by

$$E_{\mathbf{k}} = \sqrt{\xi^2_{\mathbf{k}} + |\Delta_{\mathbf{k}}|^2}, \tag{4.13}$$

so that, even at $\xi_{\mathbf{k}} = 0$, there remains a finite energy Δ_k which must be invested in order to excite the system. This gap in the energy spectrum justifies our earlier labelling of Δ_k.

4.5 Populating the quasi-particles

In this diagonal representation, we may write the gap as

$$\Delta_{\mathbf{k}} = -\sum_{\mathbf{k}'} V_{\mathbf{k}\mathbf{k}'} \langle a_{-\mathbf{k}'\downarrow} a_{\mathbf{k}\uparrow} \rangle = -\sum_{\mathbf{k}'} V_{\mathbf{k}\mathbf{k}'} u^*_{\mathbf{k}'} v_{\mathbf{k}'} \langle 1 - \gamma^\dagger_{\mathbf{k}'0}\gamma_{\mathbf{k}'0} + \gamma^\dagger_{\mathbf{k}'1}\gamma_{\mathbf{k}'1} \rangle. \tag{4.14}$$

In thermal equilibrium, the quasi-particles behave as noninteracting fermions so they distribute themselves according to Fermi statistics:

$$f(E_{\mathbf{k}}) = \frac{1}{e^{\beta E_{\mathbf{k}}} + 1}. \tag{4.15}$$

By writing

$$\langle 1 - \gamma^\dagger_{\mathbf{k}'0}\gamma_{\mathbf{k}'0} + \gamma^\dagger_{\mathbf{k}'1}\gamma_{\mathbf{k}'1}\rangle = 1 - 2f(E_{\mathbf{k}'}), \tag{4.16}$$

we may convert Eq. (4.14) to the following form

$$\Delta_{\mathbf{k}} = -\frac{1}{2}\sum_{\mathbf{k}'} V_{\mathbf{k}\mathbf{k}'}\frac{\Delta_{\mathbf{k}'}}{2E_{\mathbf{k}'}}\tanh\frac{\beta E_{\mathbf{k}'}}{2}. \tag{4.17}$$

In deriving Eq. (4.17) we have used the trigonometric identity $\tanh(x/2) = 1 - 2f(x)$. Equation (4.17) is called the gap equation. It is often assumed that the potential is constant $V_{\mathbf{k}\mathbf{k}'} = V$ which results in a constant gap $\Delta_{\mathbf{k}'} = \Delta$. This considerably simplifies the problem since a factor of Δ may be removed from both sides of the equation resulting in

$$\frac{1}{V} = -\sum_{\mathbf{k}}\frac{\tanh(\beta E_{\mathbf{k}}/2)}{2E_{\mathbf{k}}}. \tag{4.18}$$

We may perform the same transformation on the expectation value of the number operator to derive a second equation

$$\begin{aligned} n_\sigma = \sum_{\mathbf{k}}\langle a^\dagger_{\mathbf{k}\sigma}a_{\mathbf{k}\sigma}\rangle &= \sum_{\mathbf{k}}|u_{\mathbf{k}}|^2 f(E_{\mathbf{k}}) + |v_{\mathbf{k}}|^2(1 - f(E_{\mathbf{k}})) \\ &= \sum_{\mathbf{k}}\frac{1}{2}\left(1 - \frac{\xi_{\mathbf{k}}}{E_{\mathbf{k}}}\tanh(\beta E_{\mathbf{k}}/2)\right). \end{aligned} \tag{4.19}$$

Equations (4.18) and (4.19) are a closed set of equations forming the foundations of BCS theory. Unfortunately, due to the form of the potential $V_{\mathbf{k}\mathbf{k}'}$ that we have chosen, these equations will diverge. This divergence, however, may be remedied by a proper renormalization. In the case of superconductors, the divergence is often remedied by cutting the integral at the Debye energy since only a very limited shell of states about the Fermi surface are thought to contribute. However, for atomic systems, the renormalization may be performed by matching the potentials to the T-matrix describing the full 2-body scattering processes. This was explained in detail in Chapter 2.6.

4.6 Critical temperature

For dilute interactions, we may assume that the potential is given by $V = 4\pi\hbar^2 a_{sc}/m$, where m is the mass of each fermion and a_{sc} is the s-wave scattering length. At the critical point the gap vanishes, $\Delta = 0$, and we may solve Eqs. (4.18) and (4.19) for the critical temperature T_c. Under the assumption that $k_F a_{sc} \ll 1$, we find for the critical temperature:

$$\frac{T}{T_F} \approx .614 e^{-\pi/(2k_F|a_{sc}|)}. \tag{4.20}$$

The exponential form of Eq. (4.20), although only approximate, shows that we must enhance the scattering in order to raise the critical temperature. For $k_F a_{sc} \sim 1$ we have a critical temperature $T_c/T_F \sim 0.1$–a temperature which is accessible to modern experiments. One method to enhance the scattering, and obtain critical temperatures of this magnitude, would be by tuning the particle-particle interactions with a Feshbach resonance. In the next section, we discuss how to incorporate these resonant scattering interactions into this model.

Chapter 5

Resonant superfluid Fermi gases

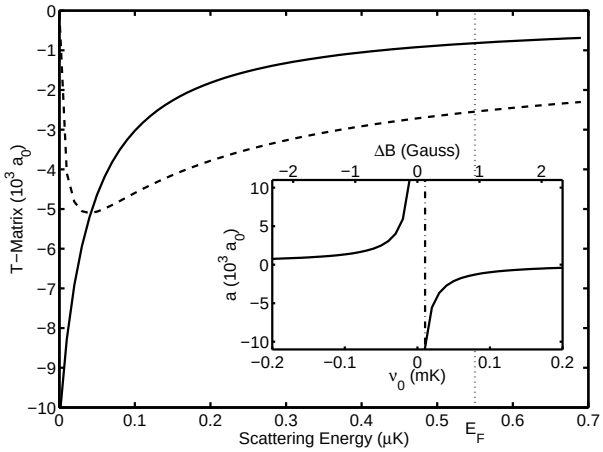

Figure 5.1: Real (solid line) and imaginary (dashed line) components of the T-matrix for collisions of the lowest two spin states of ^{40}K at a detuning of 20 E_F, shown in length dimensions, i.e., $T_k/(4\pi\hbar^2/m)$. The inset shows the scattering length as a function of detuning, with 20 E_F detuning indicated by the dashed-dot line.

5.1 Signatures

In this chapter we will develop a Feshbach resonance field theory for interacting Fermi gases and show that the enhanced interactions do indeed increase the critical temperature. Once the critical point is reached it remains to distinguish a clear signature of the phase transition. Various approaches have been proposed to detect the superfluid state: measurements of the pair distribution [60, 61], experiments involving the breakup

of Cooper pairs [62], measurements of the moment of inertia [63], and probes of collective excitations [64, 65, 66]. In this chapter we will show that a more direct signature of the transition to superfluidity is provided by the density distribution in an inhomogeneous system. We demonstrate that, in a harmonic trap, the superfluid state manifests in the appearance of a density bulge in the central atomic density.

5.2 Resonant Hamiltonian for a Fermi gas

We will now extend the concepts of BCS theory, detailed in the last chapter, and well accounted for in the literature of trapped atomic gases [67, 68, 69, 70, 71], to incorporate resonantly interacting Fermi gases [49, 72] . To begin, we consider a resonance such as that of ^{40}K, illustrated in Fig. 5.1, for s-wave scattering of atoms in the lowest two hyperfine spin states $\sigma \in \{\uparrow, \downarrow\}$. The scattering length is the intercept at zero scattering energy which, for this case, is approximately -10000 a_0, where a_0 is the Bohr radius. The large variation in the T-matrix over the relevant energy range indicates that a quantum field theory developed from this microscopic basis will need to correctly incorporate this strong energy dependence. The inset shows the resonant form of the scattering length which obeys the usual dispersive form $a = a_{\rm bg}(1 - \kappa/\bar{\nu})$. For ^{40}K, the dispersion parameters are $a_{\rm bg} = 176\, a_0$ and $\kappa = 0.657\,$mK[73].

In analogy to the Hamiltonian presented in Eq. (3.2), we write down the following Hamiltonian for the Fermi system:

$$\begin{aligned} H &= \sum_\sigma \int d^3x\ \psi^\dagger_\sigma(\mathbf{x}) H_\sigma(x) \psi_\sigma(\mathbf{x}) + \int d^3x\ \psi^\dagger_m(\mathbf{x}) H_m(x) \psi_m(\mathbf{x}) \\ &+ \int d^3x d^3x'\ \psi^\dagger_\downarrow(\mathbf{x}) \psi^\dagger_\uparrow(\mathbf{x}') U(\mathbf{x}-\mathbf{x}') \psi_\uparrow(\mathbf{x}) \psi_\downarrow(\mathbf{x}) \\ &+ \int d^3x d^3x'\ \left(\psi^\dagger_m(\frac{\mathbf{x}+\mathbf{x}'}{2}) g(\mathbf{x}-\mathbf{x}') \psi_\downarrow(\mathbf{x}) \psi_\uparrow(\mathbf{x}') + \text{h.c.} \right). \end{aligned} \tag{5.1}$$

We define the free atomic dispersion for each spin state as $H_\sigma(x) = -\frac{\hbar^2}{2m}\nabla_x^2 + V_\sigma(\mathbf{x}) - \mu_\sigma$ and the free molecular dispersion as $H_m(x) = -\frac{\hbar^2}{4m}\nabla_x^2 + V_m(\mathbf{x}) - \mu_m$. $V_{\sigma,m}$ are the external potentials and $\mu_{\sigma,m}$ are the various chemical potentials for each species. The

Feshbach resonance is controlled by the magnetic field which is incorporated by the detuning $\nu = \mu_m - \mu_\uparrow - \mu_\downarrow$ between the chemical potential of each of the two spin states and the molecular fields.

The field operators $\psi^\dagger_\sigma(\mathbf{x}), \psi_\sigma(\mathbf{x})$ create and destroy atoms of spin σ at point $\mathbf{x}$ and $\psi^\dagger_m(\mathbf{x}), \psi_m(\mathbf{x})$ create and destroy molecules at point $\mathbf{x}$. The atomic field operators now commute like fermions whereas the molecular fields retain a bosonic nature:

$$\begin{aligned} \left[\psi_{\sigma_1}(\mathbf{x}), \psi^\dagger_{\sigma_2}(\mathbf{x}')\right]_A &= \delta_{\sigma_1,\sigma_2}\delta^3(\mathbf{x}-\mathbf{x}'), \\ \left[\psi_m(\mathbf{x}), \psi^\dagger_m(\mathbf{x}')\right] &= \delta^3(\mathbf{x}-\mathbf{x}'), \end{aligned} \tag{5.2}$$

where the above subscript A refers to anti-commutation. The bosonic nature of the molecular field, although comprised of a pair of fermions, is justified with the understanding that the closed channel molecules are extremely well bound and have a relative size much smaller than all other length scales in the problem. They, therefore, are well characterized as bosons.

We now consider the general structure of the theory for the homogeneous case. Equation (5.1) is written in position space, however, we would now like to change to momentum space. This may be done by introducing the plane wave expansion of the operators:

$$\begin{aligned} \psi_\sigma(\mathbf{x}) &= \frac{1}{\sqrt{V}}\sum_{\mathbf{k}} a_{\mathbf{k}\sigma} e^{i\mathbf{k}\cdot\mathbf{x}} \\ \psi_m(\mathbf{x}) &= \frac{1}{\sqrt{V}}\sum_{\mathbf{k}} b_{\mathbf{k}} e^{i\mathbf{k}\cdot\mathbf{x}}, \end{aligned} \tag{5.3}$$

in a volume V. With this expansion, Eq. (5.1) transforms to:

$$\begin{aligned} H &= \sum_{\mathbf{k}\sigma}(\epsilon_{\mathbf{k}\sigma} - \mu_\sigma)\, a^\dagger_{\mathbf{k}\sigma} a_{\mathbf{k}\sigma} + \sum_{\mathbf{k}}(\epsilon_{\mathbf{k}m} + \nu) b^\dagger_{\mathbf{k}} b_{\mathbf{k}} \\ &+ U\sum_{\mathbf{qkk}'} a^\dagger_{\mathbf{q}/2+\mathbf{k}\uparrow} a^\dagger_{\mathbf{q}/2-\mathbf{k}\downarrow} a_{\mathbf{q}/2-\mathbf{k}'\downarrow} a_{\mathbf{q}/2+\mathbf{k}'\uparrow} + g\sum_{\mathbf{kq}}\left(b^\dagger_{\mathbf{q}} a_{\mathbf{q}/2-\mathbf{k}\downarrow} a_{\mathbf{q}/2+\mathbf{k}\uparrow} + \text{h.c.}\right), \end{aligned} \tag{5.4}$$

where h.c. denotes the hermitian conjugate. The free dispersion relation for the fermions and bosons respectively are $\epsilon_{\mathbf{k}\sigma} = \hbar^2 k^2/2m$ and $\epsilon_{\mathbf{k}m} = \hbar^2 k^2/4m$, and ν denotes the

detuning of the boson resonance state from the zero edge of the collision continuum. In deriving Eq. (5.4) we have introduced contact potentials so must again renormalize as in Appendix A.1.

5.3 Construction of dynamical equations for fermions

From this Hamiltonian (Eq. (5.4)), we construct the dynamical Hartree-Fock-Bogoliubov (HFB) equations for both the bosonic and fermionic mean-fields. These equations involve the mean fields corresponding to the spin density $n = \sum_{\mathbf{k}} \langle a^\dagger_{\mathbf{k}\sigma} a_{\mathbf{k}\sigma} \rangle$ (taken to be identical for both spins), the pairing field $p = \sum_{\mathbf{k}} \langle a_{-\mathbf{k}\downarrow} a_{\mathbf{k}\uparrow} \rangle$, and the condensed boson field $\phi_m = \langle b_{\mathbf{k}=0} \rangle$. Note that since we only consider the condensate portion of molecules, and are dealing with a homogeneous system, we may neglect the kinetic contribution of the molecules. The single particle density matrix [54] is defined as:

$$\mathcal{G}_{i,j} = \langle A^\dagger_j A_i \rangle \,, \qquad A = \begin{pmatrix} a_{\mathbf{k}\uparrow} \\ a_{\mathbf{k}\downarrow} \\ a^\dagger_{-\mathbf{k}\uparrow} \\ a^\dagger_{-\mathbf{k}\downarrow} \end{pmatrix}, \tag{5.5}$$

and evolves according to the Bogoliubov self-energy Σ

$$i\hbar \frac{d\mathcal{G}}{dt} = [\Sigma, \mathcal{G}] \,. \tag{5.6}$$

The differences between Eq. (5.6) and Eq. (3.10) arise due to the particle statistics. The self-energy for fermions now has a Hermitian structure

$$\Sigma = \begin{pmatrix} U_k & 0 & 0 & \Delta \\ 0 & U_k & -\Delta & 0 \\ 0 & -\Delta^* & -U_k & 0 \\ \Delta^* & 0 & 0 & -U_k \end{pmatrix}, \tag{5.7}$$

where the single particle energy is $U_k = \epsilon_k - \mu + Un$, we define a gap $\Delta = Up + g\,\phi_m$, and μ is the chemical potential. Finally, the dynamical equations are closed by the

evolution equation for the boson mode:

$$i\hbar\frac{d\phi_m}{dt} = \nu\,\phi_m + g\,p\,. \tag{5.8}$$

5.4 Application to a trapped system

In order to solve this set of equations, the self-energy Σ is diagonalized locally at each k by the Bogoliubov transformation (see Appendix B) generating quasi-particles with an energy spectrum $E_k = \sqrt{U_k^2 + |\Delta|^2}$. In equilibrium, the quasi-particle states are occupied according to the Fermi-Dirac distribution $n_k = [\exp(\beta E_k) + 1]^{-1}$. The corresponding maximum entropy solution for the molecule amplitude is found by $i\hbar d\phi_m/dt = \mu_m\phi_m$, where $\mu_m = 2\mu$, so that Eq. (5.8) implies

$$\phi_m = g\,p/(\mu_m - \nu). \tag{5.9}$$

The mean fields can then be determined by integration of the equilibrium single particle density matrix elements given by:

$$\begin{aligned} n &= \frac{1}{(2\pi)^2}\int_0^K dk k^2\,[(2n_k - 1)\cos 2\theta_k + 1]\,, \\ p &= \frac{1}{(2\pi)^2}\int_0^K dk k^2\,(2n_k - 1)\sin 2\theta_k\,, \end{aligned} \tag{5.10}$$

where $\tan 2\theta_k = |\Delta|/U_k$ is the Bogoliubov transformation angle. Since θ_k depends on n and p, these equations need to be solved self-consistently. As a technical point, it should be noted that the $p = 0$ solution should be discarded when the superfluid state is present since it then corresponds to an unstable point on the free energy surface. Perhaps it is useful to rewrite Eqs. (5.10) in the following form

$$\begin{aligned} 1 &= -\left(U - \frac{g^2}{\nu - 2\mu}\right)\int \frac{d^3k}{(2\pi)^3}\frac{\tanh(\beta E_{\mathbf{k}}/2)}{2E_{\mathbf{k}}} \\ n &= \frac{1}{2}\int \frac{d^3k}{(2\pi)^3}\left(1 - \frac{U_{\mathbf{k}}}{E_{\mathbf{k}}}\tanh(\beta E_{\mathbf{k}}/2)\right). \end{aligned} \tag{5.11}$$

The form of Eqs. (5.11) clearly relate the resonance equations to the BCS gap and number equation (Eqs. (4.18) and (4.19)).

So far this theory has been presented for a homogeneous system, while we are interested in a gas of N atoms confined to an external trapping potential $V(\mathbf{r})$. However, a full quantum mechanical treatment of the trapping states is not required. For instance, in our case, with a temperature on the order of $T = 0.2\,T_F$, the harmonic oscillator level spacing is smaller than both the Fermi and thermal energies. Under these conditions, we may incorporate the effect of the trap through a semi-classical, local-density approximation [75, 76]. This involves replacing the chemical potential by a local one

$$\mu(\mathbf{r}) = \mu - V(\mathbf{r}), \tag{5.12}$$

and determining the thermodynamic solution at each point in space as for the homogeneous system.

In general, the validity of the semi-classical approximation requires a slow variation in the occupation of the discrete quantum levels as a function of energy. Remarkably, in both bosonic and fermionic gases, this condition can often be satisfied even at very low temperatures because of strong correlations in a BEC due to repulsive interactions and because of exchange effects in a quantum Fermi gas. In both cases, the zero temperature, semi-classical approximation for dilute gases is usually referred to as the Thomas-Fermi approximation.

5.5 Thermodynamic results and signatures of superfluidity

We evaluate the thermodynamic quantities at given T and N in three steps:

(1) For given μ, we determine the local chemical potential $\mu(\mathbf{r}) = \mu - V(\mathbf{r})$ and use this value to find the self-consistent solution for the density $n(\mathbf{r})$ and pairing field $p(\mathbf{r})$ at each point in space, according to the solution of Eqns. (5.10).

(2) We modify the global chemical potential μ until the density integral $N = \int d^3r\, n(\mathbf{r})$ gives the desired atom number.

(3) We use the resulting solution for μ to calculate observable quantities, such as the density, gap, compressibility, and so forth.

The resulting solution for the density distribution is illustrated in Fig. 5.2. A striking signature of the resonance superfluidity is evident in the predicted density profile which has a notable bulge in the region of the trap center. This signature would appear to be directly accessible experimentally. One approach to measure this density bulge would be to fit the expected density profile for a quantum degenerate gas with no superfluid phase to the wings of the distribution (outside the dotted lines shown in Fig. 5.2). The excess density observed at the trap center could then be recorded. Fig. 5.3 illustrates the emergence of the superfluid as the temperature is decreased. Qualitatively, this situation is reminiscent of the central condensate peak observed for a Bose-Einstein condensed gas in a harmonic potential.

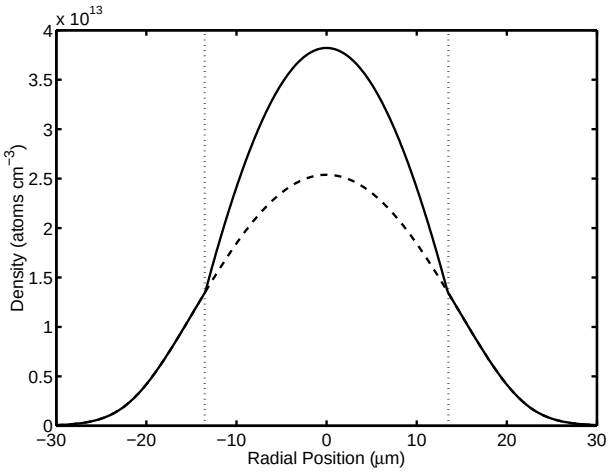

Figure 5.2: Density profile at temperature $T = 0.2\,T_F$ and detuning $\nu = 20\,E_F$ showing accumulation of atoms at the trap center (solid line). We compare with the profile resulting from the same μ but artificially setting the pairing field p to zero so that no superfluid is present (dashed line).

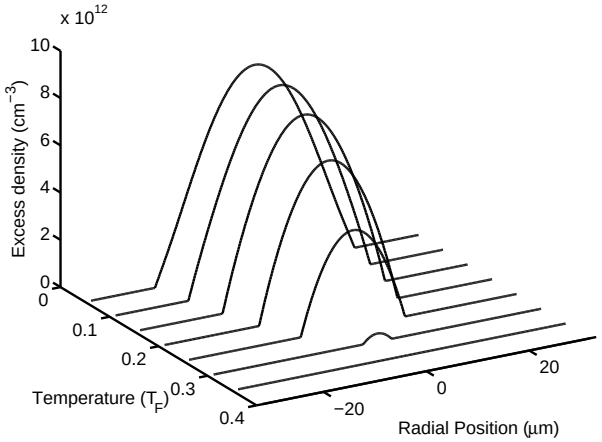

Figure 5.3: Emergence of the coherent superfluid for $\nu = 20\ E_F$. The superfluid occupies an increasing volume as the temperature is reduced. Shown is the excess density (difference between the dashed and solid lines in Fig. 5.2) at each temperature.

We explain the observed behavior by considering the compressibility of the normal and superfluid gas. Thermodynamically, the isothermal compressibility C is defined as

$$C^{-1} = n(\partial P/\partial n)_T, \tag{5.13}$$

where P is the pressure and is shown in Fig. 5.4. The compressibility is positive everywhere, indicating that, in spite of the large attractive interactions, the Fermi pressure makes the configuration mechanically stable. A significant feature is the discontinuous behavior at the radius from the trap center at which the superfluid changes from zero to a non-zero value. This discontinuity is a manifestation of a second-order phase transition occurring in space. The discontinuity is a consequence of the local density approximation and cannot occur in a finite system. However, a rapid change in the compressibility is expected. In principle, this could be probed by studies of shock waves generated by the abrupt jump in the speed of sound as a density fluctuation passes through the discontinuous region.

5.6 Conclusions

This section has shown how we may derive a resonant theory for dilute Fermi gases and has applied this theory to the case of a trapped ensemble. We demonstrated that there exists a direct signature of superfluidity in trapped Fermi gases. The onset of superfluidity leads to a density bulge in the center of the trap which can be detected by absorption imaging. The critical conditions for superfluidity are satisfied initially in the trap center and the region of non-zero pairing field spreads out from the center as the temperature is lowered further. The increase in the density profile in the superfluid region is caused by a jump in the compressibility. Direct measures of this behavior are possible by the study of the propagation of sound waves. We have applied our method here to ^{40}K, but a similar approach is easy to derive for other interesting atoms, including, in particular, ^{6}Li which is another fermionic alkali currently being investigated experimentally.

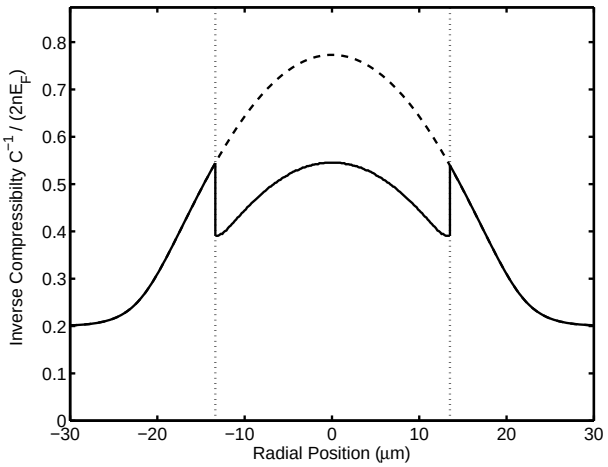

Figure 5.4: Inverse isothermal compressibility C^{-1} in units of the Fermi energy (solid line). Here $\nu = 20\,E_F$ and $T = 0.2\,T_F$ (as can be seen from the limiting behavior at large radial position). A discontinuity appears at the radius at which the superfluid emerges (dotted line). We compare this solution to that corresponding to zero pairing field and no superfluid phase transition (dashed line).

Chapter 6

Feshbach Resonant Crossover Physics

6.1 Historical background

In the early stages of developing a theory for superconductivity it was suggested that superconductivity was a result of a Bose-condensation of pairs of electrons into localized bound states. This mechanism came to be known as "Schafroth condensation" and was extended upon in the work of Schafroth, Blatt, and Butler in, what they had coined, "quasi-chemical equilibrium theory" [77, 78]. In this theory, they considered the size of the bound pairs to be small compared to the inter-particle spacing. Superconductivity would result as a continuum of Bose-Einstein excitations above a ground state without an energy gap. Due to the complexity of this theory, and the extreme success of the soon to be unveiled theory of Bardeen, Cooper, and Schrieffer (BCS), the quasi-chemical equilibrium theory fell into obscurity. Later, however, it was shown by Blatt and coworkers [79] that their Bose-condensation approach could be extended to give the same results as the BCS pairing theory.

At the time, the differences between these two approaches were highly emphasized and it was thought that superfluidity should be understood in terms of momentum-space pairing and not of real-space pairing. However, the similarities between the two approaches remain so the question may be asked: How does one reconcile the difference between BCS superfluidity of highly-overlapping, long-range fermion pairs and that of Bose-Einstein condensation of non-overlapping, localized pairs. These two cases are

the extremes and the problem of how to move from one to the other is known as the "crossover problem" (see Fig. 6.1).

One of the first attempts to understand this crossover was put forth by Eagles in a 1969 paper on pairing in superconducting semiconductors [80]. He proposed moving between these two limits by doping samples, in this case, by decreasing the carrier density in systems of $SrTiO_3$ doped with Zr. In a 1980 paper by Leggett [81], motivated by the early ideas of quasi-chemical equilibrium theory, he modelled the crossover at zero temperature by way of a variational wavefunction:

$$\psi_{BCS} = \prod_k (u_k + v_k a_k^\dagger a_{-k}^\dagger)|0\rangle. \tag{6.1}$$

This wavefunction is simply the BCS wavefunction and assumes that at $T = 0$ all the fermions form into Cooper pairs. What Leggett was able to show was that he could smoothly interpolate between conventional BCS theory and the process of BEC.

In 1985, Nozières and Schmitt-Rink (NSR) extended this theory to finite temperatures in order to calculate the critical temperature T_c [82]. NSR derived the conventional BCS gap and number equation, but introduced into the number equation the self-energy associated with the particle-particle ladder diagram (or scattering T-matrix) to lowest order (see Fig. 6.2). This very influential paper would be built upon by many other groups and was transformed into a functional form by Randeria et *al.* [83].

A compelling reason for understanding the crossover problem comes from the fact that many high-T_c superconductors seem to fall within the region intermediate between BCS and BEC. In the copper oxides, for instance, the coherence length of the Cooper pairs has been measured to be only a few times the lattice spacing. In contrast, in conventional superconductors, the coherence lengths are usually much greater than the lattice spacings. An understanding of the crossover may be one of the keys to understanding and manipulating high-T_c materials. In Chapter 7 we will extend the NSR model of Randeria to account for Feshbach resonant interactions and the formation

of molecules. In Chapter 8 we will attempt to go beyond this formalism by adapting a dynamical Green's function approach, originally designed to model high-T_c systems, to the case of Feshbach resonant interactions.

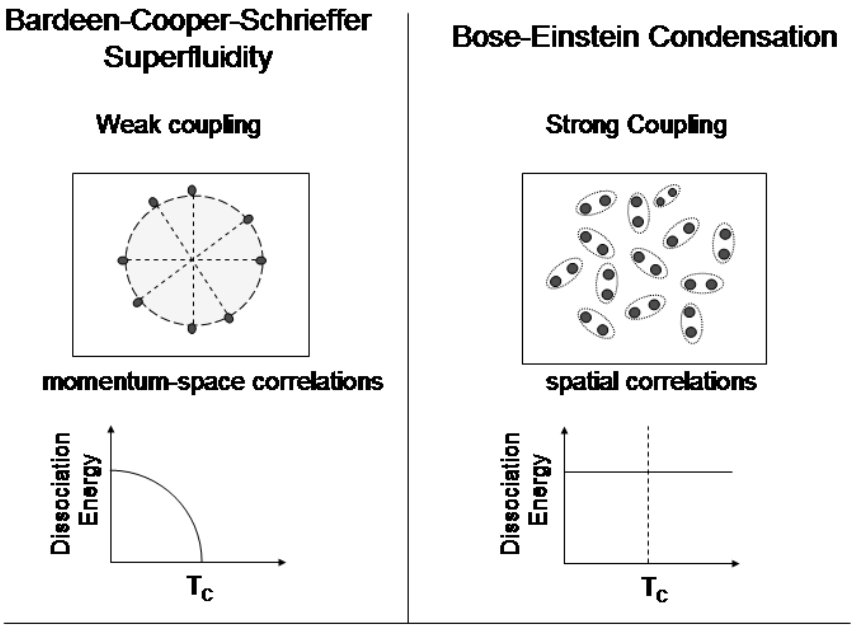

Figure 6.1: An illustration of the differences between Bardeen-Cooper-Schreiffer (BCS) superfluidity and Bose-Einstein condensation (BEC) of molecules in a Fermi gas. BCS theory describes weakly-bound fermions which are paired along the Fermi surface in k-space so may be highly overlapping in real space. The Cooper pairs break up at the critical temperature T_c signifying the phase transition. BEC results from from tightly-bound, real-space fermion pairs. Above the critical temperature T_c, these bosonic pairs loose their mutual phase coherence, but may remain bound into pairs.

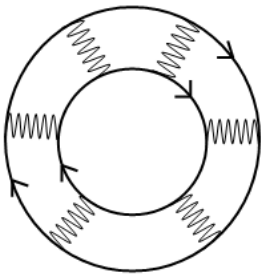

Figure 6.2: Diagrammatic contribution of pair fluctuations to the thermodynamic potential included by NSR. The solid lines are free propagators and the wavy lines are interactions.

Chapter 7

Path integral approach to the crossover problem

7.1 Resonant action

To begin our discussion of the resonant crossover problem we consider a Feshbach resonance for s-wave scattering of atoms in the lowest two hyperfine states $\sigma \in \{\uparrow, \downarrow\}$ of a fermionic alkali atom [84]. For a homogeneous system we have the following generalized Hamiltonian:

$$\begin{aligned}\hat{H}(t) &= \sum_{\sigma} \int \psi_{\sigma}^{\dagger}(x)(\hat{H}_{\sigma} - \mu)\psi_{\sigma}(x)d^3x + \int \psi_{m}^{\dagger}(x)(\hat{H}_{m} - 2\mu + \nu)\psi_{m}(x)d^3x \\ &+ \int \psi_{\uparrow}^{\dagger}(x)\psi_{\downarrow}^{\dagger}(x')U(\mathbf{x}-\mathbf{x}')\psi_{\downarrow}(x')\psi_{\uparrow}(x)d^3xd^3x' \\ &+ \int \left(\psi_{m}^{\dagger}(\frac{x+x'}{2})g(\mathbf{x}-\mathbf{x}')\psi_{\downarrow}(x)\psi_{\uparrow}(x') + \text{h.c.}\right) d^3xd^3x', \end{aligned} \tag{7.1}$$

where the operators $\psi_{\sigma}^{\dagger}$ (ψ_{σ}) create (annihilate) fermions at $x = (\mathbf{x}, t)$, and $\psi_{m}^{\dagger}$ (ψ_{m}) create (annihilate) composite bosons. The free dispersion Hamiltonian for fermions (bosons) is $\hat{H}_{\sigma}$ ($\hat{H}_{m}$) and ν is the detuning of the resonant molecular state from the collision continuum. The collisional interactions are described by both background fermion-fermion scattering, U, and an interconversion between composite bosons and fermions, g.

Functional methods prove to be especially convenient in describing the thermodynamics of the resonant system. For a finite-temperature field theory, the connection with statistical mechanics is made by Wick rotating the time coordinate $t \to -i\tau$ so that one works in terms of the spatial coordinate x and temperature τ [85]. The action

is defined in the usual way:

$$S = \sum_l \int_0^\beta d\tau \int d^3x \psi_l^\dagger(\mathbf{x},\tau)\partial_\tau \psi_l(\mathbf{x},\tau) - \int_0^\beta \hat{H}(\tau)d\tau, \tag{7.2}$$

where the sum in l runs over both the Fermi and the Bose degrees of freedom. In this functional formulation we treat the fermion fields ψ_σ as Grassmann variables and the composite Bose fields ψ_m as classical fields [86].

Let us consider a system comprised of fermions at some finite temperature τ inside a box of volume V (for convenience, let us work in the set of units where $\hbar = k_b = 1$). By imposing periodic boundary conditions upon the fields ψ_σ and ψ_m, we form the following Fourier series expansions:

$$\begin{aligned} \psi_\sigma(\mathbf{x},\tau) &= (\beta V)^{-1/2} \sum_{\mathbf{k},\omega} e^{i(\omega\tau + \mathbf{p}\cdot\mathbf{x})} a_\sigma(\mathrm{p}), \\ \psi_m(\mathbf{x},\tau) &= (\beta V)^{-1/2} \sum_{\mathbf{q},v} e^{i(v\tau + \mathbf{q}\cdot\mathbf{x})} b(\mathrm{q}), \end{aligned} \tag{7.3}$$

with even thermal (Matsubara) frequencies for the bosons ($v = 2\pi n/\beta$, where n is an integer) and odd frequencies for the fermions ($\omega = 2\pi(n+1)/\beta$) [87]. Here $a_\sigma(\mathrm{p})$ annihilates a fermion at $\mathrm{p} = (\mathbf{k},\omega)$ and $b(\mathrm{q})$ annihilates a molecule at $\mathrm{q} = (\mathbf{q},\omega)$.

By making use of the above transformation, Eq. (7.3), we may write out the action for the resonant system in terms of the Fourier coefficients $a_\sigma(\mathrm{p})$ and $b(\mathrm{q})$. To help clarify the following calculation, we split the resulting resonant action into two parts, the first being the usual BCS action

$$S_{BCS} = \sum_{\mathrm{p},\sigma} (i\omega - \frac{p^2}{2m} + \mu) a_\sigma^*(\mathrm{p}) a_\sigma(\mathrm{p}) - \frac{1}{\beta V} \sum_{\mathrm{p_1}+\mathrm{p_2}=\mathrm{p_3}+\mathrm{p_4}} U a_\uparrow^*(\mathrm{p_1}) a_\downarrow^*(\mathrm{p_2}) a_\downarrow(\mathrm{p_3}) a_\uparrow(\mathrm{p_4}), \tag{7.4}$$

and the second we will label the molecular action

$$\begin{aligned} S_M &= \sum_{\mathrm{q}} (iv - \frac{q^2}{4m} - \nu + 2\mu) b^*(\mathrm{q}) b(\mathrm{q}) \\ &\quad - \frac{1}{\sqrt{\beta V}} \sum_{\mathrm{q}=\mathrm{p_1}+\mathrm{p_2}} g \left(b^*(\mathrm{q}) a_\downarrow(\mathrm{p_1}) a_\uparrow(\mathrm{p_2}) + a_\uparrow^*(\mathrm{p_2}) a_\downarrow^*(\mathrm{p_1}) b(\mathrm{q}) \right). \end{aligned} \tag{7.5}$$

In deriving Eqs. (7.4) and (7.5) we have inserted contact potentials for the couplings $U(\mathbf{x}-\mathbf{x}') \to U\delta(\mathbf{x}-\mathbf{x}')$ and $g(\mathbf{x}-\mathbf{x}') \to g\delta(\mathbf{x}-\mathbf{x}')$. The full partition function for our

resonant system, under the model Hamiltonian of Eq. (7.1), can now be written as

$$Z = \int \left(\prod_{\sigma} \mathrm{D}a_{\sigma}^{*} \mathrm{D}a_{\sigma} \right) \left(\prod \mathrm{D}b^{*} \mathrm{D}b \right) \, \mathrm{e}^{S_{BCS}+S_{M}}, \tag{7.6}$$

with the functional integral, $\mathrm{D}c \equiv \prod_i dc^i$, ranging over all Fermi and Bose fields.

7.2 Saddle-point approximation

From the form of the action in Eq. (7.6), it should be apparent that all of the resonant contributions are contained within the molecular action. In practice this gives rise to the integral of a displaced Gaussian that can be easily evaluated (see Appendix C). After integrating out the molecular degrees of freedom, we are left with the following partition function:

$$Z = Z_B(q^2/4m + \nu - 2\mu) \int \mathrm{D}a_{\sigma}^{*} \mathrm{D}a_{\sigma} \mathrm{e}^{S_{BCS'}}. \tag{7.7}$$

Here $Z_B(q^2/4m+\nu-2\mu)$ is a Bose partition function describing the formation of bound molecules and $S_{BCS'}$ is the BCS action with a potential that is now dependent on both thermal frequencies and momentum. The interaction potential in the BCS action, therefore, is modified in the following way:

$$U \to U - \frac{g^2}{q^2/4m + \nu - 2\mu - iv}. \tag{7.8}$$

With the above partition function, Eq. (7.7), we may go on to calculate all thermodynamic properties of interest. Here we are primarily interested in calculating the critical temperature of the superfluid phase transition. This can be done by solving for a gap and number equation and then self-consistently solving these two equations for both the chemical potential μ and the critical temperature τ. The procedure is straightforward since the full resonant calculation has been reduced to the usual BCS calculation (however, we must now deal with the interaction given by Eq. (7.8)). Following Popov's derivation [86], we perform a Hubbard-Stratonovich transformation about an auxiliary

Bose field $c(q)$ (see Appendix C) to derive the gap equation at the critical point

$$1 = \left(-U + \sum_j \frac{g_j^2}{\nu_j - 2\mu} \right) \sum_k \frac{\tanh(\beta(k^2/2m - \mu)/2)}{2(k^2/2m - \mu)}. \tag{7.9}$$

A self-consistent equation for the total particle number can be found by expanding the action to lowest order about the auxiliary field $c(\mathrm{q}) = c^*(\mathrm{q}) = 0$. This is commonly referred to as the saddle-point approximation. The thermodynamic identity $N = -\partial \ln Z/\partial\mu$ yields:

$$N = N_b + N_f = 2\sum_k \frac{1}{e^{\beta(k^2/4m + \nu - 2\mu)} - 1} + 2\sum_k \frac{1}{e^{\beta(k^2/2m - \mu)} + 1}. \tag{7.10}$$

Thus, our number equation counts all free fermions, N_f, plus an additional boson population N_b. Equations (7.9) and (7.10) provide a set of equations for determining the critical temperature T_c and chemical potential μ. In conventional BCS theory, this level of approximation proves reasonable for calculating T_c for weak, attractive interactions, but diverges as the interaction strength grows. The reason for this is that the mechanism which signals the phase transition within the weak coupling BCS limit is the formation and disassociation of Cooper pairs. As the coupling increases, the particles tend to pair at higher and higher temperatures which means that the critical transition is no longer signaled by the formation of Cooper pairs, but rather by a coherence across the sample caused by condensation of pre-formed Cooper pairs. Since we are interested in describing the resonant system at all detunings, the equations that we have derived so far are insufficient because they do not account for this process. We should, therefore, next focus on how to more accurately incorporate atom pairing into our model.

7.3 Beyond the saddle-point approximation

To account for fluctuations in the fermion field, we follow the method of Nozières and Schmitt-Rink [82] in its functional form as put forth by Randeria et *al.* [83, 88]. This procedure will introduce a next order (Gaussian) correction to the saddle-point

calculation of the previous section. By expanding the action to second order in $c(\mathrm{q})$, and then calculating the number equation in the same way as was done when deriving Eq. (7.10), we introduce an additional population into the equation. The action becomes

$$S(c(\mathrm{q}), c^*(\mathrm{q}))_{BCS'} \approx S_{BCS'}(0,0) + \sum_{\mathrm{q}} |c(\mathrm{q})|^2 \chi(\mathrm{q}), \tag{7.11}$$

where we have defined the auxiliary function $\chi(\mathrm{q})$ as

$$\chi(\mathrm{q}) = \left(U - \frac{g^2}{\frac{q^2}{4m} + \nu - 2\mu - i\omega} \right) \sum_k \frac{1 - f(\epsilon_{\frac{q}{2}+k}) - f(\epsilon_{\frac{q}{2}-k})}{\epsilon_{\frac{q}{2}+k} + \epsilon_{\frac{q}{2}-k} - i\omega}. \tag{7.12}$$

Here $f(\epsilon_k)$ is the Fermi distribution function and $\epsilon_k = k^2/2m - \mu$. $\chi(\mathrm{q})$ is often referred to as the susceptibility (or the pair propagator) and results from the Matsubara summation of the single particle, free Green's functions G_0 (see Appendix D):

$$\frac{1}{\beta} \sum_{\omega} G_0(\mathbf{p}, \nu) G_0(\mathbf{k}, \omega - \nu). \tag{7.13}$$

Once again we make use of the thermodynamic identity $N = -\partial \ln Z / \partial \mu$ resulting in a modified number equation

$$\begin{aligned} N &= N_b + N_f + N_p \qquad (7.14) \\ &= 2\sum_k \frac{1}{e^{\beta(k^2/4m + \nu - 2\mu)} - 1} + 2\sum_k \frac{1}{e^{\beta(k^2/2m - \mu)} + 1} - \frac{1}{\beta} \sum_{\mathbf{q},\omega} \frac{\partial}{\partial \mu} \log[1 - \chi(\mathbf{q}, i\omega)]. \end{aligned}$$

This inclusion of the first order fluctuations introduces a new population which we will refer to as atom pairs N_p to distinguish them from the other bosonic population N_b already accounted for at the saddle-point level. We are now able to solve for the fluctuation corrected critical temperature from a self-consistent solution of Eqs. (7.9) and (7.14).

Due to the contact form of the couplings that we have chosen, however, we are immediately plagued with problems of divergences in our equations. These may be remedied by a proper renormalization as oulined in Chapter 2.6. We may also account for mean-field shifts due to all 2-body scattering processes by adjusting the chemical

potential $\mu = \bar{\mu} - \langle U n_k \rangle$ where n_k is the Fermi distribution and $\langle\rangle$ denotes an averaging. This shift, however, is sufficiently small to neglect; inclusion has demonstrated corrections of the order of 1% or less.

7.4 Bound states and asymptotes

The renormalization of the resonance theory forces us to take a closer look at the bound state physics of the system. In Fig. 7.1 we show the bound state energies for a single resonance system with a positive background scattering length. The figure results from a coupled square well calculation of the bound state energies, as in Chapter 2.4, and shows an avoided crossing between two molecular states. The upper state behaves to a fairly good approximation as $E_b = (m a_{\rm eff}^2)^{-1}$, which is the molecular binding energy regularly associated with a contact interaction [89]. The lower state, however, is offset from the detuning by an energy $\sim \kappa$ and goes linear with the detuning. We find this similar behavior in the first term of Eq. (7.14). Taking the cutoff to infinity, which is justified since this term does not diverge, the renormalized detuning approaches $\nu \to \bar{\nu} - \bar{g}^2/\bar{U}$. This produces a constant shift of $\bar{g}^2/\bar{U} = \kappa$ between the detuning and the molecular binding energy. Keeping this term in the number equation would incorrectly cause a transfer of the entire population into the wrong molecular state. In order to avoid this unwanted behavior, we set this term to zero, i.e., $N_b = 0$. In the case of a negative background scattering length, we would not have encountered this problem and only one molecular state would have appeared (see Fig. 7.2). We will show in the next section that the pairing term fully accounts for the correct population of molecules in this system with $a_{\rm bg} > 0$.

However, before we present the full crossover solution for the case of ^{40}K, let us look at the analytical solutions to Eqs. (7.9) and (7.14) in the strong (BEC) and weak (BCS) coupling regimes. We will first turn our attention to the weak coupling (BCS) limit. In this limit we would expect only free fermions to contribute to the

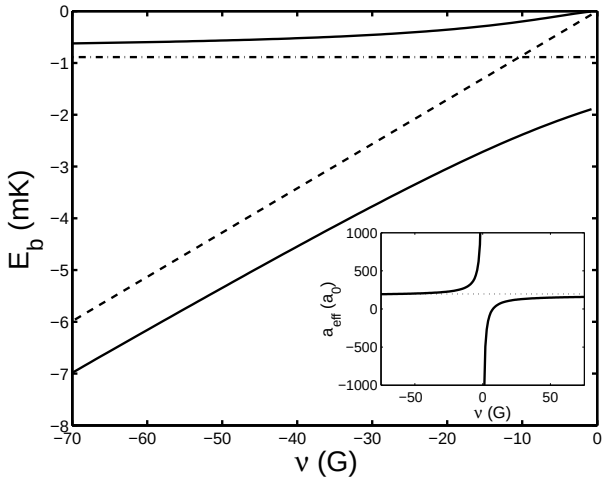

Figure 7.1: Binding energies for ^{40}K resonance at positive background scattering length $a_{bg} = 176a_0$. A single resonance with a positive background scattering length produces an effective scattering length $a_{eff} = a_{bg}(1 - \kappa/\nu)$, as seen in the figure inset where we plot the effective scattering length vs. detuning (the dotted line is at $176a_0$). A positive a_{bg}, which is larger than the range of the potential, implies that another bound state is not far below threshold (dash-dotted line). In combination with the Feshbach state (dashed detuning line) this results in an avoided crossing and the molecular state of interest asymptotes quickly to the dash-dotted line.

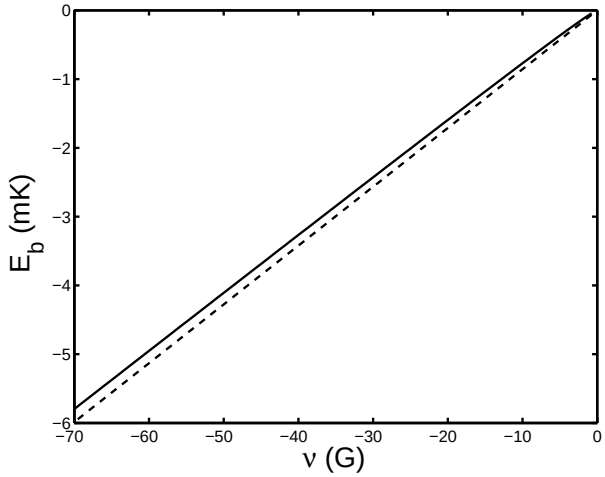

Figure 7.2: Same as Fig. 7.1, but now for an artifical situation with $a_{bg} < 0$. A resonance system with a negative background scattering length has only one bound state relatively close to threshold, which is shifted positive of the detuning. The next bound state in the potential is too far away to be of any significant influence. The line styles are the same as for Fig. 7.1.

population, so from equation (7.14) we find that the chemical potential is at the Fermi surface ($\mu = E_{\rm F}$). With this information, we solve the gap equation for the critical temperature. The result is the usual exponential dependence on the effective scattering length

$$T_c/T_F \approx \frac{8}{\pi} e^{\gamma-2} \exp(\frac{-\pi}{2k_{\rm F}|{\rm a_{eff}}|}), \tag{7.15}$$

where $\gamma \sim 0.5772$ is the Euler-Mascheroni constant, $k_{\rm F}$ is the Fermi wave number, and ${\rm a_{eff}} < 0$ is the effective scattering length produced by the Feshbach resonance ${\rm a_{eff}} = a_{\rm bg}(1 - \kappa/\bar{\nu})$.

The other limit we may consider is the strong coupling (BEC) limit. When the argument of the tanh function in the gap equation, Eq. (7.9), becomes sufficiently negative, it is a good approximation to use its asymptotic value of unity. What this implies, physically, is that the fermion statistics are unimportant in determining the value of the gap. This allows us to solve the gap equation for the chemical potential as a function of detuning. In the limit of large negative detuning we find that $\mu \to -E_b/2$, where $E_b \approx 1/ma_{\rm eff}^2$. Within this limit the entire population has been converted to molecules and we can solve the number equation to get the noninteracting BEC condensation temperature of $T_c/T_F \sim 0.218$.

7.5 Numerical results

To study the transition between the BEC and BCS regimes, we numerically solve Eqs. (7.9) and (7.14) for ^{40}K. The single resonance curve is produced using a background scattering length of $176a_0$ and $\kappa = 7.68$G at a density of $10^{14}{\rm cm}^{-3}$.

Figure 7.3 shows the critical temperature as a function of magnetic field detuning. The crossover calculation clearly merges with the BEC result for large-positive detunings and smoothly connects between positive and negative detunings, limiting to the Bose condensation temperature of $T_c/T_F \sim 0.218$ for large negative detuning. This approach

gives a maximum near zero detuning ($T_c/T_F \sim 0.26$).

Figure 7.4 shows the chemical potential as a function of detuning, beginning at the Fermi energy for positive detuning and approaching half the bound state energy at large negative detuning $\mu \to -E_b/2$. Figure 7.5 shows the change in population as a function of detuning. For large positive detuning, the system is composed solely of free fermions. As the detuning is decreased (i.e., from positive to negative) the contribution of the fermions begins to decrease until all the population is transferred into the atom pair component at $\nu \sim -0.5G$. The chemical potential is then equal to $-E_b/2$ and we may identify the atom pairs from that point on as the molecules. The superfluid behavior then comes from the condensation of these molecules.

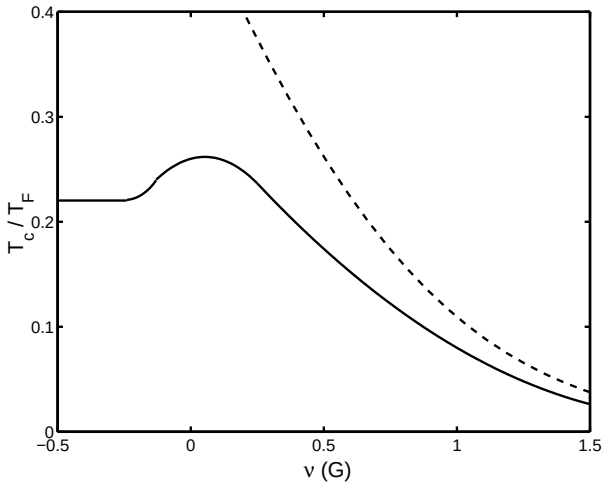

Figure 7.3: Critical temperature T/T_F as a function of detuning ν in Gauss. The dashed line corresponds to the usual BCS solution, which limits to the full crossover theory at large positive detuning. At negative detuning, T_c drops to the BEC condensation temperature of $T_c/T_F \sim 0.218$.

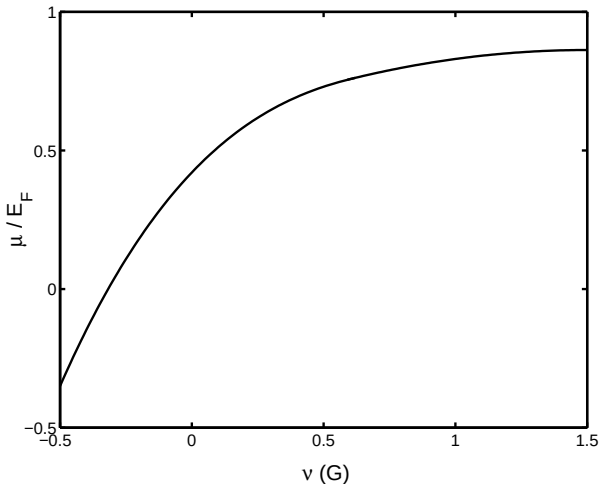

Figure 7.4: Chemical potential as a function of detuning ν in Gauss. For large negative detuning 2μ approaches the bound state energy of the molecular state. At increasing positive detuning, the chemical potential slowly approaches the Fermi energy.

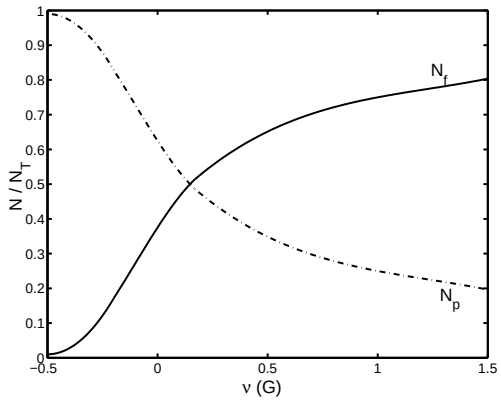

Figure 7.5: The fraction of the total population as a function of detuning ν in Gauss. The dot-dashed line corresponds to the pairing fraction N_p and the solid to the free fermion fraction N_f.

Chapter 8

Pseudogapped Crossover Theory

8.1 Introduction

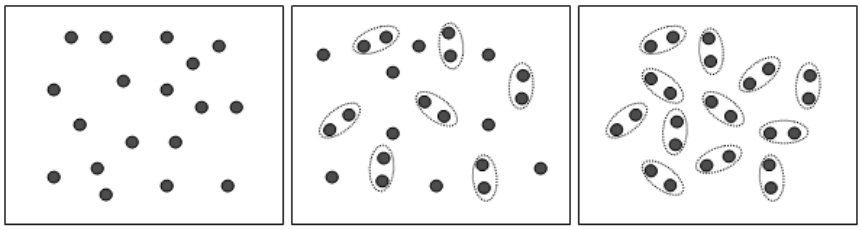

Figure 8.1: For weak coupling (left)the normal phase consists of interacting fermions. As the coupling is increases (middle) preformed pairs may appear. At lower temperatures these pairs may become coherent resulting in a superfluid transition. For strong couplings (right), the system is composed only of fermion pairs which may condense at low enough temperature.

The resonant crossover work discussed in the previous chapter introduced the idea of preformed pairs which form above the critical temperature for superfluidity. One would expect that the presence of these pairs would alter the nature of the gas from that of a simple degenerate Fermi gas. For instance, just as the presence of coherent, Cooper pairing modifies the energy spectrum below T_c, leading to the effects witnessed in superfluidity, we might expect that incoherent pairs might also modify the energy spectrum leading to other novel phenomena (see Fig. (8.1)). These above T_c effects are often referred to as "pseudogap" effects and the region between superfluidity and a

normal Fermi gas (the temperature noting this second phase is often referred to as T^*) is known as the pseudogap region.

Unfortunately, although beginning to account for the presence of preformed pairs, the work of the previous section has several shortcomings [90, 91], most notably, it does not account for the effects of the pseudogapped region above T_c. In fact, the form of the pair propagator given in Eq. (7.12) treats the pairs as composed of two free fermions uncoupled from the medium (i.e., there is no self-energy term in the propagators). In this section we wish to account for pseudogap effects by adapting a theory originally proposed by Kadanoff and Martin [92] and extended to account for high-T_c effects by several authors [93, 94, 95]. An alternative approach to including these pseudogap effects, in a non-resonant system, may be found in reference [96], although we feel this approach may overemphasize the importance of these contributions.

Although, at first it may appear quite different, the mode coupling approach we are about to present [97] is quite similar to the dynamical approach followed in Chapter 5. Now, however, higher-order correlations are to be accounted for. These correlations will result in the process of pair formation and will lead to the pseudogapped behavior we wish to incorporate.

8.2 Dynamical Green's function method

We begin with a discussion of dynamical Green's functions [98]. One method to solve for the single-particle Green's function, which encompasses all the information of a system, is to derive an infinite hierarchy of dynamical equations and then to truncate, or decouple, those equations at a given order. To see how this may be done we first define the single-particle Green's function:

$$\begin{aligned} G^{\alpha}(\mathbf{x}_1 t_1, \mathbf{x}_{1'} t_{1'}) &= -i \left\langle \mathrm{T}(\psi_\alpha(\mathbf{x}_1, \mathrm{t}_1)\psi_\alpha^\dagger(\mathbf{x}_{1'}, \mathrm{t}_{1'})) \right\rangle \\ &= -i \left(\Theta(t_1 - t_1') \left\langle \psi_\alpha(\mathbf{x}_1, t_1)\psi_\alpha^\dagger(\mathbf{x}_{1'}, t_{1'}) \right\rangle - \Theta(t_1' - t_1) \left\langle \psi_\alpha^\dagger(\mathbf{x}_{1'}, t_{1'})\psi_\alpha(\mathbf{x}_1, t_1) \right\rangle \right), \end{aligned} \tag{8.1}$$

where $\psi^\dagger_\alpha(\mathbf{x},t)$ ($\psi_\alpha(\mathbf{x},t)$) creates(destroys) a particle of spin index α at position x at time t and $\Theta(t_1 - t_1')$ is the step function defined as:

$$\Theta(t-t') = \begin{cases} 0, & t < t' \\ \\ 1, & t > t' \end{cases}. \tag{8.2}$$

The inclusion of the step function in the second line of Eq. (8.1) defines the time ordering T in the first. Higher-order Green's functions may be defined in a similar way

$$\begin{aligned} G_2^{\alpha\beta}(\mathbf{x}_1 t_1, \mathbf{x}_2 t_2; \mathbf{x}_{1'} t_{1'}, \mathbf{x}_{2'} t_{2'}) &= (-i)^2 \left\langle \psi_\alpha(\mathbf{x}_1,t_1)\psi_\beta(\mathbf{x}_2,t_2)\psi^\dagger_\beta(\mathbf{x}_{2'},t_{2'})\psi^\dagger_\alpha(\mathbf{x}_{1'},t_{1'})\right\rangle \\ G_3^{\alpha\beta\gamma}(\mathbf{x}_1 t_1, \mathbf{x}_2 t_2, \mathbf{x}_3 t_3; \mathbf{x}_{1'} t_{1'}, \mathbf{x}_{2'} t_{2'}, \mathbf{x}_{3'} t_{3'}) &= ...\text{etc.} \end{aligned} \tag{8.3}$$

We may also define the noninteracting Green's function by the useful relation

$$G_0^{-1}(\mathbf{x}_1,t_1)G_0(\mathbf{x}_1 t_1, \mathbf{x}_{1'} t_{1'}) = \delta(\mathbf{x}_1 t_1, \mathbf{x}_{1'} t_{1'}), \tag{8.4}$$

where we have suppressed the spin indexes in this last formula.

We would now like to generate a set of equations from which we may solve for the single-particle Green's function describing the interacting system. In what follows, we will focus on a two component system of interacting fermions and begin by defining the single-channel Hamiltonian ($\hbar = 1$):

$$H_A = \sum_\alpha \int d^3\mathbf{x}\ \psi^\dagger_\alpha(\mathbf{x})(-\frac{\nabla^2}{2m})\psi_\alpha(\mathbf{x}) + \int d^3\mathbf{x} d^3\mathbf{x}'\ \psi^\dagger_\uparrow(\mathbf{x})\psi^\dagger_\downarrow(\mathbf{x}')U(\mathbf{x},\mathbf{x}')\psi_\downarrow(\mathbf{x}')\psi_\uparrow(\mathbf{x}), \tag{8.5}$$

where α runs over all spin components. An entire hierarchy of dynamical equations can be generated starting with the equation of motion for the field operator

$$i\frac{\partial}{\partial t}\psi_\alpha(\mathbf{x}t) = -\frac{\nabla^2}{2m}\psi_\alpha(\mathbf{x}t) + \int d^3\bar{\mathbf{x}}\ U(\mathbf{x},\bar{\mathbf{x}})\psi^\dagger_\beta(\bar{\mathbf{x}}t)\psi_\beta(\bar{\mathbf{x}}t)\psi_\alpha(\mathbf{x}t). \tag{8.6}$$

For example, the equation of motion for the first order Green's function is

$$\begin{aligned} \left(i\frac{\partial}{\partial t_1} + \frac{\nabla_1^2}{2m}\right) G^\alpha(\mathbf{x}_1 t_1, \mathbf{x}_{1'} t_{1'}) &= \delta^3(\mathbf{x}_1 - \mathbf{x}_{1'})\delta(t_1 - t_{1'}) \\ &- i\int d^3\bar{\mathbf{x}}\ U(\mathbf{x}_1,\bar{\mathbf{x}})G_2^{\alpha\beta}(\mathbf{x}_1 t_1, \bar{\mathbf{x}}t_1; \mathbf{x}_{1'} t_{1'}, \bar{\mathbf{x}}t_1^+). \end{aligned} \tag{8.7}$$

Here we have introduced the argument t^+ to denote an infinitesimal positive time above t so that we may cast the equation in the above form. Likewise, we may solve for the equation of motion of the second order Green's function

$$\left(i\frac{\partial}{\partial t_1}+\frac{\nabla_1^2}{2m}\right)G_2^{\alpha\beta}(\mathbf{x}_1t_1,\mathbf{x}_2t_2;\mathbf{x}_{1'}t_{1'},\mathbf{x}_{2'}t_{2'}) = \delta^3(\mathbf{x}_1-\mathbf{x}_{1'})\delta(t_1-t_{1'})G^{\alpha}(\mathbf{x}_2t_2,\mathbf{x}_{2'}t_{2'}) - i\int d\bar{\mathbf{x}}^3U(\mathbf{x}_1,\bar{\mathbf{x}})G_3^{\alpha\beta\beta}(\mathbf{x}_1t_1,\mathbf{x}_2t_2,\bar{\mathbf{x}}t_1;\mathbf{x}_{1'}t_{1'},\mathbf{x}_{2'}t_{2'},\bar{\mathbf{x}}t_1^+). \quad (8.8)$$

This procedure, of course, may be continued ad nauseam, but, in order to make use of these equations, the hierarchy will need to be truncated at a given order. The method chosen for performing this truncation sets the level of approximation at which we are calculating the single-particle Green's function. The next section discusses various ways in which this may be done.

8.3 Truncation of the equations of motion

For the work that follows in this chapter, we will chose to truncate this hierarchy of equations at the order of the two-particle Green's function G_2. We must, therefore, decide how to properly account for the coupling of Eq. (8.8) to the three-particle Green's function G_3. For the moment, we will not consider anomalous correlations, but instead will focus on the region $T > T_c$ where we assume only conserving correlations are relevant. Under this condition, and the assumption that we have an equal mixture of spin states, we may keep only correlations which conserve both spin and number. A lowest order approximation of this type would be to factorize G_3 as:

$$G_3^{\alpha\beta\beta}(1,2,\bar{1};1'2',\bar{1}^+) \approx G(1,1')G(2,2')G(\bar{1},\bar{1}^+) - G(1,1')G(2,\bar{1}^+)G(\bar{1},2'). \quad (8.9)$$

We have introduced the 4-vector notation $(1) = (\mathbf{x},t)$ for convenience in writing the various correlation functions. The above factorization is just the usual Hartree-Fock (HF) approximation encountered throughout this thesis and neglects the effects of all but pairwise correlations. This is the level of approximation used in Chapter 5, however,

we would like to go beyond this approximation to begin to account for higher order correlations between the particles.

A next order factorization would involve writing G_3 in terms of factors of GG_2 and GGG. This is known as a cumulant expansion and may be written [92]:

$$\begin{aligned} G_3^{\alpha\beta\beta}(1,2,\bar{1};1',2',\bar{1}^+) \approx\ & G(2,2')G_2^{\alpha\beta}(1,\bar{1};1',\bar{1}^+) + G(\bar{1},\bar{1}^+)G_2^{\alpha\beta}(1,2;1',2') \\ -\ & G(2,\bar{1}^+)G_2^{\alpha\beta}(1,\bar{1};1',2') - G(\bar{1},2')G_2^{\alpha\beta}(1,2;1',\bar{1}^+) \\ -\ & G(1,1')G(2,2')G(\bar{1},\bar{1}^+) + G(1,1')G(2,\bar{1}^+)G(\bar{1},2'). \end{aligned} \tag{8.10}$$

In the above equation we have dropped the correlated component of $G(1,1')G_2^{\beta\beta}(2,\bar{1};2',\bar{1}^+)$ since only particles of opposite spin may collide. Notice that if we were to Wick expand the various G_2 functions we would indeed get the HF result of Eq. (8.9). Physically, the form for the three-particle Green's function G_3, which we have written, describes the interaction of three particles taking into account that two of the particles may be correlated during the interaction process and neglects all higher order correlations (see Fig. 8.2).

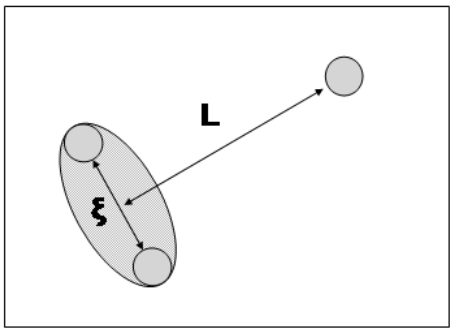

Figure 8.2: The factorization performed in Eq. (8.10) approximates the collisions of three particles by the scattering of a particle off a correlated pair. The approximation should remain valid, even for strong pair-correlations, so long as the pair size ξ remains smaller than the mean inter-particle spacing L.

Substituting the form of G_3 given by Eq. (8.10) into Eq. (8.8), we may write Eq. (8.8)

as:

$$\left(i\frac{\partial}{\partial t_1}+\frac{\nabla_1^2}{2m}\right)L_2^{\alpha\beta}(1,2;1',2') = -i\int d\bar{1}\; U(1,\bar{1})[G(\bar{1},\bar{1}^+)L_2^{\alpha\beta}(1,2;1',2')) - G(2,\bar{1}^+)G_2^{\alpha\beta}(1,\bar{1};1',2') - G(\bar{1},2')L_2^{\alpha\beta}(1,2;1',\bar{1}^+)], \tag{8.11}$$

where I have made use of Eqs. (8.4) and (8.7), and have introduced the notation

$$L_2^{\alpha\beta}(1,2;1',2') = G_2^{\alpha\beta}(1,2;1',2')' - G(1,1')G(2,2'). \tag{8.12}$$

This new function L_2 accounts for the correlated part of the Green's function G_2. Now, by absorbing the shift given by the first term on the right hand side of Eq. (8.11) into the definition of the free-particle Green's function, we may simplify things even further:

$$\tilde{G}_0^{-1}(1)L_2^{\alpha\beta}(1,2;1',2') = i\int d\bar{1}\; U(1,\bar{1})\Big[G(2,\bar{1}^+)G_2^{\alpha\beta}(1,\bar{1};1',2') \;+\; G(\bar{1},2')L_2^{\alpha\beta}(1,2;1',\bar{1}^+)\Big], \tag{8.13}$$

where

$$\tilde{G}_0^{-1}(1) = G_0^{-1}(1) + i\int d\bar{1}\; U(1,\bar{1})G(\bar{1},\bar{1}^+), \tag{8.14}$$

and we have identified the free particle Green's function

$$G_0^{-1}(1) = \left(i\frac{\partial}{\partial t_1}+\frac{\nabla_1^2}{2m}\right). \tag{8.15}$$

The first term on the right hand side of Eq. (8.13) will produce a series of ladder diagrams. The second term, which represents all the multiple scattering events where the interaction lines cross, we will drop. It is hoped that the ladder summation will account for the dominant processes involved. These statements might be made clearer by representing Eq. (8.13) diagrammatically, as shown in Fig. 8.3.

The above approximation, as noted in the caption of Fig. 8.2, should remain valid in the regime where the correlation length between pairs of atoms remains smaller than the mean inter-particle spacing. This is just the sort of term that we are interested in since it introduces the process of an atom scattering off a correlated pair, in analogy to

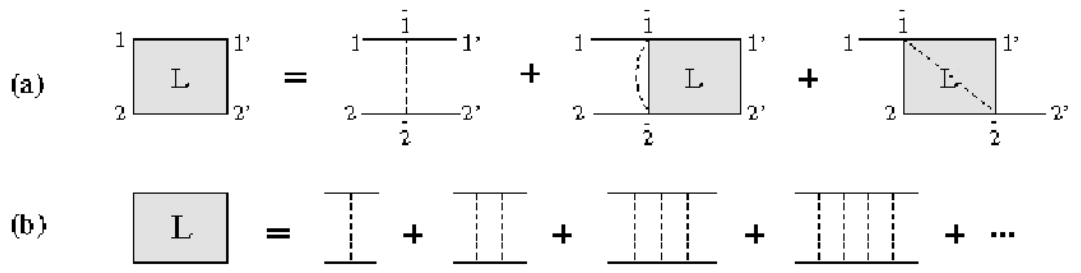

Figure 8.3: (a) Diagrammatic representation of Eq. 8.13. The thin lines denote the free Green's functions $\tilde{G}_0$, thick lines are the full Green's functions G, and dotted lines represent the interaction U. (b) Diagrammatic representation of the resulting ladder summation.

the scattering of an atom and a molecule. The final result is an integral equation for G_2 which may be written as:

$$G_2^{\alpha\beta}(1,2;1',2') = G(1,1')G(2,2') + i\int d\bar{1}\ d\bar{2}\ \tilde{G}_0(1,\bar{1})U(\bar{1},\bar{2})G(2,\bar{2})G_2^{\alpha\beta}(\bar{1},\bar{2};1',2') \tag{8.16}$$

We have written the above equation in this form to illustrate the extension from the Hartree-Fock approach (notice the lowest order term is just the HF result).

8.4 Extension to resonant Hamiltonian

Equation (8.16) was derived for the single-channel Hamiltonian of Eq. (8.5). We would like to extend these results to account for a molecular channel so, as we have done earlier, we include the resonant molecular processes in the hamiltonian:

$$\begin{aligned} H_B &= \int d^3x \varphi_m^\dagger(\mathbf{x}) \left(-\frac{\nabla^2}{4m} + \nu\right) \varphi_m(\mathbf{x}) \\ &+ \int d^3x d^3x' \left[\varphi_m^\dagger(\frac{\mathbf{x}+\mathbf{x}'}{2}) g(\mathbf{x}-\mathbf{x}') \psi_\downarrow(\mathbf{x}) \psi_\uparrow(\mathbf{x}) + h.c.\right]. \end{aligned} \tag{8.17}$$

In analogy to the previous section, we first define the molecular Green's function

$$D(\mathbf{x}_1 t_1, \mathbf{x}_{1'} t_{1'}) = -i\langle T(\varphi_m(\mathbf{x}_1, t_1)\varphi_m^\dagger(\mathbf{x}_{1'}, t_{1'}))\rangle. \tag{8.18}$$

We could likewise define higher order molecular Green's functions in much the same way as we defined the higher order Fermi Green's functions. For the moment, let us only introduce this definition. What's more, we must now write down what we may refer to simply as "mixed" Green's function

$$M(\mathbf{x}_1 t_1, \mathbf{x}_2 t_2; \mathbf{x}_{1'} t_{1'}) = (-i)^2 \langle T(\psi_\uparrow(\mathbf{x}_1, t_1)\psi_\downarrow(\mathbf{x}_2, t_2)\varphi_m^\dagger(\mathbf{x}_{1'}, t_{1'}))\rangle, \tag{8.19}$$

which accounts for correlations between atoms and molecules. We will quickly see that these two definitions are all we will need.

Using the full resonant Hamiltonian we may derive the equation of motion for the molecular field operator as:

$$i\frac{\partial}{\partial t}\varphi_m(\mathbf{x}t) = \frac{-\nabla^2}{4m}\varphi_m(\mathbf{x}t) + \int d^3\bar{x} g(\mathbf{x}, \bar{\mathbf{x}})\psi_\downarrow(\bar{\mathbf{x}})\psi_\uparrow(\mathbf{x}) \tag{8.20}$$

From this equation, naturally, follows the equation for the lowest order molecular Green's function

$$\begin{aligned}\left(i\frac{\partial}{\partial t_1} + \frac{\nabla_1^2}{4m}\right) D(\mathbf{x}_1 t_1, \mathbf{x}_{1'} t_{1'}) &= \delta^3(\mathbf{x}_1 - \mathbf{x}_{1'})\delta(t_1 - t_{1'}) \\ &- i\int d^3\bar{x}\ g(\mathbf{x}_1, \bar{\mathbf{x}}) M(\bar{\mathbf{x}}t_1, \bar{\mathbf{x}}t_1; \mathbf{x}_{1'} t_{1'}).\end{aligned} \tag{8.21}$$

From Eq. (8.21) we see that the coupling to higher order terms is through the mixed function M. If we now look at the equation of motion for the mixed Green's function, once again making use of Eq. (8.20), we find:

$$\left(i\frac{\partial}{\partial t_1} + \frac{\nabla_1^2}{4m}\right) M(\mathbf{x}_1 t_1, \mathbf{x}_1 t_1; \mathbf{x}_{1'} t_{1'}) = -\int d^3\bar{x} g(\mathbf{x}_1, \bar{\mathbf{x}}) G_2^{\alpha\beta}(\mathbf{x}_1 t_1, \bar{\mathbf{x}}t_1; \mathbf{x}_{1'} t_{1'}, \bar{\mathbf{x}}t_1^+). \tag{8.22}$$

Notice that this equation can be solved for M and plugged into our earlier Eq. (8.21) to derive a relation for the full molecular Green's function in terms of G_2. From this result we find that the modification to Eq. (8.7) is equivalent to the substitution

$$V_{eff}(\mathbf{x}, \mathbf{x}') = U(\mathbf{x}, \mathbf{x}') - D_0(\mathbf{x}, \mathbf{x}')g(\mathbf{x}, \mathbf{x}')^2, \tag{8.23}$$

where we have defined the free molecular Green's function

$$D_0^{-1} = i\frac{\partial}{\partial t_1} + \frac{\nabla_1^2}{4m}. \tag{8.24}$$

Therefore, as far as the fermionic part of our problem is concerned, the only modification that the resonant part of the Hamiltonian incurs is that the fermions now interact through the effective potential V_{eff}. This is an equivalent result as to what we found in Chapter 7 (see Eq. (7.8)) in our adaptation of the NSR approach to the resonant molecular system.

8.5 Self-energy and definition of the t-matrix

It is much easier to work in momentum space since the integral equations found in the previous section convert into algebraic equations. From Eqs. (8.7) and (8.16) we may immediately write an equation for the full Green's function

$$G = \tilde{G}_0 + i\tilde{G}_0\frac{\chi V_{eff}}{1+\xi}\tilde{G}_0 G, \tag{8.25}$$

where we define the pair susceptibility to be

$$\chi = -iV_{eff}\tilde{G}_0 G. \tag{8.26}$$

This should be compared to the resonant NSR susceptibility of Eq. (7.12) which is composed of two free propagators. The inclusion of the fully dressed Green's function G in the susceptibility is one of the major extensions of this approach since the presence of a self-energy couples the pairs to the medium.

In deriving Eq. (8.25) we have made the minor simplification of replacing one GG pair, appearing in the numerator, with a $\tilde{G}_0 G$ pair. This is equivalent to replacing the upper, left-most, full Green's function arm, in the ladder diagram of Fig. 8.3, with a bare Green's function $\tilde{G}_0$. This results in the irreducible self-energy:

$$\Sigma = \tilde{G}_0^{-1} - G^{-1} = i\frac{\chi V_{eff}}{1+\xi}\tilde{G}_0. \tag{8.27}$$

To further simplify the equations, we make an approximation in how we incorporate the Hartree shift of the free Green's function (as given in Eq. 8.14), that is, we put it back into the self-energy at lowest order and replace $\tilde{G}_0$ with G_0. This results in the following equation for the self-energy.

$$\Sigma = G_0^{-1} - G^{-1} = \frac{-iV_{eff}G_0}{1+\chi} \equiv tG_0. \tag{8.28}$$

This last equation gives a general definition for the t-matrix t. The t-matrix will prove to be a useful quantity since it may be used to define the critical point of superfluidity. This statement, known as the Thouless criterion, states that the onset of superfluidity occurs as an instability in the t-matrix or:

$$t^{-1} = 0. \tag{8.29}$$

We will often refer back to this condition in the following section.

8.6 Foundations of a pseudogapped resonant crossover theory

Before moving to a discussion on the application of sections 8.3-8.5 to the superfluid regime, $T < T_c$, let us first summarize the major results which we have found. To this end, we begin with the Hamiltonian describing the atomic resonance system written in momentum space:

$$\begin{aligned} H \quad - \quad \mu N &= \sum_{\mathbf{k},\sigma} \epsilon_{\mathbf{k}} a^\dagger_{\mathbf{k},\sigma} a_{\mathbf{k},\sigma} + \sum_{\mathbf{q}} (\epsilon^m_{\mathbf{q}} + \nu) b^\dagger_{\mathbf{q}} b_{\mathbf{q}} \\ &+ \sum_{\mathbf{q},\mathbf{k},\mathbf{k}'} U(\mathbf{k},\mathbf{k}') a^\dagger_{\mathbf{q}/2+\mathbf{k},\uparrow} a^\dagger_{\mathbf{q}/2-\mathbf{k},\downarrow} a_{\mathbf{q}/2-\mathbf{k}',\downarrow} a_{\mathbf{q}/2+\mathbf{k}',\uparrow} \\ &+ \sum_{\mathbf{q},\mathbf{k}} \left(g(\mathbf{k}) b^\dagger_{\mathbf{q}} a_{\mathbf{q}/2-\mathbf{k},\downarrow} a_{\mathbf{q}/2+\mathbf{k},\uparrow} + \text{h.c.} \right). \end{aligned} \tag{8.30}$$

The above Hamiltonian, which should be familiar to the reader by now, contains both fermions $a_{\mathbf{k},\sigma}$ and (spinless) bosonic molecules $b_{\mathbf{q}}$ (the sum in σ runs over both spin states $\{\uparrow,\downarrow\}$). The free dispersion relations for fermions and bosons are given by:

$$\epsilon_{\mathbf{k}} = k^2/2m - \mu \quad \text{and} \quad \epsilon^m_{\mathbf{q}} = q^2/2M - 2\mu, \tag{8.31}$$

respectively, where we assume an equal proportion of spins $\mu_\uparrow = \mu_\downarrow$ and the mass of the boson is just twice that of the a single fermion $M = 2m$. Once again, ν is the detuning of the resonance state.

Until this point we have solely made use of contact potentials within all our many-body theories. However, for the work that follows, we will use a set of Gaussian, separable potentials. For instance, we set the direct s-wave interaction $U(\mathbf{k}, \mathbf{k}') = U\varphi_{\mathbf{k}}\varphi_{\mathbf{k}'}$ and the Feshbach coupling $g(\mathbf{k}) = g\varphi_{\mathbf{k}}$, where the function $\varphi_{\mathbf{k}}^2 = \exp\{-(k/K_c)^2\}$ provides a momentum cutoff K_c (note, we have set $\hbar = k_B = 1$). This choice of potentials, although at the same level of accuracy as the contact potential model, proves more amenable to our later numerical calculations and may be renormalized by the relations given in Appendix A.3.

We have recognized the relevant propagators for the resonant system. These are the propagator for the fermion pairs $t(Q)$, for the molecular bosons $D(Q)$, and for the individual fermions $G(Q)$. As we have seen, the interaction effects induced by the molecular field are equivalent to an effective pairing interaction. For the separable Gaussian potentials we have introduced, this may be written as

$$\tilde{g}_{eff}(Q, K, K') = g_{eff}(Q)\varphi_{\mathbf{k}}\varphi_{\mathbf{k}'}, \tag{8.32}$$

with

$$g_{eff}(Q) \equiv U + g^2 D_0(Q), \tag{8.33}$$

where $D_0(Q) \equiv 1/[i\Omega_n - q^2/2M - \nu + 2\mu]$ is the non-interacting molecular boson propagator (see Eq. (8.23)).

We have also found a particular form for the fermion pair-susceptibility, or the pair propagator $\chi(Q)$:

$$\chi(Q) = \sum_K G(K)G_0(Q - K)\varphi_{\mathbf{k}-\mathbf{q}/2}^2, \tag{8.34}$$

provided that the fermion self-energy appearing in the dressed propagator G is

$$\Sigma(K) = \sum_{Q} t(Q) G_0(Q-K) \varphi^2_{\mathbf{k}-\mathbf{q}/2}. \tag{8.35}$$

Here and throughout, we take the convention $\sum_K \equiv T\sum_{\omega_n}\sum_{\mathbf{k}}$, where K is a 4-vector of wavenumber $\mathbf{k}$ and Matsubara frequency ω_n. The form of Eq. (8.34) will allow us to account for non-condensed atom pairs and, in contrast to that found by NSR, accounts for a *dressed* fermion pair.

8.7 Extension below T_c and the appearance of an order parameter

So far we have only considered the region $T > T_c$ and would now like to extend our results to temperatures below the critical temperature, $T < T_c$. To properly incorporate the onset of the phase transition one could imagine going back through the work of sections 8.2-8.5 to incorporate anomalous contributions into the various propagator expansions. In fact, this is just what Kadanoff and Martin did [92] at the level of the Hartree-Fock approximation (for the nonresonant case), resulting in the conventional equations of BCS theory. The resulting t-matrix they found was the following:

$$t(Q) = -\frac{\Delta^2}{T}\delta(Q). \tag{8.36}$$

The singular nature of such a function leads us to think that it is this contribution to the t-matrix that dominates the onset of long-range order and that, perhaps, higher order anomalous contributions are negligible. We propose that the full scattering t-matrix should be composed of the BCS pairing interaction and an additional interaction which leads to non-condensed Cooper pairs:

$$t = t_{sc} + t_{pg}, \tag{8.37}$$

where t_{sc} is the superfluid condensate component and t_{pg} is the pseudogapped contribution. For the resonant system these may be defined as

$$t_{sc}(Q) = -\frac{\tilde{\Delta}^2_{sc}}{T}\delta(Q), \tag{8.38}$$

$$t_{pg}(Q) = \frac{g_{eff}(Q)}{1 + g_{eff}(Q)\chi(Q)}, \qquad Q \neq 0. \tag{8.39}$$

Equation (8.38) is just a restatement of Eq. (8.36) for the resonant system and Eq. (8.39) comes from our $T > T_c$ result of the pseudogap process, Eq. (8.28). The effective, resonant interaction $g_{eff}(Q)$ is defined in Eq. (8.33) and the susceptibility $\chi(Q)$ is given by Eq. (8.34).

We identify the order parameter previously encountered in Chapter 5:

$$\tilde{\Delta}_{sc} = \Delta_{sc} - g\phi_m, \tag{8.40}$$

where $\phi_m = \langle b_{\mathbf{q}=0} \rangle$ is the condensed molecular component and $\Delta_{sc} = -U \sum_{\mathbf{k}} \langle a_{-\mathbf{k}\downarrow} a_{\mathbf{k}\uparrow} \rangle \varphi_{\mathbf{k}}$ is the standard BCS gap. The order parameter is a linear combination of both a pairing field and the closed-channel condensed molecules. It is, perhaps, enlightening to contrast this choice of an order parameter with the classic work of Fano on resonances [99]. For a potential resonance dominated by a bound state Fano chose the following ansatz for the wavefunction of eigenvalue E:

$$\Psi_E = a\varphi + \int dE' b_{E'} \psi_{E'}. \tag{8.41}$$

The above form is composed of a linear combination of a bound state φ and a range of continuum states ψ'_E (a and b being constants). Fano found that this choice of wavefunction could be used to exactly solve the resonant problem. Although, strictly speaking, Eq. (8.41) is derived from a 2-body picture it shows a striking resemblance to the order parameter of Eq. (8.40).

It is worthwhile to write the order parameter, Eq. (8.40), in a form more closely resembling that of BCS theory. In Chapter 5.4 we found that the two components of the order parameter, ϕ and Δ_{sc}, are not independent, but are connected by the relation

$$\phi_m = \frac{g\Delta_{sc}}{(\nu - 2\mu)U}. \tag{8.42}$$

This implies that

$$\tilde{\Delta}_{sc} = -g_{eff}(0) \sum_{\mathbf{k}} \langle a_{-\mathbf{k}\downarrow} a_{\mathbf{k}\uparrow} \rangle \varphi_{\mathbf{k}}, \tag{8.43}$$

as one might expect.

8.8 Self-consistent equations for $T < T_c$

The form of the order parameter, Eq. (8.40), implies that the molecular bosons condense at the same temperature as a pairing field develops. Another way to state this would be:

$$D^{-1}(0) = t^{-1}(0) = 0, \qquad T \leq T_c, \tag{8.44}$$

where D is the full bosonic Green's function. This statement simply relates the Thouless criterion to the criterion for Bose-Einstein condensation. Equation (8.44) leads to the important result:

$$t^{-1}(0) = g_{eff}^{-1}(0) + \chi(0) = 0, \qquad T \leq T_c. \tag{8.45}$$

Equations (8.44) and (8.45) demand the following form for the bosonic self-energy:

$$\Sigma_B(Q) \equiv -g^2\chi(Q)/[1 + U\chi(Q)], \tag{8.46}$$

which remains valid for $T \leq T_c$. Therefore, the full bosonic propagator is given by

$$D(Q) \equiv \frac{1}{i\Omega_n - E_q^0 - \nu + 2\mu - \Sigma_B(Q)}. \tag{8.47}$$

Equation (8.45) implies that t_{pg} is extremely sharp for all temperatures $T \leq T_c$. We may make use of the sharpness of the t-matrix to approximate Eq. (8.35) to yield a BCS-like self-energy

$$\Sigma(K) \approx -G_0(-K)\Delta^2\varphi_{\mathbf{k}}^2, \tag{8.48}$$

with the following definition for the full gap:

$$\Delta^2 \equiv \tilde{\Delta}_{sc}^2 + \Delta_{pg}^2, \tag{8.49}$$

and where we have defined the pseudogap parameter Δ_{pg}

$$\Delta_{pg}^2 \equiv -\sum_{Q\neq 0} t_{pg}(Q). \tag{8.50}$$

For a more detailed discussion of the validity of this approximation see Maly et *al.* [100].

With these results, Eq. (8.45) can now be written as

$$g_{eff}^{-1}(0) + \sum_{\mathbf{k}} \frac{1 - 2f(E_{\mathbf{k}})}{2E_{\mathbf{k}}} \varphi_{\mathbf{k}}^2 = 0, \qquad T \leq T_c \,, \tag{8.51}$$

where $E_{\mathbf{k}} = \sqrt{\epsilon_{\mathbf{k}}^2 + \Delta^2 \varphi_{\mathbf{k}}^2}$. Equation (8.51) is identical in form to the conventional BCS equation, but the full excitation gap Δ, as distinguished from the order parameter $\tilde{\Delta}_{sc}$, now appears in the dispersion $E_{\mathbf{k}}$.

To close these equations, we must now calculate the total particle number from the propagators involved. The number of molecular bosons is given directly by $n_b = -\sum_Q D(Q)$. The number of fermions is

$$n_f = \sum_{\mathbf{k}} \left[1 - \frac{\epsilon_{\mathbf{k}}}{E_{\mathbf{k}}} + 2 \frac{\epsilon_{\mathbf{k}}}{E_{\mathbf{k}}} f(E_{\mathbf{k}}) \right] \,, \tag{8.52}$$

as follows from the condition $n_f = 2\sum_K G(K)$. The total number N of particles is, therefore, given by

$$n_f + 2n_b + 2n_b^0 = N \,, \tag{8.53}$$

where $n_b^0 = \phi_m^2$ is the number of molecular bosons in the condensate. Equations (8.50), (8.51), and (8.53) form a closed set of equations for our resonance system. It should be noted that at $T = 0$ the pseudogap parameter, Eq. (8.50), vanishes ($\Delta_{pg} \to 0$) so that $\tilde{\Delta}_{sc}(0) = \Delta(0)$ and we reproduce BCS theory. In fact, one of the defining characteristics of this theory is that, at zero temperature, we reproduce the Leggett groundstate suggested in [81]. This would say that all the pseudogap behavior results from finite-temperature effects and at $T = 0$ the system is accurately described by conventional BCS theory.

An essential distinction between this and previous crossover studies based on the NSR approach [84, 101], below T_c, is that the modification to the energy spectrum is not fully accounted for by the superconducting gap, $\Delta \neq \tilde{\Delta}_{sc}$. This distinction, also absent in strict BCS theory, is to be associated with non-condensed bosonic excitations

of the superfluid. The spectrum of these excitations are modified due to the presence of other excitations. That is, the particles acquire a self-energy from other pairs present within the medium, which is fed back into the propagator for the pairs.

8.9 Numerical solution of the pseudogapped theory

We now numerically solve Eqs. (8.50), (8.51), and (8.53) for a homogeneous system. Although most atomic gas experiments are confined to a harmonic trapping potential, we don't expect the inhomogeneity of the trap to qualitatively alter the results we present here. To aid us in this task, we make use of the divergence of the t-matrix, expressed by Eq. (8.45). This allows us to Taylor expand the quantity $\chi(Q)$ in Eqs. (8.53) and (8.50) to first order in Ω and q^2:

$$\chi(Q) \approx \chi(0) + a_0(i\Omega_n - B_0 q^2). \tag{8.54}$$

We may expand $g_{eff}(Q)$ and $\Sigma_B(Q)$ in a similar fashion. These expansions considerably simplify the analysis (see Appendix E for a discussion of the expansion coefficients a_0 and B_0 and for a detailed discussion of implementing the pseudogap equations).

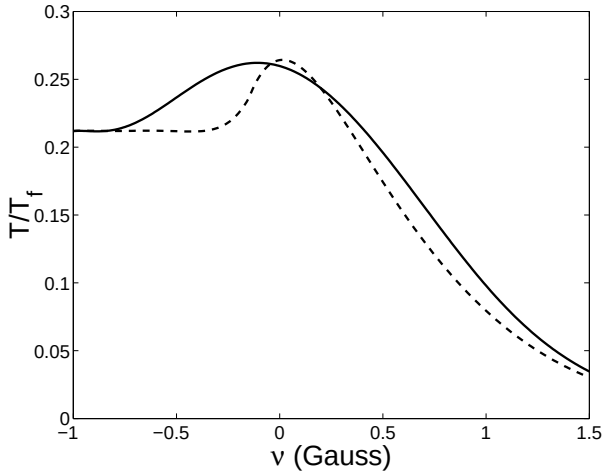

Figure 8.4: Comparison between the NSR approach (dashed line) and the pseudogap theory (solid line) for the critical temperature T_c/T_F of ^{40}K as a function of detuning ν. All parameters are chosen to be the same as those of Fig. 7.3.

We begin by comparing the results of the pseudogap theory to our earlier work of Chapter 7 where we analyzed the crossover for the case of ^{40}K. Figure 8.4 shows a direct comparison between the critical temperature prediction of the resonant NSR approach and the pseudogap equations we have just presented. With the inclusion of higher order corrections we still retain a pronounced maximum in T_c near the resonance at about $0.26T_F$.

To aid in illustrating the behavior of the resonant pseudogap equations we will leave the case of ^{40}K aside for a moment and instead explore a model atom more conducive to our discussion. We make this switch due to the positive value of the background scattering length in ^{40}K. This implies the presence of a bound state in the open channel which leads to an avoided crossing when the resonant molecular state is lowered well below threshold. Since we are not interested in this process, but would rather discuss the asymptotic case of a fully populated molecular fraction, we study a model atom with negative background scattering length. We choose $\bar{g}/E_F = -42$ and $\bar{U}/E_F = -3$ as indicative of currently trapped atomic Fermi gases. These parameters are, in fact, the same as those of ^{40}K, but we have flipped the sign of the background scattering length.

First we calculate T_c as a function of $\bar{\nu}$ which is plotted in Fig. 8.5. For $\bar{\nu} \to -\infty$, T_c approaches the ideal BEC limit. As $\bar{\nu} \to +\infty$, the bosonic populations become irrelevant and the asymptote of the curve is dictated by the behavior of the open channel fermions in the presence of the background interaction $\bar{U}$. It should be noted that in this work we have chosen a small $\bar{U}$ deliberately so that $\bar{\nu} \to \infty$ limits to BCS theory. The figure indicates that, while there are differences in the shape of the T_c vs. $\bar{\nu}$ curve, the overall magnitudes are not so different from those found within our earlier NSR-based approach. More generally, we could contemplate a moderate value of $\bar{U}$ where the asymptotic superfluid state will have a pseudogap. This might be relevant in the case of an atom such as ^{6}Li where the open channel contains a bound state close to

threshold leading to a large negative background scattering length, $a_{bg} \sim -2500a_0$.

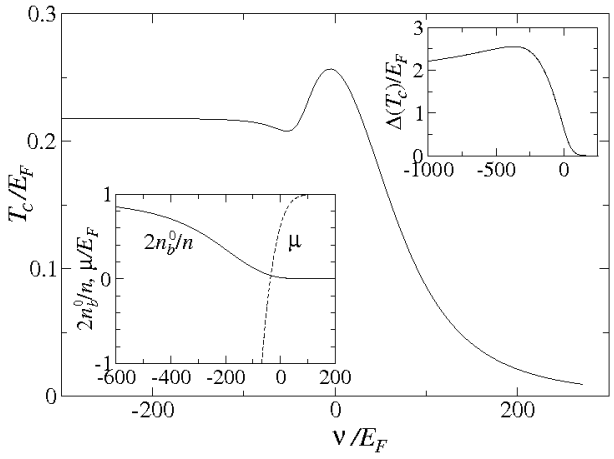

Figure 8.5: T_c vs. detuning ν with a pronounced maximum near threshold. The upper right inset plots the pseudogap at T_c vs. $\bar{\nu}$ with a maximum at large negative detuning. The lower left inset plots the molecular contribution to the condensate weight and the fermionic chemical potential.

Indicated as an inset in the figure is the behavior of $\Delta(T_c)$ as a function of $\bar{\nu}$. As $\bar{\nu}$ approaches the resonance from $+\infty$, T_c first increases following the BCS trend, which reflects an increasingly attractive pairing interaction. Likewise, the pseudogap, which starts at zero, begins to grow. At the point where the pseudogap becomes appreciable, the rise in T_c slows down. Eventually T_c decreases as fewer fermions are available to pair. An interesting feature of the pseudogap plot is that a maximum arises at large negative detuning. This behavior has not been witnessed in the non-resonant theory.

In the inset to Fig. 8.6, we plot the temperature dependence of the normalized excitation gap $\Delta(T)/\Delta(0)$ for three values of the detuning $\bar{\nu}/E_F = -200, -5, +200$. The middle value roughly corresponds to the maximum in T_c, where pseudogap effects should be the most apparent. The first and last are illustrative of the BEC and BCS limits, respectively. We, thus, refer below to these three values as the BEC, PG, and BCS cases. The order parameter, $\tilde{\Delta}_{sc}$, is not plotted here, but for all three cases it is rather close to the solid line in the inset. That $\Delta(T)$ is relatively constant with T

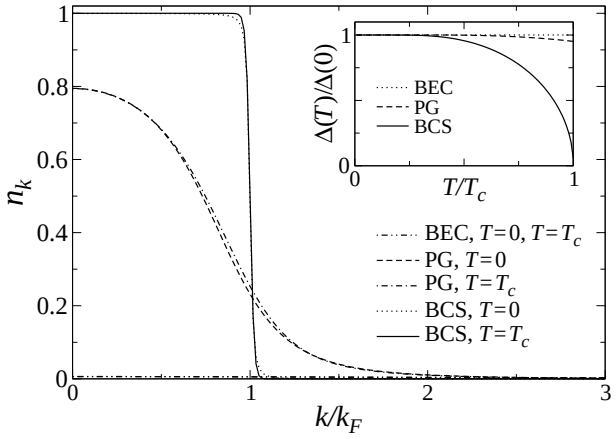

Figure 8.6: Fermionic momentum distribution function at $T = 0$ and $T = T_c$ for the three regimes. *PG* corresponds to maximal T_c. Inset plots the T dependent excitation gap below T_c.

through the superfluid transition is to be expected in the presence of preformed pairs, as we see for $\bar{\nu}/E_F = -5$ and -200.

It should be stressed that the critical temperature T_c for the phase transition to superfluidity is only apparent in $\Delta(T)$ for the BCS case. To stress this point, in the body of Fig. 8.6, we plot the fermionic momentum distribution function n_k, which is the summand in Eq. (8.52):

$$n_k = \left[1 - \frac{\epsilon_{\mathbf{k}}}{E_{\mathbf{k}}} + 2\frac{\epsilon_{\mathbf{k}}}{E_{\mathbf{k}}} f(E_{\mathbf{k}})\right], \tag{8.55}$$

at $T = 0$ and $T = T_c$. From the figure, it is clear that there is very little temperature dependence between $T = 0$ and $T = T_c$. This is a clear sign that the momentum distribution is not a good indicator of phase coherent pairing [102]. For the *PG* case, where the critical temperature is a maximum, this results in the near temperature independence of $\Delta(T)$. In the far BEC limit the excitation gap does not vary at all through T_c. In the BCS regime, $\Delta(T)$ is so small as to be barely perceptible in the figure. In order to address the question of whether a clear signature can be seen in the particle density distribution [49, 60] these results must be generalized to a trapped system. A simple approach would be to treat the system under a local density approximation as

was done in Chapter 5.

This pseudogap based phenomenology is well documented in high-T_c superconductors. For these materials, penetration depth data provides a direct probe of the transition to superconductivity. Interestingly enough, densities of state measurements in the Cuprates also show some indications of the establishment of order throughout the sample. To see how phase coherence enters in the context of atomic physics, we relax the approximation of Eq. (8.48) by noting that incoherent, or finite momentum, pairs (pg) are distinguishable from coherent, or zero momentum, pairs (sc) through lifetime effects. The incoherent nature of the non-condensed pairs is affected by scattering events and therefore incorporates a finite broadening into the self-energy Σ_{pg}. With this intuition, the self-energy can be replaced by the model self-energy [95]:

$$\Sigma(\omega, \mathbf{k}) \approx \frac{\Delta_{pg}^2}{\omega + \epsilon_{\mathbf{k}} + i\gamma} + \frac{\tilde{\Delta}_{sc}^2}{\omega + \epsilon_{\mathbf{k}}}, \tag{8.56}$$

where γ is the finite broadening. We will not directly calculate γ, but will instead treat it as a phenomenological parameter which is independent of T. To calculate the density of states we remember that

$$G^{-1} = G_0^{-1} - \Sigma, \tag{8.57}$$

relates the self-energy Σ (in this case we use the form of Eq. (8.56)) to the full propagator G. The density of states, defined by [98]:

$$N(\omega) = -2 \sum_{\mathbf{k}} \mathrm{Im}\, G(\omega + i0, \mathbf{k}), \tag{8.58}$$

can be directly evaluated given Eq. (8.56).

Figures 8.7(a)-8.7(c) show the results of evaluating Eq. (8.58), and correspond to the BEC, PG, and BCS cases displayed in the previous figures. The temperatures shown are taken just above T_c, $T = 0.75T_c$, and $T = 0.5T_c$. The BCS case is indicated by an abrupt transition at the critical temperature T_c. The density of states in the BEC regime shows very little temperature dependence throughout, since the fermions

are tightly bound into molecules at all temperatures. The PG case, which is taken near resonance at the point where T_c is a maximum, is the most interesting. A signature of superfluid order, seen by the presence of sharp coherence features, is not clearly perceptible until the temperature is well below the critical temperature. For the present case these features do not appear until a temperature of about $T = 0.5T_c$ is reached. However, the appearance of a pseudogap is clearly signalled by a suppression in the availability of low energy excitations displayed within the density of states plot. Similar observations to these are made in the high-T_c cuprates.

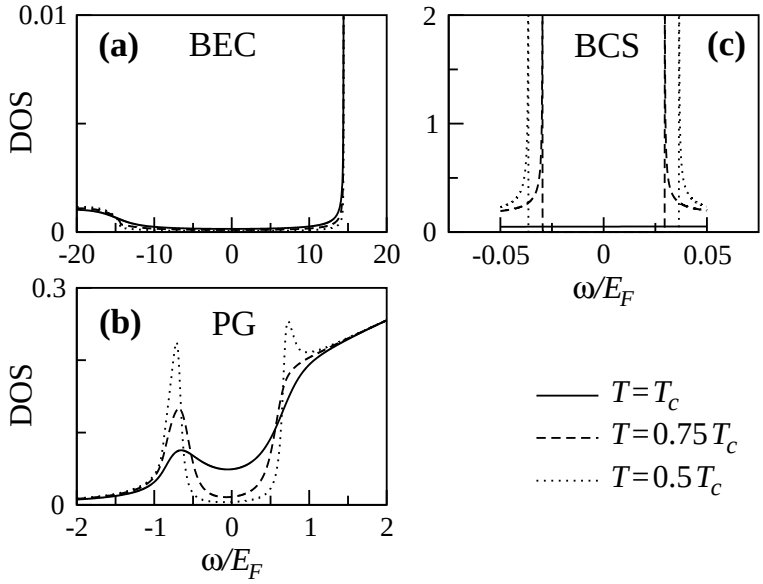

Figure 8.7: Fermionic density of states vs. energy for the three regimes at three indicated temperatures. Note the difference in the scales.

8.10 Conclusions and experimental implications

These plots have important implications for the interpretation of several predicted signatures of superfluidity. One such proposal is based on laser probing of "atomic Cooper pairs" where it has been argued that there is a conceptual analogy between normal metal-superconductor tunnelling (which measures $N(\omega)$), and the resonant scat-

tering of laser light [62]. The present work introduces a caution in interpreting future trapped atomic gas experiments. Because of the presence of a pseudogap, the signatures of superfluid onset are not as simple as in BCS or the related Bogoliubov-de Gennes theory. In general, one has to distinguish between the superfluid order parameter and the fermionic excitation gap. Nevertheless, superfluid coherence appears to be visible as fine structure effects in the fermionic density of states. While several experimentally accessible signatures, such as those displayed in the quantities $N(\omega)$ and n_k, do not provide a clear indication of superfluidity, they do establish the nature of the pairing regime as that of a pseudogapped superfluid.

Chapter 9

Fractional Quantum Hall Effect

9.1 The Hall effect

The Hall effect, discovered in 1879, occurs when a current carrying conducting plate, placed in the x-y plane, is subjected to a magnetic field B_z perpendicular to the plane. The magnetic field causes the electrons, of current density j_x moving at a velocity v_x, to experience a Lorentz force $v_x B_z$ which results in a voltage drop across the sample (see Fig. 9.1). The Hall conductance, which is a measure of the conductance across the sample is

$$\sigma_{xy} = \frac{j_x}{E_y} = \frac{nev_x}{v_x B} = \frac{ne}{B}, \tag{9.1}$$

where n is the number density. Therefore, classically, we would expect the Hall conductance to vary linearly with ne/B.

9.2 The integer quantum Hall effect

In the early 1970's, due to progress in the material sciences, new semiconductors were being produced which could be layered to form very flat, thin interfaces. By cooling these materials and applying an electric field perpendicular to the interface surface the electrons would be forced to situate themselves deep within quantum wells. The result was to quantize the motion of the electrons perpendicular to the interface. This severely limited the motion of the electrons constraining them to move, essentially, within only two-dimensions.

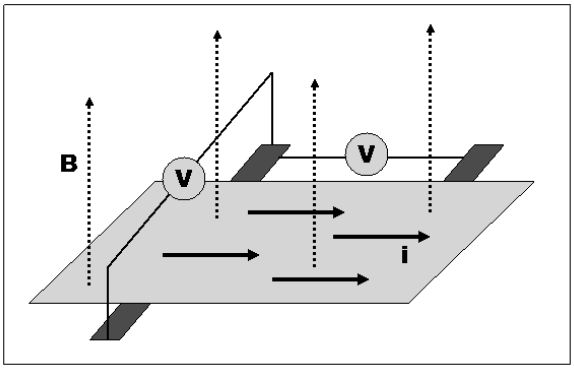

Figure 9.1: The Hall effect occurs when an electrical current is subjected to a transverse magnetic field. The Hall voltage (perpendicular to the current) drops due to the Lorentz force felt by the electrons.

In 1980, Klaus von Klitzing [103] found that at temperatures of only a few Kelvin and high magnetic field (3-10 Tesla), the Hall resistance did not vary linearly with the field. Instead, he found that it varied in a stepwise fashion (see Fig. 9.2). It was also found that where the Hall resistance was flat, the longitudinal resistance disappeared. This dissipation free transport looked very similar to superconductivity. The field at which the plateaus appeared, or where the longitudinal resistance vanished, quite surprisingly, was independent of the material, temperature, or other variables of the experiment, but only depended on a combination of fundamental constants -$\hbar/e^2$. The quantization of resistivity seen in these early experiments came as a grand surprise and would lead to a new international standard of resistivity, the Klitzing, defined as the Hall resistance measured at the fourth step.

The Integer Quantum Hall Effect (IQHE), as it later came to be known, may simply be explained in the context of non-interacting quantum mechanics. The Hamiltonian for a particle subjected to a magnetic field perpendicular to its direction of motion can be written down as:

$$H = \sum_{i}^{N} \frac{(\mathbf{p}_i - e\mathbf{A}(\mathbf{x}_i))^2}{2m}, \tag{9.2}$$

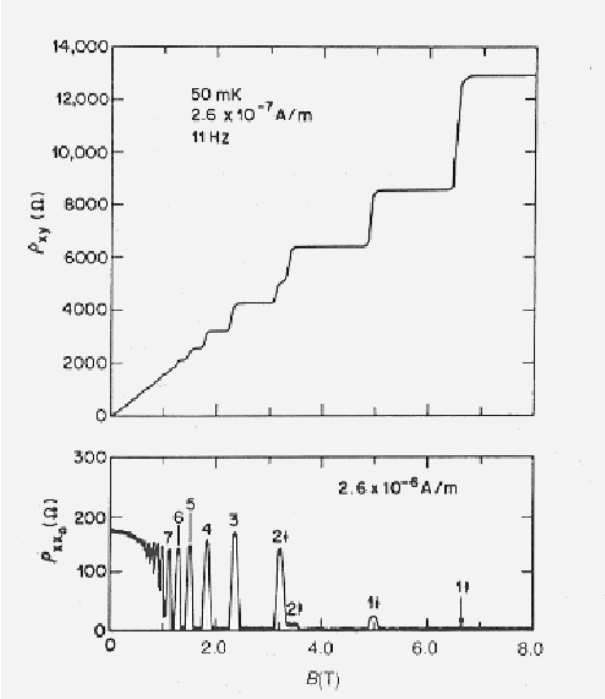

Figure 9.2: The top figure shows the stepwise behavior of the transverse resistivity and the bottom the longitudinal resistance, both as a function of magnetic field. Note, the plateaus(top) coincide with the dissipationless behavior(bottom) at each value of ν. (reprinted from reference [104])

with the vector potential $\mathbf{A}(\mathbf{x})$ chosen in the following gauge

$$\mathbf{A}(\mathbf{x}_i) = \frac{1}{2}B(y_i, -x_i), \qquad B = B\hat{z}. \tag{9.3}$$

The above Hamiltonian results in energy eigenvalues $E_{n,k_y} = (n+1/2)\hbar\omega$ for each "Landau level" (LL) which depend on the cyclotron frequency $\omega = eB/mc$ (see Appendix F). Since the LLs do not depend on the quantum number k_y, they are highly degenerate. This degeneracy, defined as the number of states per unit area, may be quantified by the relation $\rho_B = eB/hc$. This relation leads to a useful quantity for describing the IQHE, known as the filling factor:

$$\nu = \rho/\rho_B, \tag{9.4}$$

which is the number of electrons per Landau level and acts as a measure of the applied magnetic field.

In Fig. 9.2, the plateaus occur at each integer value of the filling factor ν. What occurs is that, as each of the degenerate states of a LL is filled, the conductivity decreases, or the resistivity increases, because fewer and fewer states remain unoccupied within that energy level. Once the LL level is completely full, a gap exists requiring a finite jump in energy to reach the next set of degenerate energy states (i.e., the next LL). However, due to impurities in a sample, localized states exist which may be filled, but do not contribute to the conductivity. This mechanism explains the stepwise behavior of the resistivity.

9.3 Fractional quantum Hall effect

By 1982, semiconductor technology had greatly advanced and it became possible to produce interfaces of much higher quality than where available only a few years before. That same year, Horst Stormer and Dan Tsui [105] repeated Klitzing's earlier experiments with much cleaner samples and higher magnetic fields. What they found

was the same stepwise behavior as seen previously, but to everyone's surprise, steps also appeared at fractional filling factors $\nu = 1/3, 1/5, 2/5 \ldots$ (see Fig. 9.3).

Since these fractional values occurred in the middle of the various highly degenerate Landau levels, where no gap was apparent, these observations could not be explained by the non-interacting quantum mechanical theory.

It would quickly be realized that these observations were a result of the many-body effects of interacting electrons. We should once again consider the Hamiltonian for a population of electrons in the presence of a transverse magnetic field, but now include the effects of interactions:

$$H = \sum_{i}^{N} \frac{(\mathbf{p}_i - e\mathbf{A}(\mathbf{x}_i))^2}{2m} + \sum_{i<j}^{N} \frac{e^2}{|\mathbf{x}_i - \mathbf{x}_j|} \tag{9.5}$$

For the IQHE the potential energy $e^2/\bar{r}$, where $\bar{r}$ is the average electron spacing, was small compared to the cyclotron energy $\omega = eB/mc$ and could be neglected. Now, however, the kinetic term may be neglected so that $e^2/\bar{r}$ is no longer a small term and we are left with a problem which is intrinsically one of strong correlations.

9.4 The Laughlin variational wavefunction

Strongly correlated systems are notoriously difficult to understand, but in 1983, Robert Laughlin [106] proposed his now celebrated ansatz for a variational wavefunction which contained no free parameters:

$$\psi_L = \prod_{i<j} (z_i - z_j)^{2p+1} e^{-\sum_i \frac{|z_i|^2}{4l^2}}, \tag{9.6}$$

where the position of the i^{th} particle is given by the complex coordinate $z_i = x_i + iy_i$ and $l^2 = hc/eB$ is the magnetic length . The Laughlin wavefunction, as it would come to be known, gave an accurate description of all filling fractions $\nu = 1/(2p+1)$ and was shown to almost exactly match numerical ground state wavefunctions found for small FQHE systems. There are several key points that should be mentioned about this choice of wavefunction:

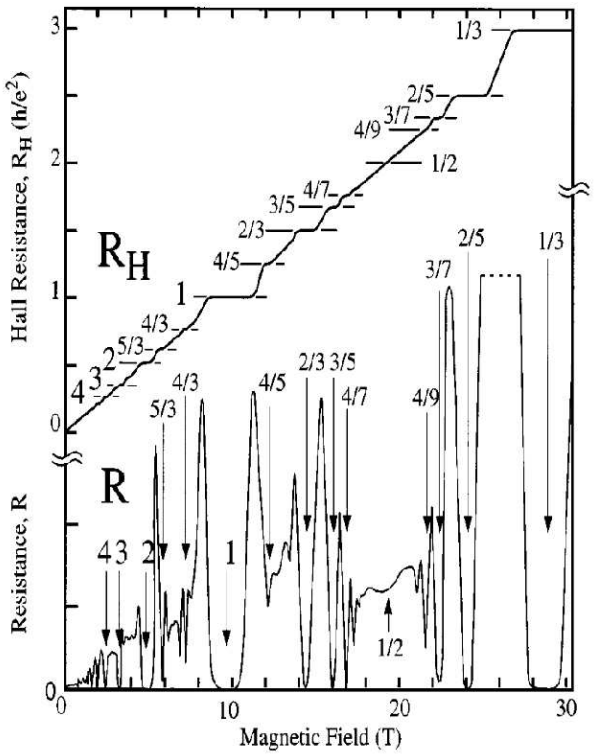

Figure 9.3: The figure shows the stepwise behavior of the transverse resistivity, superimposed with the longitudinal resistance, as a function of magnetic field. The same behavior as in figure 9.2 is seen except now at fractions of ν. (reprinted from reference [104])

- The wavefunction is extremely efficient at minimizing the Coulomb energy. Since the wavefunction has multiple zeros, occurring whenever two particles approach, the wavefunction results in a very uniform distribution. This distribution is much more efficient at lowering the Coulomb energy than, for example, a random distribution.

- The Laughlin wavefunction is the lowest energy state and is no longer degenerate, as one might naively expect. The state, therefore, is incompressible and will generate a finite energy gap for all excitations.

- The quasi-particles which result above the ground state carry with them a fractional charge.

One of the main reasons the Laughlin wavefunction is so celebrated is because it is a true, highly-correlated wavefunction. In contrast, the majority of many-body wavefunctions are simply Slater-determinants of single-particle wavefunctions. For example, the wavefunction for one filled Landau level can be written as proportional to:

$$\psi(z_1, z_2, \dots z_N) \sim \begin{vmatrix} 1 & 1 & \cdots & 1 \\ z_1 & z_2 & \cdots & z_N \\ z_1^2 & z_2^2 & \cdots & z_N^2 \\ \vdots & \vdots & \vdots & \vdots \\ z_1^{N-1} & z_2^{N-2} & \cdots & z_N^{N-1} \end{vmatrix}, \tag{9.7}$$

where we have not bothered to write out the normalization or the usual decaying exponential factors. The Laughlin wavefunction, however, cannot be written in terms of a Slater determinant and is, therefore, something much more complicated than is often encountered. In order to explain the remaining filling fractions, such as $2/5, 3/7$... it was necessary to build off the work of Laughlin to create what has come to be known as the hierarchy picture.

9.5 Composite fermions and Chern-Simons theory

In 1989, Jainendra Jain [107] identified a suitable set of quasi-particles for the FQHE system, calling them "composite fermions". In terms of these quasi-particles, the FQHE behaves exactly as does the IQHE. When each of the composite fermion Landau levels is filled there exists an energy gap separating it from the next composite Landau level. This scheme was able to explain both the Laughlin fractions $1/3, 1/5 \ldots$ as well as many of the remaining fractions $2/5, 3/7 \ldots$. The idea of composite particles may be clarified by the illustrations of Figs. 9.4, 9.5, and 9.6.

A system of composite fermions may seem strange at first thought since the quasi-particles are composed of both particles (the electrons) and fields (the flux quanta). A field theory of this sort is known as a gauge field theory since it will require a gauge transformation to move from particles to quasi-particles. In the context of the FQHE, this transformation is known as the Chern-Simons theory [108]. We will discuss the Chern-Simons theory more in the next chapter where we apply it to describe a resonant gas of Bosons.

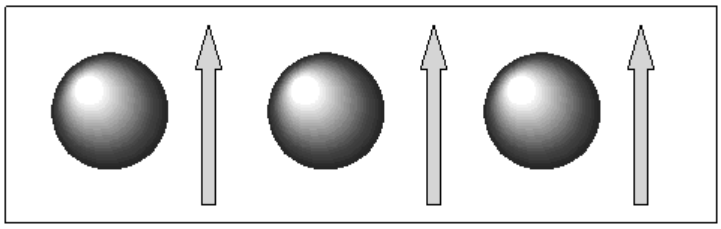

Figure 9.4: The IQHE may be depicted by the above illustration. For each particle (balls) there exists one associated flux quanta (arrows) and the particles are weakly interacting. This results in a filling fraction of $\nu = 1$.

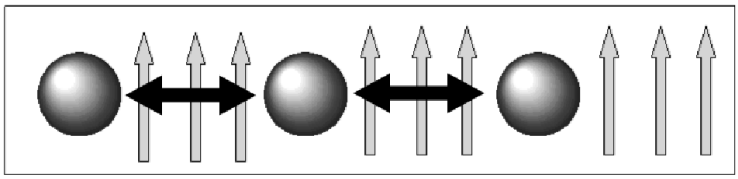

Figure 9.5: At a filling fraction of $\nu = 1/3$, for example, there exist three flux quanta for each particle, but the particles are now strongly interacting.

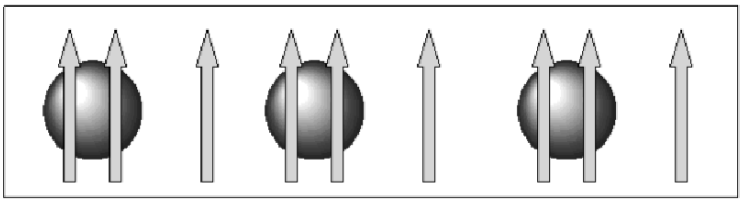

Figure 9.6: By associating two flux quanta with each particle, the system at $\nu = 1/3$ reduces to a weakly interacting system of composite particles (one particle and two flux quanta) at $\nu = 1$. We are left with the IQHE of figure 9.4, but in terms of composite fermions.

Chapter 10

Resonant Manipulation of the Fractional Quantum Hall Effect

10.1 Resonant theory of a rapidly rotating Bose gas

There is a considerable amount of interest in the behavior of rotating Bose gases confined to an effective two-dimensional space. Beginning with the generation of a single vortex [109], experiments have progressively created increasingly dense vortex arrays [110, 111]. By driving the stirring frequency ever closer to the critical trap frequency, experiments are now creating scenarios where there exist a similar number of vortices as particles. One of the major goals is to push these systems well into the regime where the system is thought to display strong correlation effects.

Recently, Wilkin et *al.* [112] have shown that there exists a direct mapping between the two-dimensional Hamiltonian of a rotating Bose gas and of electrons subjected to a transverse magnetic field. The analog of the magnetic field is realized by the angular rotation and the Coulomb interaction is replaced by the two-particle scattering. The group later went on to show, through exact diagonalization studies of a small number of particles, that one could generate a Laughlin state (as well as many other novel FQHE type states) when there exists on the order of one vortex per particle [113]. This was also confirmed by Paredes et *al.* [114]. Unfortunately, if a state such as the Laughlin state were to be created in the laboratory, it would remain a major challenge to resolve it from the next excited state due to the extreme fineness of the gap. The size of the energy gap, however, is directly related to the strength of interatomic interactions.

A natural strategy for increasing the gap, and thus making the FQHE states more accessible to experiment, would be to exploit a mechanism, such as a Feshbach resonance, to enhance the interaction strength. To account for the full effects of the resonance, however, we cannot simply scale the mean-field energy, but must incorporate the entire resonant structure into the model. We must, therefore, include the process of molecular formation to the description of the rotating system.

By introducing a bound state, we not only modify the relative interaction strength, we also introduce a physical mechanism for generating pair correlations between particles (see Fig. 10.1). In the context of two-dimensional condensed matter systems, such a mechanism, which may arise from the long range nature of the Coulomb interaction [115], can have a dramatic effect on the properties of the ground state. In a resonant atomic gas, although the range of the potential is quite small, the effective scattering length may well exceed the inter-particle spacing so that even a small overlap between particles may lead to significant interaction effects. The closed channel bound state responsible for this enhancement, in effect, matches pairs of atoms within the gas resulting in a large increase in correlations.

A natural starting point for studying resonant effects in a rotating Bose gas is to look at the effect of the resonant interactions on the ground state wavefunction. By focusing on the most fundamental FQHE state, the Laughlin state, we will show that as the detuning approaches the Feshbach resonance, the Laughlin state transforms into a unique, strongly correlated state [116].

We begin by writing down an effective Hamiltonian, in second quantized form, for a resonant gas of Bosons of mass m rotating in two dimensions with stirring frequency Ω approaching the trapping frequency ω (i.e., $\omega - \Omega \to 0^+$):

$$\begin{aligned} \hat{H} &= \int d^2x\ \hat{\psi}_a^\dagger(\mathbf{x}) \left[\frac{-1}{2m}(\nabla - i\mathbf{A}(\mathbf{x}))^2\right] \hat{\psi}_a(\mathbf{x}) \\ &+ \frac{1}{2}\int d^2x' \int d^2x\ \hat{\psi}_a^\dagger(\mathbf{x})\hat{\psi}_a^\dagger(\mathbf{x}')U(\mathbf{x},\mathbf{x}')\hat{\psi}_a(\mathbf{x}')\hat{\psi}_a(\mathbf{x}) \end{aligned} \tag{10.1}$$

$$+ \int d^2x\ \hat{\psi}_m^\dagger(\mathbf{x}) \left[\frac{-1}{4m}(\nabla - 2i\mathbf{A}(\mathbf{x}))^2 + \nu\right] \hat{\psi}_m(\mathbf{x})$$
$$+ \frac{1}{2}\int d^2x' \int d^2x \Big[\hat{\psi}_m^\dagger(\frac{\mathbf{x}+\mathbf{x}'}{2}) g(\mathbf{x},\mathbf{x}') \hat{\psi}_a(\mathbf{x}) \hat{\psi}_a(\mathbf{x}') + \text{H.c.}\Big].$$

Here $\hat{\psi}_{a,m}^\dagger(\mathbf{x}), \hat{\psi}_{a,m}(\mathbf{x})$ are the creation and destruction operators for atoms and molecules which satisfy the commutation relations $[\hat{\psi}_1(\mathbf{x}), \hat{\psi}_2^\dagger(\mathbf{x}')] = \delta^{(3)}(\mathbf{x},\mathbf{x}')\delta_{1,2}$, where $1,2 \in \{a,m\}$. We define the two-dimensional vector potential $\mathbf{A}(\mathbf{x}) = (m\omega y, -m\omega x)$, $U(\mathbf{x},\mathbf{x}')$ is the two-particle background scattering potential, $g(\mathbf{x},\mathbf{x}')$ is the resonant coupling between the open and closed channel potentials, and ν is the detuning of the open channel continuum from the level of the bound state in the closed channel.

From the work of Wilkin et *al.* [112], if we were to neglect resonant effects, we would expect the many-body ground state to be described by the Laughlin wavefunction [106]

$$\Psi_L(\mathbf{x}_1, \mathbf{x}_2, ...\mathbf{x}_N) = \prod_{i<j}(z_i - z_j)^2 \prod_k \exp\left(-|z_k|^2/2\right), \tag{10.2}$$

where the products run over the indices $i,j,k = (1,2,...N)$ at position $z = x + iy$ for N particles (as noted earlier, we are focusing on the Laughlin wavefunction arising from a 1/2 filling fraction). We will see that the inclusion of the resonant terms in Eq. (10.1) can significantly modify the form of Eq. (10.2) due to the growth of two-particle correlations.

10.2 Application of Chern-Simons theory

We approach this problem by an extension of Chern-Simons theory [108] which allows us to develop a mean-field theory for the rotating system that has removed the complications of the associated rotation. This is done by constructing a composite particle composed of the original particle and an artificially attached number of flux quanta. The composite particle is designed so that the attached flux quanta cancel the total rotation of the original system leaving a system of non-rotating, interacting composite particles. For the resonant system, the composite particles can formally be

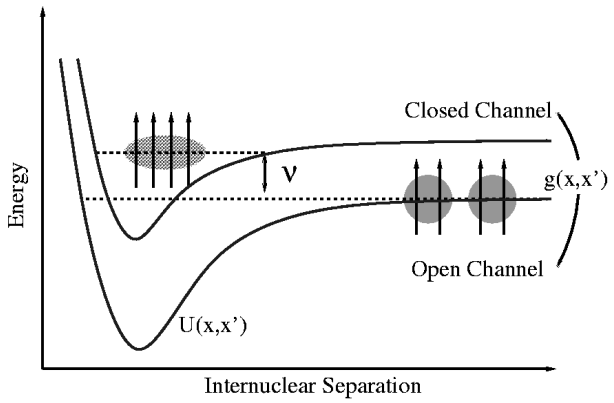

Figure 10.1: Pairs of composite atoms composed of single atoms and an associated number of angular momenta quanta (represented by the arrows) approach within an open channel potential of background value $U(\mathbf{x}, \mathbf{x}')$. They may form a composite molecule due to the presence of a closed channel bound state, at a detuning ν from the scattering continuum, which is coupled to the open channel with strength $g(\mathbf{x}, \mathbf{x}')$.

obtained by the following transformation:

$$\hat{\varphi}_{a,m}(\mathbf{x}) = \exp\Big[-2i \int d^2x' \theta(\mathbf{x}-\mathbf{x}')(\rho_a(\mathbf{x}') + 2\rho_m(\mathbf{x}'))\Big]\hat{\psi}_{a,m}(\mathbf{x}), \tag{10.3}$$

where $\rho_a(\mathbf{x}')$ and $\rho_m(\mathbf{x}')$ are the atomic and molecular spatial densities, respectively, and $\theta(\mathbf{x}-\mathbf{x}')$ is the topological phase [104].

In the composite picture, we replace the $\hat{\psi}$ operators in Eq. (10.1) with the corresponding composite operators $\hat{\varphi}$ and introduce the statistical Chern-Simons field $\mathbf{a}(\mathbf{x})$ through the gauge transformation

$$\mathbf{A}(\mathbf{x}) \to \mathbf{A}(\mathbf{x}) + \mathbf{a}(\mathbf{x}). \tag{10.4}$$

These modifications generate the Hamiltonian formulation of our composite atom/molecule theory. The composite picture can be shown to be equivalent to the single particle picture of Eq. (10.1).

We will now shift to a functional representation of the composite atom/molecule system to clarify the resonant modifications of the Chern-Simons theory and then return to the Hamiltonian formulation to derive the ground state wavefunction. Defining the

action within one temporal and two spatial dimensions

$$S = \int d^3x \sum_{\sigma=a,m} \varphi^*_\sigma(\mathbf{x}) i\partial_0 \varphi_\sigma(\mathbf{x}) - \int dx_0 \hat{H}, \tag{10.5}$$

we generate a Chern-Simons term which couples to the statistical vector field $a_\mu(\mathbf{x})$

$$S_{CS} = -\int d^3x \frac{1}{8\pi} \epsilon^{\mu\nu\lambda} a_\mu(\mathbf{x}) \partial_\nu a_\lambda(\mathbf{x}), \tag{10.6}$$

where the indices of μ, ν, and λ run over the three dimensions $(0, 1, 2)$ and a summation convention over repeated indices is invoked. We have also introduced the antisymmetric tensor $\epsilon^{012} = 1$. To simplify the following calculations we assume contact interactions of the form $U(\mathbf{x}, \mathbf{x}') = U\delta(\mathbf{x}, \mathbf{x}')$ and $g(\mathbf{x}, \mathbf{x}') = g\delta(\mathbf{x}, \mathbf{x}')$. Any complications arising from this replacement of the true potentials with contact potentials should be remedied as explained in Appendix A.

We next perform the lowest order variation of the action. Varying with respect to the zeroth component of the gauge field

$$\frac{\partial S}{\partial a_0} = 0, \tag{10.7}$$

reproduces the Chern-Simons condition

$$\nabla \times \mathbf{a}(\mathbf{x})|_z = -4\pi \left(|\varphi_a(\mathbf{x})|^2 + 2|\varphi_m(\mathbf{x})|^2 \right). \tag{10.8}$$

Equation (10.8) is a statement of Gauss's law for the statistical gauge field associating an even number of rotational flux quanta with each particle. This relation is simply a restatement of our choice of quasi-particle.

10.3 Calculation of the ground state wavefunction

Since we will be interested in the ground state properties of the atom/molecule system, let us assume that the fields $\varphi_a(\mathbf{x})$ and $\varphi_m(\mathbf{x})$ are uniform. By minimizing the action with respect to the atomic and molecular fields

$$\frac{\partial S}{\partial \varphi_a} = 0 \quad \text{and} \quad \frac{\partial S}{\partial \varphi_m} = 0, \tag{10.9}$$

we generate the following constraint equation for the molecules:

$$\varphi_m = \frac{g\varphi_a^2}{2[\nu + |\mathbf{A}+\mathbf{a}|^2/m]}. \tag{10.10}$$

Equation (10.10) allows us to eliminate the molecular field from the theory and arrive at a self-consistent relationship for the gauge field

$$|\mathbf{A}+\mathbf{a}|^2 = \left(U + \frac{g^2}{4(\nu + |\mathbf{A}+\mathbf{a}|^2/m)}\right) 2m|\varphi_a|^2. \tag{10.11}$$

Equation (10.11) is the usual result relating the gauge field to the background density only now it is dependent upon the detuning from the resonance.

We next switch back to the Hamiltonian form of our theory to derive the ground state wavefunction. After Fourier transforming the composite form of Eq. (10.1), by substitution of the field operators $\hat{\varphi}_a(\mathbf{x}) = \sum_{\mathbf{k}} \hat{a}_{\mathbf{k}} e^{i\mathbf{k}\cdot\mathbf{x}}$ and $\hat{\varphi}_m(\mathbf{x}) = \sum_{\mathbf{k}} \hat{b}_{\mathbf{k}} e^{i\mathbf{k}\cdot\mathbf{x}}$, we follow the usual Hartree-Fock-Bogoliubov (HFB) approach to construct a quadratic Hamiltonian which accounts for the lowest order pairing. As before, we assume contact interactions and now make the additional assumption that we may neglect the excited modes of the molecular field keeping only the lowest condensed mode $\hat{b}_{\mathbf{k}} = b_0$. This should remain a valid assumption so long as the molecular mode is not too greatly populated. The resulting Hamiltonian for the composite system can be written as:

$$H = H^0 + \sum_{\mathbf{k}\neq 0} A_{\mathbf{k}}^\dagger M_{\mathbf{k}} A_{\mathbf{k}}. \tag{10.12}$$

H^0 is composed of all terms of less than quadratic order in the operator $\hat{a}_{\mathbf{k}}$, we define a column vector $A_{\mathbf{k}} = (\hat{a}_{\mathbf{k}}, \hat{a}_{-\mathbf{k}}^\dagger)$, and $M_{\mathbf{k}}$ is the self-energy matrix. For our purposes we need only concern ourselves with the structure of the second term in Eq. (10.12). Here the self-energy matrix is expressed as

$$M_{\mathbf{k}} = \begin{pmatrix} E_{\mathbf{k}} & \Delta \\ \Delta^* & E_{-\mathbf{k}} \end{pmatrix} \tag{10.13}$$

with the additional definitions for the diagonal and off-diagonal terms

$$E_{\mathbf{k}} = E^0_{\mathbf{k}} + U(|\varphi_a|^2 + n), \tag{10.14}$$

$$\Delta = U(\varphi_a^2 + p) + g\varphi_m. \tag{10.15}$$

Equations (10.14) and (10.15) are expressed in terms of the pairing-field $p = \sum_{\mathbf{k}'} \langle \hat{a}_{\mathbf{k}'} \hat{a}_{-\mathbf{k}'} \rangle$, the normal-field $n = \sum_{\mathbf{k}'} \langle \hat{a}^\dagger_{\mathbf{k}'} \hat{a}_{\mathbf{k}'} \rangle$, and $E^0_{\mathbf{k}}$ is the effective kinetic term which contains the contribution from the gauge field $A(\mathbf{x})$.

By rewriting Eq. (10.12) in terms of the quasi-particles

$$\hat{\alpha}_{\mathbf{k}} = \frac{1}{\sqrt{(E_{\mathbf{k}} + \omega_{\mathbf{k}})^2 + |\Delta|^2}} \left((E_{\mathbf{k}} + \omega_{\mathbf{k}}) \hat{a}_{\mathbf{k}} + \Delta \hat{a}^\dagger_{-\mathbf{k}} \right), \tag{10.16}$$

$$\hat{\alpha}^\dagger_{-\mathbf{k}} = \frac{1}{\sqrt{(E_{\mathbf{k}} + \omega_{\mathbf{k}})^2 + |\Delta|^2}} \left((E_{\mathbf{k}} + \omega_{\mathbf{k}}) \hat{a}_{-\mathbf{k}} + \Delta^\dagger \hat{a}_{\mathbf{k}} \right), \tag{10.17}$$

the result is a diagonal Hamiltonian

$$\mathcal{H} = \mathcal{H}^0 + \sum_{\mathbf{k} \neq 0} \omega_{\mathbf{k}} \hat{\alpha}^\dagger_{\mathbf{k}} \hat{\alpha}_{\mathbf{k}}, \tag{10.18}$$

where $\mathcal{H}^0$ contains the ground state contribution to the energy and the excitations are given by the spectrum of frequencies $\omega_{\mathbf{k}} = \sqrt{E^2_{\mathbf{k}} - |\Delta|^2}$.

Since there are no quasi-particles present in the ground state $|gs\rangle$, which is what one would expect from an interacting bosonic system at $T = 0$, the ground state must satisfy the condition

$$\hat{\alpha}_{\mathbf{k}} |gs\rangle = 0. \tag{10.19}$$

Substitution of Eqs. (10.16) and (10.17) for the quasi-particle operators result in the relation

$$(E_{\mathbf{k}} + \omega_{\mathbf{k}}) \hat{a}_{\mathbf{k}} |gs\rangle = -\Delta \hat{a}^\dagger_{-\mathbf{k}} |gs\rangle. \tag{10.20}$$

Because $\hat{a}_{\mathbf{k}}$ and $\hat{a}^\dagger_{\mathbf{k}}$ are canonically conjugate variables, there is no loss of generality in making the replacement $\hat{a}_{\mathbf{k}} \rightarrow \partial / \partial \hat{a}^\dagger_{\mathbf{k}}$ [117]. This converts Eq. (10.20) into a simple differential equation for the ground state with the solution:

$$|gs\rangle = \exp \left[\sum_{\mathbf{k}} \frac{-\Delta}{E_{\mathbf{k}} + \omega_{\mathbf{k}}} \hat{a}^\dagger_{-\mathbf{k}} \hat{a}^\dagger_{\mathbf{k}} \right] |0\rangle. \tag{10.21}$$

To derive the many-body wavefunction, we must now move from second to first quantization. We follow the method of reference [118] in what follows. The relationship which links the second quantized ground state $|gs\rangle$ with the first quantized wavefunction Ψ_{CB} can be written for an even number of noncondensed particles $2N$ as

$$\Psi_{CB}(\mathbf{x}_1, \mathbf{x}_2, ...\mathbf{x}_{2N}) = \langle 0|\hat{\varphi}_a(\mathbf{x}_{2N})...\hat{\varphi}_a(\mathbf{x}_2)\hat{\varphi}_a(\mathbf{x}_1)|gs\rangle, \tag{10.22}$$

where it should be noted that Ψ_{CB} is the full-many body wavefunction for the composite Bose particles. If we are able to assume that $E_{\mathbf{k}} + \omega_{\mathbf{k}} \gg \Delta$, an assumption which will remain valid as long as we are not too close to resonance, we may truncate the power expansion of the exponent in Eq. (10.21). This results in the composite boson wavefunction

$$\Psi_{CB}(\mathbf{x}_1, \mathbf{x}_2, ...\mathbf{x}_{2N}) = \mathcal{S}(\psi_{12}\psi_{34}...\psi_{(2N-1)2N}), \tag{10.23}$$

comprised of a symmetrized product $\mathcal{S}$ of paired wavefunctions

$$\psi_{ij} = \sum_{\mathbf{k}} \frac{-\Delta}{E_{\mathbf{k}} + \omega_{\mathbf{k}}} e^{i\mathbf{k}\cdot(\mathbf{x}_i - \mathbf{x}_j)}. \tag{10.24}$$

If we were dealing with a system of fermions, Eq. (10.23) would be antisymmetrized and would result in a Pfaffian wavefunction [119]. Here, because of the statistics of the particles, we generate a bosonic analogue to this result. The many-body wavefunction for the bare particles can now be extracted from the composite wavefunction (see reference [118]) resulting in:

$$\Psi_{MB} = \Psi_{CB}(\mathbf{x}_1, \mathbf{x}_2..., \mathbf{x}_{2N}) \times \Psi_L(\mathbf{x}_1, \mathbf{x}_2..., \mathbf{x}_{2N}), \tag{10.25}$$

which is a product of the composite particle wavefunction of Eq. (10.23) and the Laughlin wavefunction of Eq. (10.2).

10.4 Discussion of resonant effects

Equation (10.25) is the final result for the ground state wavefunction of the resonant rotating Bose system. This result has important consequences for the generation

of a Laughlin state within a resonant atomic gas. It would imply that since a Feshbach resonance necessarily increases two-particle correlations between composite particles, resonantly increasing the interactions will eventually result in a modification to the ground state wavefunction. As is clear from the form of Eq. (10.23), for large detuning from the resonance, corresponding to small pairing and molecular field, the many-body wavefunction reduces to the Laughlin wavefunction. As one moves nearer to the resonance, however, the off-diagonal part of the self-energy matrix, Δ, grows. This results in an increasing modification of the many-body wavefunction from the Laughlin wavefunction. The ability to tune a Feshbach resonance, therefore, allows for the direct study of this crossover from a Laughlin wavefunction to a paired wavefunction.

A similar, yet distinct, Moore-Read type wavefunction, as in Eq. (10.25), was found for electronic FQHE systems [120]. This has been used to explain the previously unresolved, even denominator filling fractions which result from a pairing instability, such as the observed incompressibility of the 5/2 filling. In this case, a straightforward generalization of the Laughlin wavefunction would result in a symmetric wavefunction, violating the asymmetry of the fermions. However, the generation of an antisymmetric Pfaffian wavefunction which multiplies the generalized Laughlin state allows the overall ground state to be correctly antisymmetrized. For the bosonic system we have treated, the overall wavefunction must remain symmetric, so the corresponding paired wavefunction is symmetric in comparison to the antisymmetric Pfaffian wavefunction.

In conclusion, the introduction of Feshbach resonance interactions to the problem of a rotating Bose gas forces one to account for the effects of molecular formation. The growth of pair correlations among the composite particles leads to a modification of the nonresonant ground state for a rapidly rotating Bose gas. The new ground state wavefunction, which is generated by the Feshbach resonance, exists as a strongly correlated state unique to trapped Bose gases. Currently, the major challenge in realizing the simplest of FQHE states, the Laughlin state, is the need to reach extremely low

temperatures to resolve the ground state from the excited states. Since the size of this energy gap is directly related to the strength of interatomic interactions, by increasing the interactions, it would seem natural that one could increase the energy gap, making the system more accessible to experiment. The results of this paper would imply that any attempt to increase the gap with a Feshbach resonance would result in modifying the ground state from the desired Laughlin state. Unfortunately, at the level of the present calculation, we are unable to comment on the resonant behavior of the gap so defer this discussion for now. These results, nonetheless, reveal the exciting possibility of directly studying the crossover transition between a bosonic Moore-Read type state and the Laughlin state.

These conclusions have several other important implications for the resonant production of FQHE states within atomic gases. For instance, many of the observable properties of the gas may be modified, such as the density profile for both atoms and molecules and the nature of collective excitations. It should also be noted that the crossover transition we have discussed is only a part of a much more general crossover theory made accessible by the tunability of a Feshbach resonance. Although the methods presented here are invalid close to the resonance, one could imagine extending these ideas to describe the resonant system as one passes from a gas of interacting rotating atoms, through the resonance, to a system of tightly bound, rotating molecules. This would be the analog for the rotating system of the crossover problem we have discussed at such length within this thesis.

Bibliography

[1] M. H. Anderson *et al.*, Science **269**, 198 (1995).

[2] C. C. Bradley, C. A. Sackett, J. J. Tollett, and R. G. Hulet, Phys. Rev. Lett. **75**, 1687 (1995).

[3] K. B. Davis *et al.*, Phys. Rev. Lett. **75**, 3969 (1995).

[4] B. DeMarco and D. S. Jin, Science **285**, 1703 (1999).

[5] J. Anglin and W. Ketterle, Nature **416**, 211 (2002).

[6] F. Schreck *et al.*, Phys. Rev. Lett. **87**, 080403 (2001).

[7] A. G. Truscott *et al.*, Science **291**, 2570 (2001).

[8] S. R. Granada, M. E. Gehm, K. M. O'Hara, and J. E. Thomas, Phys. Rev. Lett. **88**, 120405 (2002).

[9] Z. Hadzibabic *et al.*, Phys. Rev. Lett. **88**, 160401 (2002).

[10] G. Roati, F. Riboli, G. Modungo, and M. Inguscio, Phys. Rev. Lett. **89**, 150403 (2002).

[11] S. Inouye *et al.*, Nature **392**, 151 (1998).

[12] P. Courteille *et al.*, Phys. Rev. Lett. **81**, 69 (1998).

[13] J. L. Roberts *et al.*, Phys. Rev. Lett. **81**, 5109 (1998).

[14] V. Vuletic, A. J. Kerman, C. Chin, and S. Chu, Phys. Rev. Lett. **82**, 1406 (1999).

[15] T. Loftus *et al.*, Phys. Rev. Lett. **88**, 173201 (2002).

[16] K. Dieckmann *et al.*, Phys. Rev. Lett. **89**, 203201 (2002).

[17] T. Bourdel *et al.*, Phys. Rev. Lett. **91**, 020402 (2003).

[18] S. Jochim *et al.*, Phys. Rev. Lett. **89**, 273202 (2002).

[19] E. A. Donley, N. R. Claussen, S. T. Thompson, and C. E. Wieman, Nature **417**, 529 (2002).

[20] S. Dürr, T. Volz, A. Marte, and G. Rempe, Phys. Rev. Lett. **92**, 020406 (2004).

[21] J. Cubizolles *et al.*, Phys. Rev. Lett. **91**, 240401 (2003).

[22] S. Jochim *et al.*, Phys. Rev. Lett. **91**, 240402 (2003).

[23] K. E. Strecker, G. B. Partridge, and R. G. Hulet, Phys. Rev. Lett. **91**, 080406 (2003).

[24] K. Xu *et al.*, Phys. Rev. Lett. **91**, 210402 (2003).

[25] M. Greiner, C. A. Regal, and D. S. Jin, Nature **426**, 537 (2003).

[26] M. W. Zwierlein *et al.*, Phys. Rev. Lett. **91**, 250401 (2003).

[27] S. Jochim *et al.*, Science **302**, 2101 (2003).

[28] C. A. Regal, M. Greiner, and D. S. Jin, Phys. Rev. Lett. **92**, 040403 (2004).

[29] M. Zwierlein *et al.*, cond-mat/0403049 (unpublished).

[30] H. Feshbach, Ann. Phys. **5**, 357 (1958).

[31] H. Feshbach, Theoretical Nuclear Physics (Wiley, New York, 1992).

[32] J. R. Taylor, Scattering Theory (Wiley, New York, 1972).

[33] A. J. Moerdijk, B. J. Verhaar, and A. Axelsson, Phys. Rev. A **51**, 4852 (1998).

[34] S. J. J. M. F. Kokkelmans, B. J. Verhaar, and K. Gibble, Phys. Rev. Lett. **81**, 951 (1998).

[35] P. J. Leo, E. Tiesinga, and P. S. Julienne, Phys. Rev. Lett. **81**, 1389 (1998).

[36] E. G. M. van Kempen, S. J. J. M. F. Kokkelmans, D. J. Heinzen, and B. J. Verhaar, Phys. Rev. Lett. **81**, 951 (1998).

[37] S. J. J. M. F. Kokkelman *et al.*, Phys. Rev. A **65**, 053617 (2002).

[38] S. Kokkelmans and B. J. Verhaar, the calculation is based on the analysis of the lithium interactions as described in [123]. An alternative analysis has been described in [124]. (unpublished).

[39] E. A. Donley *et al.*, Nature **412**, 295 (2001).

[40] R. A. Duine and H. T. C. Stoof, Phys. Rev. Lett. **86**, 2204 (2001).

[41] L. Santos and G. V. Shlyapnikov, Phys. Rev. A **66**, 011602 (2002).

[42] H. Saito and M. Ueda, Phys. Rev. A **65**, 033624 (2002).

[43] C. M. Savage, N. P. Robins, and J. J. Hope, Phys. Rev. A **67**, 014304 (2003).

[44] G. S. Jeon, S. W. Rhee, and D. J. Thouless, Phys. Rev. A **66**, 011603 (2002).

[45] J. N. Milstein, C. Menotti, and M. J. Holland, New Journal of Physics **5**, 52. 1 (2003).

[46] S. J. J. M. F. Kokkelmans and M. J. Holland, Phys. Rev. Lett. **89**, 180401 (2002).

[47] M. Mackie, K. A. Suominen, and J. Javanainen, Phys. Rev. Lett. **89**, 180403 (2002).

[48] T. Köhler, T. Gasenzer, and K. Burnett, Phys. Rev. A **67**, 013601 (2003).

[49] M. L. Chiofalo, S. J. J. M. F. Kokkelmans, J. N. Milstein, and M. J. Holland, Phys. Rev. Lett. **88**, 090402 (2002).

[50] E. Timmermans *et al.*, Phys. Rev. Lett. **83**, 2691 (1999).

[51] M. Holland, J. Park, and R. Walser, Phys. Rev. Lett. **86**, 1915 (2001).

[52] J. Ranninger and S. Robaszkiewicz, Phys. Rev. B **53**, 468 (1985).

[53] R. Friedberg and T. D. Lee, Phys. Rev. B **40**, 6745 (1989).

[54] J. P. Blaizot and G. Ripka, Quantum theory of finite systems (MIT Press, Cambridge, Massachusettes, 1986).

[55] C. W. Gardiner and P. Zoller, Quantum noise (Springer-Verlag, Germany, 2000).

[56] J. Bardeen, L. N. Cooper, and J. R. Schrieffer, Phys. Rev. **108**, 1175 (1957).

[57] L. N. Cooper, Phys. Rev. **104**, 1189 (1956).

[58] M. Tinkham, Introduction to superconductivity (McGraw Hill, New York, 1980).

[59] J. R. Schrieffer, Theory of Superconductivity, 3rd ed. (Perseus Books, Reading, MA, 1983).

[60] W. P. Zhang, C. A. Sackett, and R. G. Hulet, Phys. Rev. A **60**, 504 (1999).

[61] F. Weig and W. Zwerger, Europhys. Lett. **49**, 282 (2000).

[62] P. Törma and P. Zoller, Phys. Rev. Lett. **85**, 487 (2000).

[63] M. Farine, P. Schuck, and X. Vinas, Phys. Rev. A **62**, 013608 (2000).

[64] A. Minguzzi, G. Ferrari, and Y. Castin, Eur. Phys. J. D **17**, 49 (2001).

[65] A. Minguzzi and M. P. Tosi, Phys. Rev. A **63**, 023609 (2001).

[66] M. A. Baranov and D. S. Petrov, Phys. Rev. A **62**, 041601 (2000).

[67] H. T. C. Stoof, M. Houbiers, C. A. Sackett, and R. G. Hulet, Phys. Rev. Lett. **76**, 10 (1996).

[68] M. Houbiers and H. T. Stoof, Phys. Rev. A **59**, 1556 (1999).

[69] R. Combescot, Phys. Rev. Lett. **83**, 3766 (1999).

[70] G. Bruun, Y. Castin, and R. Dum, Eur. Phys. J. D. **7**, 433 (1999).

[71] H. Heiselberg, C. J. Pethick, H. Smith, and L. Viverit, Phys. Rev. Lett. **85**, 2418 (2000).

[72] M. Holland, S. J. J. M. F. Kokkelmans, R. Walser, and M. L. Chiofalo, Phys. Rev. Lett. **87**, 120406 (2001).

[73] J. L. Bohn, Phys. Rev. A **61**, 053409 (2000).

[74] L. P. Gorkov and T. K. Melik-Barkhudarov, J. Exptl. Theoret. Phys. **40**, 1452 (1961).

[75] V. Bagnato, D. E. Pritchard, and D. Kleppner, Phys. Rev. A **35**, 4534 (1987).

[76] K. Molmer, Phys. Rev. Lett. **80**, 1804 (1998).

[77] M. R. Schafroth, J. M. Blatt, and S. T. Butler, Helv. Phys. Acta. **30**, 93 (1957).

[78] M. R. Schafroth, Phys. Rev. **111**, 72 (1958).

[79] J. M. Blatt, Prog. Theoret. Phys. (Kyoto) **27**, 1137 (1962).

[80] D. M. Eagles, Phys. Rev. **186**, 456 (1969).

[81] A. J. Leggett, in Modern Trends in the Theory of Condensed Matter (Springer-Verlag, Berlin, 1980), pp. 13–27.

[82] P. Nozières and S. Schmitt-Rink, J. Low Temp. Phys. **59**, 195 (1985).

[83] M. Randeria, in Bose Einstein Condensation, edited by A. Griffin, D. Snoke, and S. Stringari (Cambridge Univ. Press, Cambridge, 1995), pp. 355–92.

[84] J. N. Milstein, S. J. J. M. F. Kokkelmans, and M. J. Holland, Phys. Rev. A **66**, 043604 (2002).

[85] A. A. Abrikosov, L. P. Gorkov, and I. E. Dzyaloshinski, Methods of quantum field theory in statistical physics (Dover Publications, New York, 1963).

[86] V. N. Popov, Functional integrals and collective excitations (Cambridge University Press, New York, NY, 1987).

[87] G. D. Mahan, Many-particle physics (Plenum Press, New York, 1990).

[88] C. A. R. S. de Melo, M. Randeria, and J. R. Engelbrecht, Phys. Rev. Lett. **71**, 3202 (1993).

[89] R. G. Newton, Scattering theory of waves and particles (McGraw-Hill, New York, 1996).

[90] J. O. Sofo and C. A. Balseiro, Phys. Rev. B **45**, 8197 (1992).

[91] J. Serene, Phys. Rev. B **40**, 10873 (1989).

[92] L. P. Kadanoff and P. C. Martin, Phys. Rev. **124**, 670 (1961).

[93] B. Janko, J. Maly, and K. Levin, Phys. Rev. B **56**, R11407 (1997).

[94] Q. J. Chen, I. Kosztin, B. Janko, and K. Levin, Phys. Rev. Lett. **81**, 4708 (1998).

[95] J. Maly, B. Janko, and K. Levin, Phys. Rev. B **59**, 1354 (1999).

[96] R. Haussmann, Phys. Rev. B **49**, 12975 (1994).

[97] J. Stajic *et al.*, cond-mat/0309329 (unpublished).

[98] A. L. Fetter and J. D. Walecka, Quantum theory of Many-Particle Systems (Dover Publications, New York, 2003).

[99] U. Fano, Phys. Rev. **124**, 1866 (1961).

[100] J. Maly, B. Janko, and K. Levin, Physica C **321**, 113 (1999).

[101] Y. Ohashi and A. Griffin, Phys. Rev. Lett. **89**, 130402 (2002).

[102] L. Viverit, S. Giorgini, L. Pitaevskii, and S. Stringari, Phys. Rev. A **69**, 013607 (2004).

[103] K. von Klitzing, G. Dorda, and M. Pepper, Phys. Rev. Lett. **45**, 494 (1980).

[104] Z. F. Ezawa, Quantum Hall Effects (World Scientific, River Edge, NJ, 2000).

[105] D. C. Tsui, H. L. Stormer, and A. C. Gossard, Phys. Rev. Lett. **48**, 1559 (1982).

[106] R. B. Laughlin, Phys. Rev. Lett. **50**, 1395 (1983).

[107] J. K. Jain, Phys. Rev. Lett. **63**, 199 (1989).

[108] S. C. Zhang, T. H. Hansson, and S. Kivelson, Phys. Rev. Lett. **62**, 82 (1989).

[109] M. R. Matthews *et al.*, Phys. Rev. Lett. **83**, 2498 (1999).

[110] J. R. Abo-Shaeer, C. Raman, J. M. Vogels, and W. Ketterle, Science **292**, 476 (2001).

[111] P. Engels, I. Coddington, P. C. Haljan, and E. A. Cornell, Phys. Rev. Lett. **89**, 100403 (2002).

[112] N. K. Wilkin, J. M. F. Gunn, and R. A. Smith, Phys. Rev. Lett. **80**, 2265 (1998).

[113] N. K. Wilkin and J. M. F. Gunn, Phys. Rev. Lett. **84**, 6 (2000).

[114] B. Paredes, P. Fedichev, J. I. Cirac, and P. Zoller, Phys. Rev. Lett. **87**, 010402 (2001).

[115] F. D. M. Haldane and E. H. Rezayi, Phys. Rev. Lett. **60**, 956 (1988).

[116] S. Bhongale, J. N. Milstein, and M. J. Holland, Phys. Rev. A (2004).

[117] P. A. M. Dirac, The Principles of Quantum Mechanics (Clarendon Press, Oxford, 1958).

[118] T. Morinari, Phys. Rev. B **62**, 15903 (2000).

[119] N. Read, Phys. Rev. Lett. **62**, 86 (1989).

[120] G. Moore and N. Read, Nucl. Phys. B **360**, 362 (1991).

[121] J. Goldwin, S. B. Papp, B. DeMarco, and D. S. Jin, Phys. Rev. A **65**, (2002).

[122] K. M. O'Hara *et al.*, Science **298**, 2179 (2002).

[123] F. A. van Abeelen, B. J. Verhaar, and A. J. Moerdijk, Phys. Rev. A **55**, 4377 (1997).

[124] E. R. I. Abraham *et al.*, Phys. Rev. A **55**, R3299 (1997).

[125] M. E. Peskin and D. V. Schroeder, An introduction to quantum field theory (Perseus Books, Cambridge, MA, 1995).

[126] S. Hassani, Foundations of mathematical physics (Allyn and Bacon, Needham Heights, MA, 1991).

Appendix A

Renormalization of model potentials

Throughout this thesis we have made use of contact and separable pseudo-potentials to simplify the evaluation of the resonant field theories. This has introduced a need to renormalize the resulting equations. Equation (2.41), which defines our renormalization scheme, will now be solved for three different pseudo-potentials: contact, Lorentzian, and Gaussian.

A.1 Contact

The contact potential has the Fourier representation: $\lambda(k) = \sqrt{U}$ and $g(k) = g$. To prevent Eq. (2.41) from diverging we must impose a cutoff K bounding the integral. After performing the integrals, Eq. (2.41) may be solved for $T(k)$. The Feshbach theory, as given by Eqs. (2.20) and (2.25), may be compared to this result by series expanding to order $\mathcal{O}(k)$. Matching terms, order by order, we get a series of algebraic equations which may be solved to find the following relationships between U, g, ν and the physical quantities $\bar{U}, \bar{g}, \bar{\nu}$:

$$\begin{aligned} U &= \bar{U}\Gamma \\ g &= \bar{g}\Gamma \\ \nu &= \bar{\nu} + \alpha\Gamma\bar{g}^2, \end{aligned} \tag{A.1}$$

where we introduce the following definitions:

$$\Gamma = (1 - \alpha\bar{U})^{-1} \quad \text{and} \quad \alpha = mK/(2\pi^2\hbar^2). \tag{A.2}$$

A.2 Lorentzian

In Fourier space the Lorentzian has the form: $\lambda(k) = \sqrt{U}(1 + (k/K)^2)^{-1}$ and $g(k) = g(1 + (k/K)^2)^{-1}$. The form of the pseudo-potentials regularizes the integrals so we do not need to impose a cutoff and the integrals may extend to infinity. The relations given in Eqs. (A.1) again hold and we find

$$\Gamma = (1 - \alpha\bar{U})^{-1} \quad \text{and} \quad \alpha = mK/(4\pi\hbar^2). \tag{A.3}$$

A.3 Gaussian

In Fourier space we have: $\lambda(k) = \sqrt{U}e^{-(k/K)^2}$ and $g(k) = ge^{-(k/K)^2}$. Again the potentials regularize the integrals. Equations (A.1) still hold and we find

$$\Gamma = (1 - \alpha\bar{U})^{-1} \quad \text{and} \quad \alpha = mK/(4\pi^{3/2}\hbar^2). \tag{A.4}$$

Appendix B

Bogoliubov Transformation

Very few many-body problems allow for an exact solution. Among the few that do, one of the more commonly encountered forms are Hamiltonians which are quadratic in creation and annihilation operators. In this appendix we will sketch the general method of solving these quadratic Hamiltonians for the case of both bosons and fermions. A much more thorough treatment can be found in various books such as that of reference [54].

B.1 Hermitian quadratic Hamiltonian

A general, quadratic Hamiltonian of this sort may be written in the form

$$H = \sum_{ij} A_{ij} a_i^\dagger a_j + \frac{1}{2} \sum_{ij} (B_{ij} a_i^\dagger a_j^\dagger + B_{ij}^* a_j a_i), \tag{B.1}$$

where the following conditions are satisfied

$$A = A^\dagger, \qquad B^\top = -\varepsilon B. \tag{B.2}$$

The variable ε is defined such that $\varepsilon = 1$ for fermions and $\varepsilon = -1$ for bosons. Equation (B.1) may be written in matrix form as

$$H = \frac{1}{2} \alpha^\dagger M \alpha + \frac{\varepsilon}{2} \mathrm{tr} A, \tag{B.3}$$

by introducing the row and column vectors

$$\alpha = \begin{pmatrix} a \\ a^\dagger \end{pmatrix}, \qquad \alpha^\dagger = (a^\dagger a), \tag{B.4}$$

and defining the Matrix

$$M = \begin{pmatrix} A & B \\ -\varepsilon B^* & -\varepsilon A^* \end{pmatrix}. \tag{B.5}$$

B.2 Unitary canonical transformation

We define the matrix T which moves us from the basis α to a diagonal basis β

$$\beta = T\alpha. \tag{B.6}$$

We would like this transformation to be canonical, meaning that the operators in the new basis satisfy the same commutation relations as the original operators. This can be expressed by the matrix η defined as:

$$\eta = \begin{pmatrix} [a, a^\dagger]_\varepsilon & [a, a]_\varepsilon \\ [a^\dagger, a^\dagger]_\varepsilon & [a^\dagger, a]_\varepsilon \end{pmatrix} = \begin{pmatrix} 1 & 0 \\ 0 & \varepsilon \end{pmatrix}. \tag{B.7}$$

In order for a transformation T to remain canonical, it must satisfy the following criteria:

$$T\eta T^\dagger \eta = 1 \qquad T^* = \gamma T \gamma, \tag{B.8}$$

where we have introduced the matrix

$$\gamma = \begin{pmatrix} 0 & 1 \\ 1 & 0 \end{pmatrix}. \tag{B.9}$$

It can clearly be seen that a canonical transformation of Eq. (B.3) results in the diagonal Hamiltonian

$$H = \frac{1}{2}\beta^\dagger \eta T \eta M T^{-1} \beta + \frac{\epsilon}{2}\mathrm{tr}A, \tag{B.10}$$

where $T\eta MT^{-1}$ is a diagonal matrix.

B.3 Basis transformations for bosons and fermions

A canonical basis transformation, known as the Bogoliubov transformation, that brings Eq. (B.3) into diagonal form is given by

$$\begin{pmatrix} b_\nu \\ b_\nu^\dagger \end{pmatrix} = \begin{pmatrix} \cosh\omega_\nu & e^{i\theta_\nu}\sinh\omega_\nu \\ e^{-i\theta_\nu}\sinh\omega_\nu & \cosh\omega_\nu \end{pmatrix} \begin{pmatrix} a_\nu \\ a_\nu^\dagger \end{pmatrix}, \tag{B.11}$$

for a single component system of bosons and by

$$\begin{pmatrix} b_{\uparrow\nu} \\ b_{\downarrow\nu} \\ b_{\uparrow\nu}^\dagger \\ b_{\downarrow\nu}^\dagger \end{pmatrix} = \begin{pmatrix} \cos\omega_\nu & 0 & 0 & -ie^{i\theta_\nu}\sin\omega_\nu \\ 0 & \cos\omega_\nu & ie^{i\theta_\nu}\sin\omega_\nu & 0 \\ 0 & ie^{-i\theta_\nu}\sin\omega_\nu & \cos\omega_\nu & 0 \\ -ie^{-i\theta_\nu}\sin\omega_\nu & 0 & 0 & \cos\omega_\nu \end{pmatrix} \begin{pmatrix} a_{\uparrow\nu} \\ a_{\downarrow\nu} \\ a_{\uparrow\nu}^\dagger \\ a_{\downarrow\nu}^\dagger \end{pmatrix}, \tag{B.12}$$

for a two-spin system of fermions. These transformations, of course, can be generalized to systems of higher degrees of freedom.

Appendix C

Functional Integrals and Grassmann Variables

Several useful integrals are often encountered when working with path integrals, the most ubiquitous being Gaussian integrals. We begin by discussing the evaluation of these integrals for the case of Bosons, where we may work with classical fields, and then proceed to discuss fermions and Grassmann variables [86, 125].

C.1 Bosons

For complex fields it is often useful to first decompose the fields into real and imaginary parts. For the bosonic fields x, x^* we may expand them as:

$$x = \frac{x_1 + ix_2}{\sqrt{2}}, \qquad x^* = \frac{x_1 - ix_2}{\sqrt{2}}. \tag{C.1}$$

Before solving for the basic Gaussian functional integral, it is useful to first look at the evaluation of a Gaussian integral of the complex variables x, x^*:

$$\int dx^* dx e^{-x^* a x} = \int dx_1 dx_2 e^{-\frac{1}{2}ax_1^2} e^{-\frac{1}{2}ax_2^2} = \left(\int dx e^{-\frac{1}{2}ax^2} \right)^2 = \frac{2\pi}{a}. \tag{C.2}$$

We have made use of Eq. (C.1) in the second step of Eq. (C.2). Equation (C.2) allows us to evaluate the Gaussian functional integral of the complex fields x, x^* acting on the matrix A with eigenvalues a_i:

$$\int dx^* dx \exp(-x^* A x) \quad = \quad \left(\prod_{i,j} \int dx_i^* dx_j \right) \exp(-\sum_{i,j} x_i A_{i,j} x_j) \tag{C.3}$$

$$
\begin{aligned}
&= \left(\prod_i \int dx_i^* dx_i\right) \exp(-\sum_i x_i^* a_i x_i) \\
&= \prod_i \frac{2\pi}{a_i} = \frac{(2\pi)^n}{\det A}.
\end{aligned}
$$

C.2 Fermions and Grassmann variables

Fermions require the introduction of Grassmann variables in order to satisfy the correct particle statistics. Grassmann variables are defined such that the exchange of any two variables is antisymmetric:

$$x\eta = -\eta x. \tag{C.4}$$

What's more, the product of more than one Grassmann variable yields zero:

$$x^2 = 0. \tag{C.5}$$

This definition may yield an ambiguity in sign when integrating these variables so we must choose a convention. Here we impose the convention $\int dx^* dx (xx^*) = 1$. Let's first look at how a simple Gaussian integral over Grassmann variables is modified:

$$\int dx^* dx \exp(-x^* a x) = \int dx^* dx (1 - x^* a x) = \int dx^* dx (1 + x x^* a) = a. \tag{C.6}$$

This should be contrasted to the result of Eq. (C.2) for a standard, classical variable. With this information we may evaluate the Gaussian functional integral for fermions:

$$
\begin{aligned}
\int dx dx^* \exp(-xAx) &= \left(\prod_{i,j} \int dx_i^* dx_j\right) \exp(-\sum_{i,j} x_i A_{i,j} x_j) \qquad \text{(C.7)} \\
&= \left(\prod_i \int dx_i^* dx_i\right) \exp(-\sum_i x_i^* a_i x_i) \\
&= \prod_i a_i = \det A.
\end{aligned}
$$

Note that for bosons the result was $(2\pi)^n / \det A$. Another useful integral that is often encountered is:

$$\frac{\int dx^* dx \exp(-x^* A x + \eta^* x + x^* \eta)}{\int dx^* dx \exp(-x^* A x)} = \exp(\eta^* A^{-1} \eta), \tag{C.8}$$

where

$$\eta^* x = \sum_i \eta_i^* x_i, \qquad x^* \eta = \sum_i x_i^* \eta_i. \tag{C.9}$$

The variables η_i, η_i^* anticommute with each other and x_i, x_i^*. This can be proved by a shift transformation

$$x \to x + \tilde{\eta}, \qquad x^* \to x^* + \tilde{\eta}^*, \tag{C.10}$$

which will cancel the linear terms in the exponent of Eq. (C.8). When applied in practice, this shift transformation is often known as a Hubbard-Stratonovich transformation.

Appendix D

Matsubara frequency summations

In finite-temperature field theories we often encounter Matsubara frequency summations over products of free Green's functions. In this appendix we will list some of the more common summations and detail how they are evaluated. A discussion of evaluating more complex summations than are presented here can be found in reference [87].

D.1 Common summations

In this thesis we have made use of the following useful relations:

$$\frac{1}{\beta}\sum_{i\omega_p^n} G_0(\mathbf{p}, i\omega_p^n) = n_f(\xi_{\mathbf{p}}), \tag{D.1}$$

$$-\frac{1}{\beta}\sum_{i\nu_p^n} D_0(\mathbf{p}, i\nu_p^n) = n_b(\xi_{\mathbf{p}}), \tag{D.2}$$

$$-\frac{1}{\beta}\sum_{i\omega_p^n} G_0(\mathbf{p}, i\omega_p^n) G_0(\mathbf{q}, i\omega_q^n - i\omega_p^n) = \frac{1 - n_f(\xi_{\mathbf{p}}) - n_f(\xi_{\mathbf{q}})}{i\omega_q^n - \xi_{\mathbf{p}} - \xi_{\mathbf{q}}}. \tag{D.3}$$

Equations (D.1) and (D.2) result in Fermi and Bose distributions defined, respectively, as:

$$n_f(\xi_{\mathbf{p}}) = \frac{1}{e^{\beta\xi_{\mathbf{p}}} - 1} \quad \text{and} \quad n_b(\xi_{\mathbf{p}}) = \frac{1}{e^{\beta\xi_{\mathbf{p}}} + 1}, \tag{D.4}$$

whereas Eq. (D.3) was encountered in our discussion of the pair susceptibility χ.

D.2 Evaluation of Matsubara summations

We begin our discussion of evaluating Matsubara series with the simple case of Eq. (D.1). If we explicitly write the free Fermion Green's function, the sum we wish to evaluate is:

$$S = \frac{1}{\beta} \sum_{n=-\infty}^{\infty} \frac{1}{i\omega_p^n - \xi_p}, \tag{D.5}$$

where the summation runs over integer values for the odd Matsubara frequencies $\omega_p^n = (2n+1)\pi/\beta$. Let us write this in the representative form

$$S = -\frac{1}{\beta} \sum_n f(i\omega_p^n), \tag{D.6}$$

where $f(i\omega_p^n)$ is defined through Eq. (D.5). To evaluate the sum, we transform the summation into an equivalent contour integration. Let us look at the following integral:

$$I = \lim_{R\to\infty} \int \frac{dz}{2\pi i} f(z) n_f(z). \tag{D.7}$$

We now chose the contour to be a circle of radius $R \to \infty$ and impose that the function $n_f(z)$ generates poles at all points $z_n = (2n+1)i\pi/\beta$. An appropriate function would be:

$$n_f(z) = \frac{1}{e^{\beta z} + 1}, \tag{D.8}$$

which has a residue of $-1/\beta$ at each pole z_n. The contour and these periodic poles are illustrated in Fig. D.1. The function $f(z)$ is defined as:

$$f(z) = \frac{1}{z - \xi_p}, \tag{D.9}$$

which contributes an extra pole at $z = \xi_p$. To clarify these results, we list all the poles and residues:

$$z_n = (2n+1)i\pi/\beta, \qquad R_n = -\frac{1}{\beta} \frac{1}{(2n+1)i\pi/\beta - \xi_p} \tag{D.10}$$

$$z_1 = \xi_p, \qquad R_1 = n_f(\xi). \tag{D.11}$$

According to Cauchy's theorem [126], Eq. (D.7) may be written as a sum of residues

$$I = -\frac{1}{\beta}\sum_n \frac{1}{(2n+1)i\pi/\beta - \xi_p} + n_f(\xi_p). \tag{D.12}$$

In the limit that we take the contour $R \to \infty$, assuming Jordan's lemma is satisfied [126], the integral $I \to 0$. We, therefore, have the result:

$$\frac{1}{\beta}\sum_n \frac{1}{(2n+1)i\pi/\beta - \xi_p} = n_f(\xi_p), \tag{D.13}$$

which may be written as

$$\frac{1}{\beta}\sum_{n=-\infty}^{\infty} \frac{1}{i\omega_p^n - \xi_p} = n_f(\xi_p). \tag{D.14}$$

This final result proves Eq. (D.1).

For bosons, the method is similar except the contour integral should be chosen to have poles at the even values $z_n = 2ni\pi/\beta$. It is therefore appropriate to replace Eq. (D.7) with:

$$I = \lim_{R\to\infty} \int \frac{dz}{2\pi i} f(z) n_b(z), \tag{D.15}$$

where the function $n_b(z)$ is given by

$$n_b(z) = \frac{1}{e^{\beta z} - 1}, \tag{D.16}$$

which now has a residue of $1/\beta$ at each pole z_n.

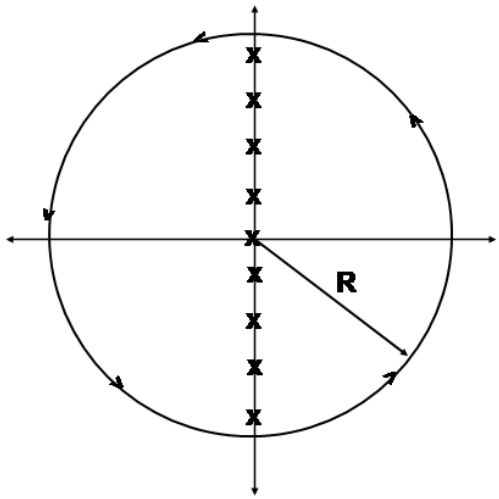

Figure D.1: A typical contour for Matsubara summation integrals. The x's represent evenly spaced poles along the vertical axis at points z_n and the contour radius is taken in the limit $R \to \infty$.

Appendix E

T_c equations from the pseudogap theory

The pseudogap equations derived in Chapter 8 are presented here in a more clear and explicit form. The Matsubara summations are performed and the expansion coefficients of Eq. (8.54) are clearly listed. A detailed discussion of their derivation is given in the text. They are valid for $T \leq T_c$ and may be thought of as an extrapolation for a small region above T_c.

E.1 Gap equation

The Gap equation is given by

$$1 = -g_{eff}(0) \sum_k \frac{1 - 2f(E_k)}{2E_k} \varphi_k^2, \tag{E.1}$$

where $E_k = \sqrt{\varepsilon_k^2 + \Delta^2 \varphi_k^2}$ is the gapped energy spectrum, $\varepsilon_k = k^2/2m - \mu$, and the gap is defined in terms of the superconducting gap Δ_{sc} and the pseudogap Δ_{pg}:

$$\Delta^2 = \Delta_{sc}^2 + \Delta_{pg}^2. \tag{E.2}$$

The Fermi distribution function is defined as $f(x) = 1/(\exp(\beta x)+1)$. The resonant interaction contribution is given as $g_{eff}(0) = U - \frac{g^2}{\nu - 2\mu}$ and the function $\varphi_k^2 = \exp[-(k/Kc)^2]$ is introduced to impose a cutoff K_c upon the integral. For this regularization to work we must define the renormalized parameters as in Appendix A.3.

E.2 Number equation

The equation for the total number of particles in the system is

$$\begin{aligned} N &= N_f + 2N_b + 2N_b^0 \\ &= 2\sum_k \left[f(E_k) + \frac{1}{2}(1 - \frac{\varepsilon_k}{E_k})(1 - 2f(E_k)) \right] + \frac{2}{1+C} \sum_q n \left(q^2 \frac{\frac{1}{2M} + BC}{1+C} \right) + 2N_b^0 \end{aligned} \tag{E.3}$$

The Bose distribution function is introduced as $n(x) = 1/(\exp(\beta x) - 1)$. Here we have also introduced the following constants a_0, B, C. The first two, a_0 and B, will be defined in a following section; the third:

$$C = \frac{g^2 a_0}{(1 - U g_{eff}^{-1}(0))^2}. \tag{E.4}$$

E.3 Pseudogap equation

The equation for the pseudogap is given by

$$\Delta_{pg}^2 = \frac{1}{a_0(1 + 1/C)} \sum_q n \left(q^2 \frac{\frac{1}{2M} + BC}{1+C} \right). \tag{E.5}$$

E.4 Coefficients a_0,B

We now define the expansion coefficients coming from Eq. (8.54) and appearing in the above equations. To begin

$$a_0 = \frac{1}{2\Delta^2} \sum_k \left[(1 - 2f(\varepsilon_k)) - \frac{\varepsilon_k}{E_k}(1 - 2f(E_k)) \right]. \tag{E.6}$$

For the Gaussian potential

$$\vec{\nabla}_k^2 \varphi_k^2 = \frac{2\varphi_k^2}{K_c^2}(2(\frac{k}{K_c})^2 - 3) \quad \text{and} \quad (\vec{\nabla}_k \varepsilon_k) \cdot (\vec{\nabla}_k \varphi_k^2) = -\frac{2}{m}(\frac{k}{K_c})^2 \varphi_k^2, \tag{E.7}$$

so

$$
\begin{aligned}
B &= -\frac{1}{6a_0\Delta^2}\sum_k \Big\{\Big[\frac{4}{m}(\epsilon_k+\mu)f'(\epsilon_k) \\
&+ \frac{2}{m}\frac{E_k(\varepsilon_k+\mu)}{\Delta^2\varphi_k^2}\Big[(1+\frac{\varepsilon_k^2}{E_k^2})(1-2f(E_k)) - 2\frac{\varepsilon_k}{E_k}(1-2f(\varepsilon_k))\Big] \\
&- \frac{1}{2m}\Big[(1-2f(\varepsilon_k)) - \frac{\varepsilon_k}{E_k}(1-2f(E_k))\Big]\Big[3-2(\frac{k}{K_c})^2\Big] \\
&- \frac{\Delta^2}{2K_c^2}\frac{1-2f(E_k)}{2E_k}\varphi_k^2\Big[3-2(\frac{k}{K_c})^2\Big]\Big\}, \qquad \text{(E.8)}
\end{aligned}
$$

where we have introduced the shorthand notation $f'(x) = -f(x)(1-f(x))\beta$.

Appendix F

Landau levels

The Hamiltonian for a charged particle moving in a transverse magnetic field may be written as

$$H = \frac{1}{2m}(\mathbf{p} - e\mathbf{A}(\mathbf{r}))^2 = \frac{1}{2m}\pi^2, \tag{F.1}$$

where we have introduced the operator π which satisfies the commutation relation $[\pi_x, \pi_y] = -i\hbar^2/l^2$, with $l = \sqrt{\hbar/|e|B}$ the magnetic length or Larmor radius. Equation (F.1) may be rewritten in terms of the ladder operators

$$\begin{aligned} a &= \frac{l}{\sqrt{2}\hbar}(\pi_x - i\pi_y), \\ a^\dagger &= \frac{l}{\sqrt{2}\hbar}(\pi_x + i\pi_y), \end{aligned} \tag{F.2}$$

which satisfy the commutation relation $[a, a^\dagger] = 1$. This substiturion results in the following Hamiltonian:

$$H = \hbar\omega_c \left(a^\dagger a + \frac{1}{2}\right), \tag{F.3}$$

where $\omega_c = |eB|/m$ is the cyclotron frequency. Equation (F.3) has eigenvalues $E_n = \hbar\omega_c \left(n + \frac{1}{2}\right)$, like those of the harmonic oscillator, each associated with a highly degenerate set of eigenvectors, known as Landau levels [104]. Often it is convenient to work within the lowest of these degenerate energy levels, referred to as the lowest Landau level (LLL), whose wavefunction may be written as

$$\psi_{0,m}(\mathbf{r}) = \frac{1}{\sqrt{2\pi 2^m m! l}} z^m e^{-|z|^2/4}, \tag{F.4}$$

where the quantum number $m = 0, \pm 1, \pm 2 \ldots$ and the complex position $z = x + iy$ is introduced.